UNIVERSIDAD CARLOS III DE MADRID


Escuela Politécnica Superior

# FORMULATION AND ANALYSES OF VAPORIZATION AND DIFFUSION-CONTROLLED COMBUSTION OF FUEL SPRAYS

**Tesis Doctoral**

Autor
Jorge Arrieta Sanagustín

Directores
Antonio Luis Sánchez Pérez  Amable Liñán Martínez

DEPARTAMENTO DE INGENIERÍA TÉRMICA Y DE FLUIDOS

Leganés, Diciembre 2011

DEPARTAMENTO DE INGENIERÍA TÉRMICA Y DE FLUIDOS
Escuela Politécnica Superior

# FORMULATION AND ANALYSES OF VAPORIZATION AND DIFFUSION-CONTROLLED COMBUSTION OF FUEL SPRAYS

Autor
Jorge Arrieta Sanagustín

Directores de Tesis
Antonio Luis Sánchez Pérez  Amable Liñán Martínez

Leganés, Diciembre 2011

*A mis padres, a Lucía y a Sara*

Tesis doctoral

# FORMULATION AND ANALYSES OF VAPORIZATION AND DIFFUSION-CONTROLLED COMBUSTION OF FUEL SPRAYS

Autor
Jorge Arrieta Sanagustín

Directores de Tesis: Antonio Luis Sánchez Pérez  Amable Liñán Martínez

Firma del Tribunal Calificador:

Firma

Presidente: D. Forman Arthur Williams

Vocal: D. Norman Riley

Vocal: D. Francisco Higuera Antón

Vocal: D. José Luis Ferrín González

Secretario: D. Pedro Luis García Ybarra

Calificación:

Leganés, 16 de Diciembre de 2011

# Agradecimientos

En primer lugar quisiera dar las gracias a las personas sin las cuales no habría sido posible la realización de esta tesis, mis directores Antonio Luis Sánchez y Amable Liñán por sus enseñanzas, su ayuda y por haber tenido el privilegio de aprender y formarme como científico junto a ellos.

Con Eduardo Fernández empecé a dar mis primeros pasos en el mundo de la investigación en el INTA, y por ello quisera agradecerle la oportunidad que me brindó, además de toda la ayuda que me ha prestado de manera desinteresada a lo largo de estos años, ya que sin ella muchos de los resultados de esta tesis no habrían sido posibles. A Alejandro Sevilla, todo mi agradecimiento por su amistad y apoyo, por nuestras charlas científicas y filosóficas que han sido tan estimulantes y gratificantes, y por recordarme la importancia y el valor de la claridad y el pensamiento exacto. A Javier Rodríguez, todos los buenos momentos compartidos, y el tratar de motivarme y animarme en las situaciones de desánimo. Al resto de profesores del Área de Mecánica de Fluidos, su interés en nuestro trabajo y su disposición siempre que he necesitado su ayuda.

A lo largo de esta tesis he tenido la oportunidad de realizar dos estancias breves en la Universidad de California, San Diego, donde pude colaborar con el Profesor Forman Williams al que agradezco la oportunidad que me dio de visitarle así como sus aportaciones a esta tesis , que sin duda han contribuido a mejorarla notablemente. No me puedo olvidar de la comunidad española en San Diego, Baldo, Juan Carlos, Silvana y Javier, que con su hospitalidad hicieron mucho más agradables las estancias allí.

I also had the opportunity of visiting the School of Mathematics at the University of East Anglia, where I had the honour to collaborate with Professor Norman Riley. I would like to acknowledge the opportunity of collaborating with him. I would also like to express my gratitude to Norman and his wife, Mary for their hospitality, their kindness and their affection. I am also very grateful to Dr. Mark Blyth for his interest in our work, his advice and his kindness.

A Antonio Soria y Luismi les doy las gracias por haberme escuchado, por sus constantes ánimos y por haber tenido las puertas siempre abiertas para hablar cuando lo he necesitado. A Merche, Néstor, Domingo, Ulpiano, Sergio y Javi Villa les agradezco su afecto y todos los buenos momentos que hemos compartido en tantas comidas y cafés, que sin duda han hecho mucho más gratos los momentos de trabajo duro. A Wil, Pablo, Cristina, Dani, Celia, Mario, Carolina, Ana, Mariano y al resto de miembros del Departamento de Ingeniería Térmica y de Fluidos, sus ánimos, su apoyo y su interés a lo largo de estos años.

Quisera agradecer a mis padres, Rolando y María Jesús y a mi hermana Lucía, toda la ayuda y el apoyo que me han dado, su compresión, su paciencia y sus ánimos a lo largo de estos años.

Por último, quisiera darle las gracias a Sara por su apoyo incondicional, por su cariño y compresión, por animarme siempre a ser mejor y por estar siempre a mi lado, porque sin ella todo habría sido mucho más difícil.

# Abstract

This dissertation focuses on the modelling of vaporization and combustion of sprays. A general two-continua formulation is given for the numerical computation of spray flows, including the treatment of the droplets as homogenized sources. Group combustion is considered, with the reaction between the fuel coming from the vaporizing droplets and the oxygen of the air modeled in the Burke-Schumann limit of infinitely fast chemical reaction, with nonunity Lewis numbers allowed for the different reactants. Linear combinations of the conservation equations for species and energy are used to formulate the gas-phase problem in terms of coupling functions satisfying chemistry-free conservation equations that contain sources associated with the vaporizing droplets. The resulting set of gas-phase conservations equations are accompanied by a Eulerian description of the liquid phase, with appropriate conservation equations written for the number density, velocity, temperature, and radius of the droplets. The formulation, which can be used in general in direct numerical simulations of spray diffusion flames and may also serve as starting point in modelling strategies of turbulent flows, is employed for the analysis of two different spray problems.

First, the two-continua formulation is used to investigate by numerical and asymptotic methods the group vaporization of a monodisperse fuel-spray jet discharging into a hot coflowing gaseous stream for steady flow. The jet is assumed to be slender and laminar, as occurs when the Reynolds number is moderately large, so that the boundary-layer form of the conservation equations can be employed in the analysis. Two dimensionless parameters are found to control the flow structure, namely, the spray dilution parameter $\alpha_c$, defined as the mass of liquid fuel per unit mass of gas in the spray stream, and the group vaporization parameter $\varepsilon$, defined as the ratio of the characteristic time of spray evolution due to droplet vaporization to the characteristic diffusion time across the jet. It is observed that, for the small values of $\varepsilon$ often encountered in applications, vaporization occurs only in a thin layer separating the spray from the outer droplet-free stream. This regime of sheath vaporization, which is controlled by heat conduction, is amenable to a simplified asymptotic description, independent of $\varepsilon$, in which the location of the vaporization layer is determined numerically as a free boundary in a parabolic problem involving matching of the separate solutions in the external streams, with appropriate jump conditions obtained from analysis of the quasisteady vaporization front. Separate consideration of dilute and dense sprays, corresponding, respectively, to the asymptotic limits $\alpha_c \ll 1$ and $\alpha_c \gg 1$, enables simplified descriptions to be obtained for the different flow variables, including explicit analytic expressions for the spray penetration distance.

Second, the general formulation is employed for the analysis of the combustion of a typical hollow cone spray issuing from a pressure swirl atomizer for injection conditions such that the breakup length from the injector is comparable to the vaporization length. The characteristic Reynolds number is large enough for the resulting flow to be slender, thereby enabling the boundary-layer approximation to be employed. Numerical computations are used to investigate the dependence of the solution on the two parameters mainly controlling the flow, namely, the characteristic dilution parameter, $\alpha_c$, and the ratio of the atomization-to-vaporization lengths, $l_{\mathrm{BU}}$, both assumed to be or oder unity.

*Abstract*

The highly simplified flow configurations investigated here facilitate understanding of the underlying physical phenomena involved in the vaporization and combustion of sprays. Despite the associated simplifications, it is expected that many of the results obtained, such as influences of dilution, apply qualitatively also to realistic configurations. Besides, by replacing the molecular diffusivity by an appropriately selected turbulent diffusivity, quantitative information, including for instance penetration distances, could also be extracted for direct use in evaluating overall combustion properties of spray flames.

# Resumen

Esta tesis aborda el estudio de la vaporización y combustión de esprays. En particular, se presenta una formulación simplificada para el cálculo y el modelado numérico de esprays reactivos. En el tratamiento propuesto se homogeneiza la fase discreta, de forma que las gotas aparecen como fuentes distribuidas. La reacción entre el combustible que se vaporiza y el oxígeno del aire se describe en el límite de Burke-Schumann de reacción infinitamente rápida. Siguiendo la metodología que introdujeron Shvab y Zeldovich para llamas gaseosas, se eliminan los términos de reacción química mediante combinaciones lineales de las ecuaciones de conservación de las especies químicas y de la energía. De este modo, es posible formular el problema para la fase gaseosa en términos de las variables reducidas fracción de mezcla y exceso de entalpía, incluyendo números de Lewis de los reactantes distintos de la unidad. Las ecuaciones de conservación resultantes, libres de términos químicos, contienen sin embargo términos fuentes asociados al calentamiento y vaporización de las gotas. La fase líquida se describe mediante una formulación Euleriana en la que la población de gotas se caracteriza mediante el número de gotas que existe por unidad de volumen, y que incluye ecuaciones de conservación para el radio de la gota, su temperatura y su velocidad.

La formulación resultante es adecuada para la simulación numérica directa de combustión de esprays y puede también servir como punto de partida para el modelado de este tipo de flujos en régimen turbulento. En esta tesis, se hace aplicación de la misma para el tratamiento simplificado de dos configuraciones de interés práctico, lo que ha permitido entender y cuantificar algunos de los fenómenos más relevantes que afectan a la vaporización y combustión de esprays.

En primer lugar, se aborda el estudio de la vaporización en grupo de un espray monodisperso que descarga a una atmósfera caliente, que puede estar en movimiento o en reposo. La descarga del espray ocurre en régimen laminar a números de Reynolds moderadamente altos, de forma que podemos hacer uso de la aproximación de capa límite para describir el flujo resultante. Se considera que en la sección de salida el espray se encuentra en equilibrio saturado. La formulación adimensional del problema incluye como parámetros más relevantes la masa de líquido por unidad de masa de gas en la corriente de alimentación, $\alpha_c$, que caracteriza el grado de dilución del espray, y el parámetro de vaporización en grupo, $\varepsilon$, que controla el proceso de vaporización. Para valores pequeños de $\varepsilon$, típicos en aplicaciones, la vaporización del espray tiene lugar en una capa delgada que separa la región interior, donde el espray sigue en equilibrio saturado, de una región exterior donde no hay gotas. Este límite, controlado por la conducción de calor, admite una descripción simplificada, independiente de $\varepsilon$, en donde la posición del frente de vaporización se obtiene como parte de la solución de un problema parabólico de frontera libre. El acople entre el espray saturado y la corriente exterior libre de gotas se realiza a través de las condiciones de salto que se obtienen del análisis de la capa de vaporización. Se obtienen además soluciones simplificadas del problema para valores extremos de la dilución, $\alpha_c \ll 1$ y $\alpha_c \gg 1$, incluyendo expresiones explícitas para la distancia de penetración del espray.

En segundo lugar, se aplica la formulación general obtenida previamente al estudio de la combustión y vaporización del espray en forma de cono hueco formado por un atomizador con giro. En la configuración

simplificada que se estudia se supone que el flujo es laminar, estacionario y esbelto, y se desprecia el movimiento de giro de las corrientes gaseosas exteriores. Se supone que, tal y como ocurre en el caso de los combustibles líquidos más habituales, la masa de aire que se requiere para quemar la unidad de masa de combustible es muy grande, por lo que la llama se posiciona lejos del espray. Las integraciones numéricas indican que la solución depende del parámetro de dilución $\alpha_c$, que determina la distancia de penetración del chorro y la forma de la llama circundante, y de la distancia de atomización, siendo la dependencia de este último parámetro mucho más débil.

# Contents

CHAPTER
**ONE**

# Introduction

## 1.1 Spray flows: general considerations and relevant applications

A spray is a type of two-phase flow in which the liquid appears in the form of droplets as the dispersed phase with the gas conforming the surrounding continuous phase. They are present in many industrial applications associated with power generation, propulsion, heat exchange and material processing. Coating and painting processes rely on the use of sprays, which are also employed for food processing and for the delivery of medicines, insectides or pesticides. Because of their importance in a wide range of applications, significant research efforts have been devoted in the past to the study of sprays, leading to better understanding of the underlying physical phenomena as well as improved designs of spray devices.

Combustion systems using liquid fuels also employ sprays as a means to introduce the fuel into the combustion chamber with a sufficiently large surface-to-mass ratio to enable complete vaporization to be achieved, as in diesel engines or gas turbines, where the fuel vapor generated by the droplets diffuses, mixes and reacts with the surrounding oxygen. Because of its relevance in many industrial applications, the combustion and vaporization of fuel sprays has been the subject of many previous investigations (see, e.g. , [1–6] for reviews of the early work). Although individual droplet combustion may occur in liquid-fuel burners provided the resulting spray is sufficiently dilute, it was early recognized that in many practical situations fuel sprays evaporate or burn as a group [7–10], with the fuel that originates from the vaporizing droplets burning with the ambient oxygen in a diffusion flame that stands off the droplet cloud. In many applications, the chemical reaction is very fast, and the resulting flame appears as an infinitesimally thin surface separating a region with no fuel from a region with no oxygen. The formulation of the resulting problem of spray flames in the Burke-Schumann limit of infinitely fast chemistry and its application to the analysis of vaporization and combustion problems in relevant configurations are the subjects to be explored in the present dissertation.

## 1.2 Homogenized description of spray flows

Progress in understanding of spray vaporization and combustion relies on advanced diagnostic techniques [11–13] as well as on increased computer power, which enables, for instance, analyses of droplet array combustion to be advanced well beyond the initial analytic efforts [14], an example being the recent

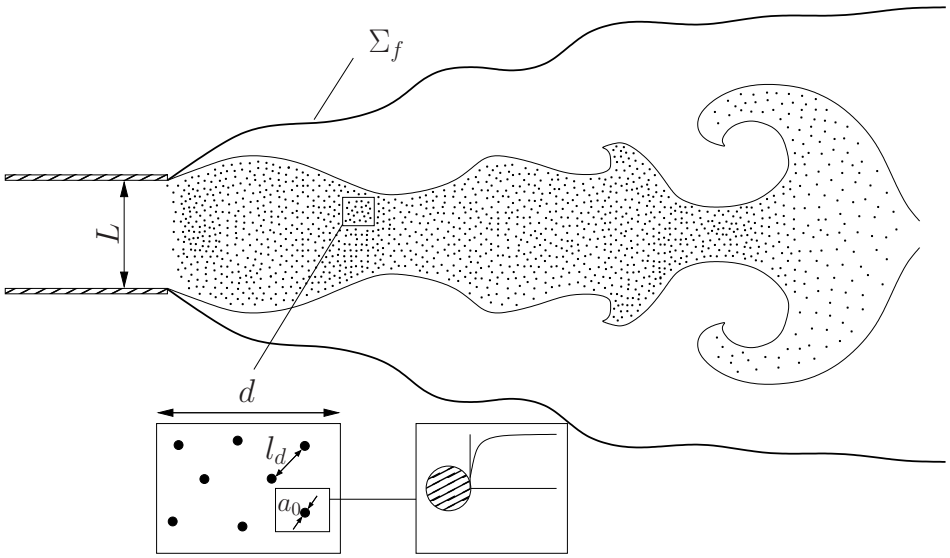


**Figure 1.1:** Schematic illustration of the disparity of length scales in spray combustion.

computation of heptane-droplet group combustion in a staggered configuration [15]. With the present computer power, direct numerical simulations of combution of turbulent sprays at moderate Reynolds numbers are feasible [16, 17], and more complex computations including detailed chemistry and higher Reynolds numbers can be envisioned in the near future. These numerical computations can be facilitated by exploiting the disparity of length scales often encountered in realistic applications, enabling as explained below a two-continua formulation to be employed for the description of the gas and liquid phases.

A prominent parameter characterizing sprays is the local ratio of the mass of liquid to the mass of gas $\alpha_c$, whose value varies across jet sprays, decreasing for increasing distances from the injector due to droplet dispersion. Its representative value can be evaluated from

$$\alpha_c = \frac{4}{3}\pi a_o^3 n_c \rho_l / \rho_c, \tag{1.1}$$

where $a_o$, $\rho_l$, $\rho_c$, and $n_c$ denote the initial droplet radius, the liquid density and the characteristic values of the gas density and of the number of droplets per unit volume, the latter quantity providing a measure of the characteristic inter-droplet distance according to $l_d = n_c^{-1/3}$. Vaporizing sprays with $\alpha_c \sim O(1)$ display a significant coupling between the liquid and gas phases through the exchange of mass, momentum and energy. For instance, in spray combustion applications appreciable liquid heating and vaporization resulting from heat transfer from the gas carrier occurs only downstream from the atomization region, once the droplet distribution becomes sufficiently dilute for $\alpha_c$ to decay to values of order unity. Since for all liquid fuels the mass $S$ of air needed to burn a unit mass of fuel is a moderately large quantity (e.g., $S = 15.3$ for octane and $S = 9.1$ for ethanol), in the main combustion region of burners employing overall fuel-to-air feed ratios not far from stoichiometric conditions, the characteristic value of $\alpha_c$ can be expected to be of order $\alpha_c \sim S^{-1}$. For these relatively small values of

$\alpha_c$ strong coupling between phases also exist, associated with the strong exothermicity of the reaction. Irrespective of this fact, there is considerable interest in sprays with $\alpha_c \sim O(1)$.

The ratio of liquid-to-gas densities $\rho_l/\rho_c$ found in combustion chambers is typically a large quantity, taking up pressure-dependent values in the range

$$10^2 \lesssim \rho_l/\rho_c \lesssim 10^3. \tag{1.2}$$

As a result, according to (1.1), sprays with $\alpha_c \sim O(1)$ correspond to inter-droplet distances $l_d$ much larger than the droplet radius, i.e.,

$$l_d/a_o \sim (\rho_l/\rho_c)^{1/3} \gg 1. \tag{1.3}$$

These scales are to be compared with those of the spray, associated with the characteristic droplet vaporization time

$$t_v \sim \frac{a_o^2}{D_{T_c}} \frac{\rho_l}{\rho_c}, \tag{1.4}$$

of the order of the droplet acceleration time, defined below in (4.1). Here, $D_{T_c}$ denotes the characteristic value of the thermal diffusivity of the gas. In many applications the Reynolds number $u_o^2 t_v/D_{T_c}$ based on the injection velocity $u_o$ is large, and the resulting flow is slender, with a streamwise length $u_o t_v$ much larger than its characteristic transverse length $L$. In laminar sprays, a value $L \sim (D_{T_c} t_v)^{1/2}$ follows from the condition that the conduction time across the spray $L^2/D_{T_c}$ be comparable to the vaporization time, thereby yielding

$$L/a_o \sim (\rho_l/\rho_c)^{1/2} \gg 1. \tag{1.5}$$

In the presence of turbulence, enhanced turbulent transport and droplet dispersion would lead to even larger values of $L$, so that the inequalities

$$L \gg l_d \gg a_o \tag{1.6}$$

can be expected to hold under most conditions of practical interest in laminar and turbulent configurations, as illustrated in figure 1.1, enabling a two-continua formulation to be employed for the description of the gas and liquid phases.

Because of the condition $a_o \ll l_d$ present in (1.6), each droplet vaporizes and moves with no significant direct effects from neighboring droplets. The main effects on the vaporization of the droplets are not due to the direct influence of their neighbours, but are associated instead with the mean gas-phase collective environment created by all the droplets. Each droplet produces in the gas relatively large variations of the composition and temperature that are felt only in the immediate vicinity of the droplet, decaying at distances of the order of $a_o$, so that in most of the gas phase between droplets the variations of the different properties are much smaller. The vaporization rate of and the force acting on each individual droplet are to be computed as those of the isolated droplet surrounded by the mean

local environment.

The description of the slow variations of the different gas-phase variables, including the velocity, temperature, density, and relevant mass fractions, which occur over distances of the order of $L$, can be obtained at any spatial point by space-averaging over a neighborhood of that point of size $d$, with $d$ in the range $L \gg d \gg l_d$. the vaporizing droplets appear as a large number of point sources of mass and momentum and point sinks of heat. Since $d \gg l_d$, each averaging cell includes many droplets, so that the corresponding point sources can be homogenized, as if they were homogeneously distributed, giving source terms that are proportional to the number of droplets per unit volume.

While a Eulerian description emerges naturally for the gas phase, the liquid phase is in principle more easily described with a Lagrangian approach in which each droplet is traced individually, with the ambient properties changing as the droplet moves across the flow field. An alternative formulation is, however, possible, in which the liquid phase is also treated as a continuum, with the droplet population described in terms of the number of droplets per unit volume through a conservation equation. This Eulerian-Eulerian approach, used in the formulation given below, is a great simplification over fine-grained descriptions that specifically consider phenomena occurring at points separated by distances of the order of $l_d$. Often-employed eddy-diffusivity approximations in fact typically are equivalent to averaging over fine-grained events separated by distances even larger than $l_d$. It should be however noticed that, although this Eulerian-Eulerian approach is often simpler and greatly facilitates analytical work, it is only well suited for the treatment of monodisperse laminar sprays, whereas in the presence of crossing droplet trajectories, as occurs in turbulent flow or with recirculating flow regions when the particle size is not small enough, this continuum description fails, and tracking of individual droplets becomes necessary.

## 1.3 Regimes of spray vaporization and combustion

Different regimes of spray combustion and vaporization appear for different values of the controlling parameters. Besides the dilution parameter $\alpha_c$ defined above in (1.1), the other prominent parameter characterizing sprays is the so-called Stokes number St, defined as the ratio of the characteristic droplet acceleration time to the characteristic flow time. This parameter measures the relative importance of the droplet inertial effects. For small values of St, the droplets behave as flow tracers, their trajectories following closely those of the gas particles, whereas in the opposite limit $\mathrm{St} \gg 1$ the droplets move in nearly ballistic trajectories, with little influence from aerodynamic forces exerted by the relative gas flow. The resulting spray characteristics depend therefore critically on the value of St. In the paradigmatic example of the counterflow configuration, often used in experiments of spray diffusion flames [18], when potential-flow boundary conditions apply the type of droplet motion encountered is known to depend on whether or not the Stokes number exceeds a critical limiting value $\mathrm{St} = 1/4$, found theoretically from calculations of trajectories of individual droplets injected in the gaseous irrotational stream on one side of the counterflow [19]. In this case, for $\mathrm{St} < 1/4$ the droplets exponentially approach the stagnation plane but never cross it, yielding an increasing droplet population in the central region, but droplets with $\mathrm{St} > 1/4$ have sufficient inertia to cross the stagnation plane and undergo an oscillatory motion of decreasing amplitude, including several penetrating excursions into the opposed counterflow

to distances comparable with the initial injection distance.

In the past, clasiffications of solutions for spray combustion and vaporization have been based on a single parameter, constructed as a combination of St and $\alpha_c$, with the various proposals for the controlling parameter being essentially equivalent [20]. For instance, the parameter $\varepsilon$ used by Correa and Sichel [8, 9] to characterize group combustion and vaporization of droplet clouds equals $\mathrm{St}/\alpha_c$ multiplied by three halfs of the Prandtl number, whereas the Thiele modulus employed by Labowsky and Rosner [10] can be written as $[2\alpha_c/(3\mathrm{PrSt}))]^{1/2}$ and the group-combustion number introduced by Chiu and coworkers [7, 21, 22] equals $2\alpha_c/(3\mathrm{PrSt})$ divided by the fuel Lewis number.

The combustion regimes appearing for different values of $\varepsilon$ [7–10] include cases where the diffusion flame lies outside the droplet cloud; there, the fuel that originates from the vaporizing droplets burns with the ambient oxygen, with droplet vaporization occurring either all throughout the cloud (external group combustion) or in a thin outer layer on the outer edge of the droplet cloud (external sheath combustion). It was also seen that individual droplet combustion may also occur, provided the spray is sufficiently dilute, with oxygen diffusing across the resulting cloud of burning droplets, each one of them being surrounded by a closed flame if their radius is large enough to sustain the flame. Besides these combustion modes, for a narrow range of conditions, there exists a transition regime termed internal group combustion [22], in which an internal diffusion flame separates a group of vaporizing droplets from a group of individually burning droplets, a configuration that has been observed in laboratory experiments (see, e.g., [11, 13]).

As mentioned in [22], experimental evidence suggests that group combustion is the predominant form of spray combustion in typical industrial burners. This limit is to be addressed below in chapter 4 in connection with the combustion of hollow cone sprays, as those typically produced in pressure-swirl atomizers. The limit of sheath vaporization arising for $\varepsilon \ll 1$, previously investigated in [8, 9] for the spherical droplet cloud, is to be considered below in chapter 3 in addressing sheath vaporization of round jet sprays.

## 1.4 Diffusion-controlled combustion of sprays

Although individual droplet combustion may occur in liquid-fuel burners provided that the resulting spray is sufficiently dilute, in most cases the droplets burn as a group, with the fuel that originates from the vaporizing droplets burning with the ambient oxygen in a diffusion flame that stands off the droplet cloud. In many applications, the gas-phase chemical reaction is fast, in that the characteristic time for fuel oxidation is much shorter than both the characteristic fluid-mechanical time and droplet-vaporization times. Under those conditions, the flame appears as an infinitesimally thin sheet, $\Sigma_f$, separating an external region $\Omega_{\mathrm{O}}$ where no gaseous fuel is present from an internal oxygen-free region $\Omega_{\mathrm{F}}$. In the resulting Eulerian description of the gas phase with infinitely fast chemistry, the chemical-reaction terms appear as Dirac delta distributions along reaction surfaces.

Burke and Schumann [23] addressed in particular the problem of infinitely fast reaction for gaseous diffusion flames when the chemistry can be modelled with a global one-step irreversible reaction, with the chemical sources in the conservation equations for the energy and the reacting species expressed in terms of a reaction rate proportional to the product of the fuel and oxygen mass fractions. They showed

that, in the limit of infinitely fast chemistry, the reaction occurs in an infinitesimally thin layer acting as a concentrated sink for the reactants, preventing their coexistence outside this reaction layer. This feature of the solution was employed in determining the shape of the flame surface for the particular case of combustion of parallel laminar streams of fuel and air.

This type of concept was extended to general problems of nonpremixed combustion by Shvab and Zeldovich [24, 25], who demonstrated that solutions can be facilitated by eliminating the chemical terms through appropriate linear combinations of the conservation equations of chemical species and energy. The resulting conservation equations, free from the chemical source terms, are written in terms of coupling functions, associated with the different linear combinations employed. The additional condition that the fuel and oxidizer cannot coexist must be employed in computing the temperature and species mass fractions from the coupling functions, thereby closing the formulation.

Although the original development of Shvab and Zeldovich was restricted to Lewis numbers of the reactants equal to unity, giving identical transport operators for all conservation equations, extensions to non-unity Lewis numbers, involving conservation equations with convective and diffusive transport of different coupling functions, have been identified [26–28]. Generalizations to account for multi-step chemistry, including an infinitely fast step describing the reaction between the fuel and oxygen to produce a chemical intermediate, have been proposed for hydrogen [29, 30] and hydrocarbon nonpremixed flames [31, 32], with the intermediates being hydrogen atoms and carbon monoxide, respectively. More recently, a coupling-function formulation has been derived for the description of group combustion in pulverized coal furnaces [33, 34]. The applicability of coupling functions in the context of spray and droplet combustion has been recently explored further [35], with some success obtained in turbulent-combustion modelling of jet-spray flames [36].

## 1.5 Spray atomization

In liquid-fuel burners, the fuel is typically introduced into the combustion chamber as a high-velocity liquid jet [37]. The atomization process is often highly complex, with the effects of injector boundary layers, droplet breakup and collision, turbulence and recirculation playing key roles in determing the characteristics of the resulting spray [37]. As previously mentioned, since the liquid density is typically a factor up to $10^3$ larger than the gas density, appreciable liquid heating and vaporization resulting from heat transfer from the gas carrier occurs only far from the injection region, once the spray stream becomes sufficiently dilute for the liquid phase to occupy a small volumetric fraction, of the order of $10^{-3}$. The processes of liquid-jet atomization leading to spray formation and those of spray vaporization and combustion therefore occur in separate spatial regions, sketched in figure 1.2, and can be consequently studied independently, with the latter being the subject of the present investigation. Although spray atomization is not to be addressed in the remaining of this dissertation, it is worth presenting in this introductory chapter a short account of the most prominent aspects of the process, the reason being that the main spray properties affecting vaporization and combustion, such as droplet radius distribution and initial droplet velocity, depend fundamentally on the way the spray is generated [38].

Sprays are effectively produced when there exists a significant velocity difference between the liquid

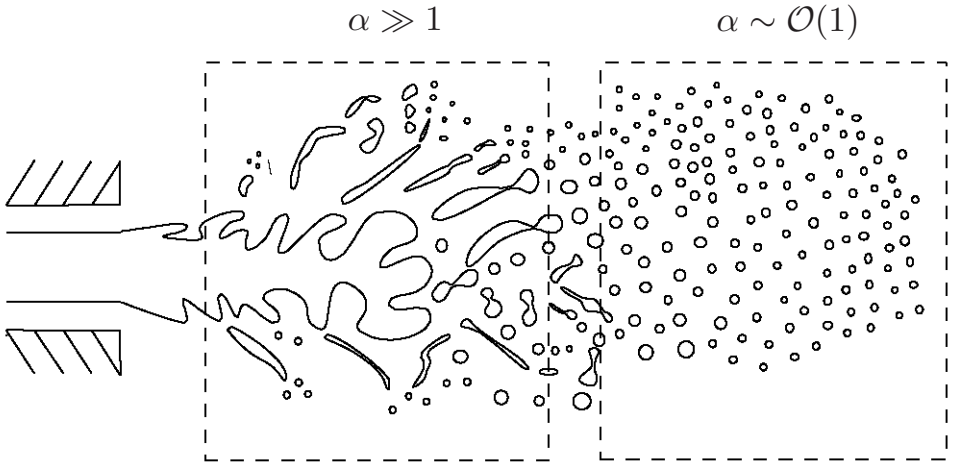


**Figure 1.2:** Air assisted atomization a liquid fuel-jet. In the atomization region no significant liquid heating occurs.

to be atomized and the surrounding gas. This can be accomplished by exposing the discharging liquid stream to a relative slow-velocity moving gas, as in pressure and rotary atomizers. Alternatively, a slow-velocity liquid can be exposed to a high-velocity air stream, a method known as air-assist, twin-fluid or airblast atomization. The geometry-dependent hydrodynamics of the liquid within the atomizer influences the structure of the emerging stream. The disintegration of this stream into ligaments and then droplets determines the characteristics of the resulting spray, including mean droplet size, droplet-size distribution and number density.

A wide variety of atomizers is available for different applications, providing different spray characteristics. A detailed description of the different nozzles, their applications, advantages, and drawbacks can be found in [38]. Among the many types of existing atomizers, airblast atomizers and pressure swirl atomizers are preferred in combustion systems because of their simplicity and their ability to produce good atomization. In many combustion applications the resulting spray is obtained by combining different atomization methods to promote flame stabilization and a good performance of the burner.

Depending on the application, a flat or a conical spray pattern may be required to achieve the appropiate dispersion of droplets. In the case of the conical sprays generated by pressure-swirl atomizers, whose combustion is to be investigated in chapter 4, expand the emerging sheet against the contracting effect of surface tension forces. The strong swirling motion created by the pumping pressure in the injection chamber decays as the liquid sheet opens up away from the injector rim, creating a conical sheet of constant streamwise velocity. The resulting thickness decreases due to flow divergence away from the injector rim. Aerodynamic forces increase the growth of the initial hydrodynamic instabilities. Due to these instabilities, as the sheet evolves and reduces its thickness downstream, perforations that are formed in the sheet lead to the formation of threads and ligaments. The ligaments obtained may vary in size, producing through breakup droplets of different radii, with droplets exceeding a critical size further disintegrating downstream into smaller droplets.

In an effort to sort out the complex interplay of surface tension and aerodynamic instabilities,

three different disintegration modes have been proposed for conical sheets produced in pressure-swirl atomizers, namely, rim, wave and perforated-sheet disintegration [38]. In the rim mode, which becomes dominant when the surface tension and viscosity of the liquid are high, the free edge of the sheet is contracted due to the effect of surface tension into thick rims that eventually break up. It tends to produce large droplets with numerous small satellites. In perforated-sheet disintegration holes appearing in the sheet grow rapidly until the rims of adjacent holes coalesce, producing ligaments that break into drops. In this case, the threads that eventully break into droplets tend to be quite uniform in size, providing a more uniform droplet-size distribution. Conversely, the wavy-sheet disintegration mode is highly irregular and results in higher variability of mean-droplet sizes. Typically, the disintegration of a conical sheet is a combination of all three modes, with the final atomization process by which ligaments and threads are broken-up into droplets being always controlled by the Rayleigh mechanism.

All these intricacies will not be further considered here. For the round-jet and hollow-cone spray problems investigated in chapters 3 and 4, the initial size and velocity of the droplets will be assumed to be known. Although the formulation of the different problems can be generalized to account for nonuniform distributions, to focus more directly on the vaporization and combustion processes, a monodisperse spray of constant velocity will be considered for simplicity in all sample computations.

## 1.6 Outline of the dissertation

The present disseration is outlined as follows. Chapter 2 presents the conservation equations for a reactive spray in the two-continua approximation. The formulation includes appropiate expressions for the source terms appearing in the conservation equations, associated with the heating and vaporization of the droplets and also with the force acting on them. The Burke-Schumann limit of infinitely fast combustion is considered next. It is shown that elimination of the singular reaction terms through linear combinations of the conservation equations leads to a set of chemistry-free coupling functions, which replace the temperature and species mass fractions in the integration of the problem. Unlike those found in gaseous combustion, these coupling functions contain source terms, associated with the droplet vaporization and heating. To describe correctly the diffusive transport of heavy fuels, nonunity Lewis numbers are in general considered in the derivation. The resulting Burke-Schumann formulation can be used in direct numerical simulations of spray diffusion flames. It can also serve as a starting point in modeling strategies addressed to two-phase turbulent flows.

In chapter 3 the steady group vaporization of a slender monodisperse fuel-spray jet is studied. Two parameters are found to control the vaporization process, namely, the dilution parameter $\alpha_c$ and the reciprocal of the group combustion number, $\varepsilon = 3\mathrm{PrSt}/(2\alpha_c)$, with Pr representing the Prandtl number for the gas mixture. For the small values of $\varepsilon$ often encountered in applications, the solution includes a thin vaporization front separating an inner region where the spray remains unperturbed from a droplet-free outer region. Correspondingly, in the asymptotic limit $\varepsilon \to 0$ associated with sheath vaporization, the vaporization layer appears as a surface whose location is to be determined as part of a free-boundary parabolic problem, leaving $\alpha_c$ as the only relevant parameter in the solution. Besides numerical integrations, asymptotic methods are used to analyze the resulting solution, including explicit expressions for the spray penetration distance for extreme values of the dilution parameter $\alpha_c$.

In chapter 4, the general coupling-function formulation derived in chapter 2 is employed to study the diffusion-controlled combustion of a simplified hollow-cone spray flow. A steady laminar slender solution is assumed, thereby enabling the use of the boundary-layer approximation for the description of the resulting flow. In the absence of a relevant fluid mechanical time, the dilution parameter $\alpha_c$ is seen to emerge as the main parameter characterizing the spray, with the ratio of the breakup length to the spray vaporization length entering as an additional controlling parameter. Consideration of the boundary layers developing over the liquid sheet upstream from the atomization location is seen to provide the initial conditions for numerical integration. The computations serve to ascertain the effect of the different parameters on the flame temperature and shape, spray velocity and penetration distance, and reactant distribution.

The main body of the dissertation ends in chapter 5 with a short presentation of conclusions and future prospects. An appendix describing in detail the numerical schemes used in integrating the different boundary-layer problems is included for completeness.

# References

[1] K. Annamalai, W. Ryan, Interactive processes in gasification and combustion. Part I: Liquid drop arrays and clouds, Prog. Energy Combust. Sci. 18 (1992) 221–295.

[2] C. Crowe, M. Sommerfeld, Y. Tsuji, Multiphase flows with droplets and particles, CRC Press, 1998.

[3] G. M. Faeth, Evaporation and combustion of sprays, Prog. Energy Combust. Sci. 9 (1983) 1–76.

[4] W. Sirignano, Fuel droplet vaporization and spray combustion theory, Prog. Energy Combust. Sci. 9 (1983) 291–322.

[5] N. Peters, B. Rogg, Reduced kinetic mechanisms for applications in combustion systems, Lecture notes in Physics 15, Springer-Verlag, 1993.

[6] F. Williams, Combustion Theory, Second ed., Benjaming Cummings, Menlo Park, CA., 1985.

[7] H. H. Chiu, T. Liu, Group combustion of liquid droplets, Combust. Sci. Tech. 17 (1977) 127–142.

[8] S. M. Correa, M. Sichel, The boundary layer structure of a vaporizing fuel cloud, Combust. Sci. Tech. 28 (1982) 121–130.

[9] S. M. Correa, M. Sichel, The group combustion of a spherical cloud of monodisperse fuel droplets, Proc. Combust. Inst. 19 (1982) 981–991.

[10] M. Labowsky, D. E. Rosner, Group combustion of droplets in fuel clouds, i. quasi-steady predictions, in: J. T. Zung (Ed.), Evaporation-Combustion of Fuels, Americal Chemical Society, 1978, pp. 63–79.

[11] G. Chen, A. Gomez, Dilute laminar spray diffusion flames near the transition regime from group combustion to individual droplet burning, Combust. Flame 110 (1997) 392–404.

[12] A. N. Karpetis, A. Gomez, An experimental study of well-defined turbulent non-premixed flames, Combust. Flame 121 (2000) 1–23.

[13] S. Russo, A. Gomez, Physical chracterization of laminar spray flames in the pressure range 0.1-0.9 MPa, Combust. Flame 145 (2006) 339–356.

[14] M. Labowsky, Calculation of the burning rates of interacting fuel droplets, Combust. Sci. Tech. 22 (1980) 217–226.

[15] D. Lee, H. Y. Kim, S. S. Yoon, C. P. Cho, Group combustion of staggeringly arranged heptane droplets at various Reynolds numbers, oxygen mole-fractions and separation distances, Fuel 89 (2010) 1447–1460.

[16] K. Luo, H. Pitsch, M. G. Pai, O. Desjardin, Direct numerical simulations and analysis of three-dimensional n-heptane spray flames in a model swirl combustor, Proc. Comb. Inst. 89 (2011) 1447–1460.

[17] J. Reveillon, L. Vervisch, Analysis of weakly turbulent dilute-spray flames and spray combustion regimes, J. Fluid Mech. 537 (2005) 317–347.

[18] M. Massot, M. Kumar, M. Smooke, A. Gomez, Spray counterflow diffusion flames of heptane: experiments and computations with detailed kinetics and transport, Proc. Combust. Inst. 27 (1998) 1975–1983.

[19] S. Li, Spray stagnation flames, Prog. Energ. and Combust. Sci. 23 (1997) 303–347.

[20] M. Sichel, S. Palaniswamy, Sheath combustion of sprays, Proc. Combust. Inst. 20 (1984) 1789–1798.

[21] H. H. Chiu, R. Ahluwalia, B. Koh, E. J. Croke, Spray group combustion, AIAA 16th Aerospece sciences meeting.

[22] H. H. Chiu, H. Kim, E. J. Croke, Internal group combustion of liquid droplets, Proc. Combust. Inst. 19 (1982) 971–980.

[23] S. Burke, T. Schumann, Diffusion flames, Indust. Eng. Chem. 20 (1928) 998–1009.

[24] V. A. Shvab, Relation between the temperature and velocity fields of the flame of a gas burner, *Issledovanie protessov gorenia naturalnogo topliva*, Gos. Energ. izd.

[25] Y. B. Zeldovich, Teorii gorenia neperemeshannykh, *English translation*: On the theory of combustion of initially unmixes gases, NACA, Tech. Memo. 1296, 1951, Zhurnal Tekhnicheskoi Fiziki 19 (1949) 1199–1210.

[26] A. Liñán, The structure of diffusion flames, in: M. Onofri, A. Tesei (Eds.), Fluid dynamical aspects of combustion theory, Longman Scientific Technical Essex, 1991, pp. 11–19.

[27] A. Liñán, F. Williams, Fundamental aspects of combustion, Oxford University Press, New York, 1993.

[28] A. Liñán, P. Orlandi, R. Verizzco, F. J. Higuera, Effects of non-unity Lewis numbers in diffusion flames, in: Proc. Summer Program, Center for Turbulence Research, NASA-Ames, Stanford University, Standford University, 1994, pp. 5–18.

[29] J. Janicka, W. Kollmann, Two variables formalism for the treatment of chemical reactions in turbulent $H_2$-air diffusion flames, Proc. Combust. Inst. 17 (1978) 421–430.

[30] A. L. Sánchez, A. Liñán, F. Wiliams, A generalized Burke-Schumann formulation for hydrogen-oxygen diffusion flames mantaining partial equilibrium of the shuffle reactions, Combust. Sci. Tech. 123 (1997) 317–345.

[31] M. Bollig, A. Liñán, A. L. Sánchez, , F. Wiliams, A simplified approach to the numerical description of methane-air flames, Proc. Combust. Isnt. 27 (1998) 595–603.

[32] A. Lépinette, A. . Liñán, B. Lázaro, A. L. Sánchez, Reduced kinetics and coupling functions for calculating CO and NO emissions in gas-turbine combustion, Combust. Sci. Tech. 177 (2005) 907–931.

[33] A. Bermúdez, J. L. Ferrín, A. Liñán, The modelling of the generation of volatiles, $H_2$ and CO, and their simultaneous diffusion controlled oxidation, in pulverized coal furnaces, Combus. Theor. Modell. 11 (2007) 949–976.

[34] A. Bermúdez, J. Ferrín, A. Liñán, L. Saavedra, Numerical simulation of group combustion of pulverized coal, Comb. Flame 158 (2011) 1852–1865.

[35] R. Bilger, A mixture fraction framework for the theory and modeling of droplets and sprays, Comb. Flame 158 (2011) 191–202.

[36] S. De, R. Lakshmisha, K. N. amd Bilger, Modeling nonreacting and reacting turbulent spray jets using fully stochastic separated flow approach, Comb. Flame 158 (2011) 1992–2008.

[37] J. C. Lasheras, E. J. Hopfinger, Liquid jet instability and atomization in a coaxial gas stream, Annu. Rev. Fluid Mech. 32 (2000) 275–308.

[38] A. Lefebvre, Atomization and sprays, Hemisphere Publishing, 1989.

CHAPTER
**TWO**

# Coupling-function formulation for monodisperse spray diffusion flames with infinitely fast chemistry

## 2.1 Introduction

As pointed out in chapter 1, because of their key role in numerous technological applications, combustion and vaporization of fuel sprays have been the subject of many modelling efforts. Direct numerical integration is hindered by many complicating factors [1–3], including disparate length and time scales associated with the fast chemistry and with the multiphase nature of the flow, which is highly turbulent in most applications. Clearly, modelling strategies aimed at removing the numerical stiffness associated with these disparities can be instrumental in enabling more efficient computations to be performed.

In many applications, the gas-phase chemical reaction is fast, in that the characteristic time for fuel oxidation is much shorter than both the characteristic fluid-mechanical and droplet-vaporization times. Under those conditions, the flame appears as an infinitesimally thin sheet, $\Sigma_f$, separating an external region $\Omega_{\mathrm{O}}$ where no gaseous fuel is present from an internal oxygen-free region $\Omega_{\mathrm{F}}$, given the flow-field structure sketched in figure 2.1. The formulation of this problem of fuel-spray combustion in the Burke-Schumann limit of infinitely fast chemistry is the objective of the present chapter, by extending to spray flows previous ideas developed for gaseous nonpremixed flames.

We shall see that, unlike the case of gaseous fuels, the coupling functions obtained by eliminating the chemical sources are not conserved scalars, in that their corresponding conservation equations include source terms associated with the vaporizing droplets. Following previous extensions of the Burke-Schumann formulation [4], the coupling functions are derived here for general non-unity Lewis numbers of the different chemical species, a feature of the proposed formulation that enables transport by diffusion to be correctly described for the fuels found in spray applications, whose Lewis numbers significantly differ from unity. Although restricted for simplicity to monodisperse sprays in the illustrative application presented here, the formulation can be readily extended to include droplet families of different sizes. The development accounts for the presence of droplets vaporizing in $\Omega_{\mathrm{O}}$, a phenomenon that may occur when large droplets with sufficient inertia cross the flame to reach the outer air stream. The resulting fuel vapor appears in very small concentrations, reacting with the existing oxygen in a distributed manner, a higher-order finite-rate effect that can be incorporated in the Burke-Schumann formulation, as shown below.

Although the presentation below involves a Euler-Euler flowfield description, the formulation of the gas phase in terms of coupling functions is independent of the type of description used for the liquid

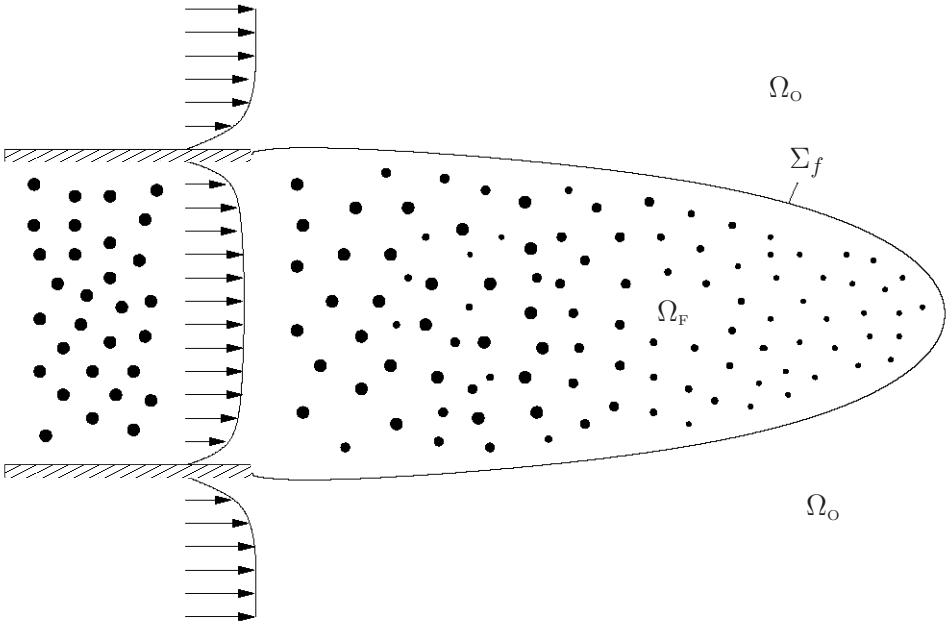


**Figure 2.1:** Diffusion flame in a round jet spray.

phase. Thus, chemistry-free modelling strategies using coupling functions for the Eulerian description of the gas phase together with a Lagrangian treatment of the dispersed phase can readily be developed following the derivation given below, an example being the formulation proposed in [5, 6] for pulverized coal combustion.

## 2.2 General formulation

The homogenized gas-phase conservation equations include the continuity and momentum equations

$$\frac{\partial \rho}{\partial t} + \nabla \left( \rho \mathbf{v} \right) = n\dot{m}, \tag{2.1}$$

$$\frac{\partial}{\partial t} \left( \rho \mathbf{v} \right) + \nabla \cdot \left( \rho \mathbf{v} \mathbf{v} \right) = \nabla \cdot \bar{\bar{\tau}} - \nabla p + n\dot{m}\mathbf{v}_d - n\mathbf{f}, \tag{2.2}$$

together with the conservation equations for chemical species and energy, which reduce simply to

$$\frac{\partial}{\partial t}\left(\rho Y_{\mathrm{F}}\right)+\nabla\cdot\left(\rho\mathbf{v}Y_{\mathrm{F}}\right)-\nabla\cdot\left(\frac{\rho D_T}{\mathrm{L}_{\mathrm{F}}}\nabla Y_{\mathrm{F}}\right)=-\omega_{\mathrm{F}}+n\dot{m}, \tag{2.3}$$

$$\frac{\partial}{\partial t}\left(\rho\hat{Y}_{\mathrm{O}}\right)+\nabla\cdot\left(\rho\mathbf{v}\hat{Y}_{\mathrm{O}}\right)-\nabla\cdot\left(\frac{\rho D_T}{\mathrm{L}_{\mathrm{O}}}\nabla\hat{Y}_{\mathrm{O}}\right)=-S\omega_{\mathrm{F}}, \tag{2.4}$$

$$\frac{\partial}{\partial t}\left(\rho Y_{\mathrm{CO_2}}\right)+\nabla\cdot\left(\rho\mathbf{v}Y_{\mathrm{CO_2}}\right)-\nabla\cdot\left(\frac{\rho D_T}{\mathrm{L}_{\mathrm{CO_2}}}\nabla Y_{\mathrm{CO_2}}\right)=s_{\mathrm{CO_2}}\omega_{\mathrm{F}} \tag{2.5}$$

$$\frac{\partial}{\partial t}\left(\rho Y_{\mathrm{H_2O}}\right)+\nabla\cdot\left(\rho\mathbf{v}Y_{\mathrm{H_2O}}\right)-\nabla\cdot\left(\frac{\rho D_T}{\mathrm{L}_{\mathrm{H_2O}}}\nabla Y_{\mathrm{H_2O}}\right)=s_{\mathrm{H_2O}}\omega_{\mathrm{F}} \tag{2.6}$$

and

$$\frac{\partial}{\partial t}\left(\rho c_pT\right)+\nabla\cdot\left(\rho\mathbf{v}c_pT\right)-\nabla\cdot\left(\kappa\nabla T\right)=-q\omega_{\mathrm{F}}-n\left[\dot{m}\left(L_v-c_pT_d\right)+\dot{q}_d\right]+\frac{\partial p}{\partial t}, \tag{2.7}$$

when the overall chemical reaction between the oxygen of the air and the fuel vapor is assumed to occur according to the global irreversible step

$$\mathrm{F}+s\mathrm{O_2}\rightarrow s_{\mathrm{CO_2}}\mathrm{CO_2}+s_{\mathrm{H_2O}}\mathrm{H_2O}+q, \tag{2.8}$$

where $s$, $s_{\mathrm{CO_2}}$, $s_{\mathrm{H_2O}}$, and $q$ are, respectively, the mass of oxygen consumed and of carbon dioxide and water vapor produced, and the amount of heat released per unit mass of fuel burnt, with $s_{\mathrm{CO_2}}+s_{\mathrm{H_2O}}=1+s$. Here $T$, $\rho$, $p$, $\kappa$, $D_T=\kappa/(\rho c_p)$, $c_p$, and $\mathbf{v}$ are the temperature, density, pressure, thermal conductivity, thermal diffusivity, specific heat at constant pressure and velocity of the gas mixture, and $\bar{\bar{\tau}}$ is the viscous stress tensor. The mass fraction and Lewis number of species $i$ are denoted by $Y_i$ and $\mathrm{L}_i$, with $\hat{Y}_{\mathrm{O}}=Y_{\mathrm{O_2}}/Y_{\mathrm{O_{2A}}}$ representing the oxygen mass fraction normalized with its value in the air stream $Y_{\mathrm{O_{2A}}}\simeq 0.232$. A low-Mach-number approximation has been used in writing the energy equation, where spatial pressure variations have been neglected along with viscous dissipation, while the time variation of the pressure has been retained, as it can be of importance for combustion in reciprocating engines. The above set of equations must be supplemented with the equation of state

$$\frac{p}{\rho}=R^oT\sum_i\frac{Y_i}{M_i}, \tag{2.9}$$

where $R^o$ is the universal gas constant and $M_i$ is the molecular mass of species $i$.

The chemical sources are written in terms of the mass of fuel consumed per unit volume per unit time $\omega_{\mathrm{F}}$, with $S=s/Y_{\mathrm{O_{2A}}}$, $s_{\mathrm{CO_2}}$, and $s_{\mathrm{H_2O}}$ entering as corresponding factors in the oxygen and product conservation equations. Additional source terms appear above associated with the presence of the droplets in the flow. Thus, the mass and fuel conservation equations have been modified to take into account the mass of fuel vapor produced per unit time and unit volume due to droplet vaporization, $n\dot{m}$, where $n$ is the number of droplets per unit volume and $\dot{m}$ is the mass rate of vaporization of an individual droplet. Momentum exchange between the liquid and gas phases is also accounted for in writing (2.2), where $\mathbf{v}_d$ is the average droplet velocity and $\mathbf{f}$ is the force of the gas on the individual

droplet. Heating of the initially cold droplets and their subsequent vaporization necessitate heat transfer from the gas phase, which is taken into account when writing the energy equation, where $\dot{q}_d$ is the heating rate of the individual droplet and $L_v$ is the specific latent heat of vaporization, $T_d$ representing the temperature on the droplet surface. Note that, in writing the droplet source terms, a monodisperse spray is assumed, so that the droplet population is described in terms of a single variable $n$, the number of droplets per unit volume. The formulation can be extended to polydispersed sprays by quantifying separately the number of droplets in each droplet class, and replacing the source terms above by appropriate summations over all droplet classes.

The number of droplets $n$ is a conserved quantity satisfying

$$\frac{\partial n}{\partial t} + \nabla \cdot (n\mathbf{v}_d) = 0. \tag{2.10}$$

On the other hand, the evolution of the droplet temperature $T_d$, droplet radius $a$ and droplet velocity $\mathbf{v}_d$ is described following the droplet trajectory by

$$\frac{4}{3}\pi\rho_l a^3 c_l \left(\frac{\partial T_d}{\partial t} + \mathbf{v}_d \cdot \nabla T_d\right) = \dot{q}_d, \tag{2.11}$$

$$\frac{\partial}{\partial t}\left(\frac{4}{3}\pi\rho_l a^3\right) + \mathbf{v}_d \cdot \nabla\left(\frac{4}{3}\pi\rho_l a^3\right) = -\dot{m}, \tag{2.12}$$

$$\frac{4}{3}\pi\rho_l a^3 \left(\frac{\partial \mathbf{v}_d}{\partial t} + \mathbf{v}_d \cdot \nabla \mathbf{v}_d\right) = \mathbf{f}, \tag{2.13}$$

where $\rho_l$ and $c_l$ are the liquid density and its specific heat. In writing (2.11) it is assumed that the temperature inside the droplets $T_d$ is uniform, a valid assumption when the heating and vaporization time for the single droplet is much larger than the inner droplet conduction time (assisted by internal convection). Note that, from the above equations, it is straightforward to write conservation equations for the entire fluid. For instance, combining (2.2), (2.10) and (2.13) yields the overall momentum equation

$$\frac{\partial}{\partial t}\left(\rho\mathbf{v} + n\frac{4}{3}\pi a^3\rho_l\mathbf{v}_d\right) + \nabla\cdot\left(\rho\mathbf{v}\mathbf{v} + n\frac{4}{3}\pi a^3\rho_l\mathbf{v}_d\mathbf{v}_d\right) = -\nabla p + \nabla\cdot\bar{\bar{\tau}}. \tag{2.14}$$

Equations (2.1)–(2.7) and (2.10)–(2.13) must be integrated with appropriate initial and boundary conditions to determine the spray evolution. To close the problem, expressions must be provided for $\mathbf{f}$, $\dot{q}_d$ and $\dot{m}$, whose determination requires in principle consideration of the near-field solution for the velocity and temperature around the droplet. Simple solutions apply in limits of practical interest when appropriate symplifying assumptions are introduced. For instance, when the droplets are small enough for the corresponding droplet Reynolds number $\mathrm{Re_d} = \rho a|\mathbf{v}-\mathbf{v}_d|/\mu$, associated with the velocity difference $|\mathbf{v}-\mathbf{v}_d|$ between the gas and the droplet, to be smaller than unity, the drag acting on the droplet can be calculated using the familiar Stokes formula

$$\mathbf{f} = 6\pi\mu a(\mathbf{v}-\mathbf{v}_d), \tag{2.15}$$

linearly proportional to the gas viscosity $\mu$, droplet radius $a$, and velocity difference $\mathbf{v} - \mathbf{v}_d$. Drag corrections associated with the Stefan flow due to gasification, considered in [7], and with the variation of the viscosity with the temperature in the vicinity of the droplet, which can be anticipated to be moderately small, could be in principle incorporated in (2.15).

The spherico-symmetrical temperature field can be used to write expressions for the droplet heating flux and vaporization rate. As explained for instance in [8], the description of these two quantities is further simplified for fuels such that $L_v \gg R_{\text{F}} T_B$, with $R_{\text{F}} = R^0/M_{\text{F}}$ and $T_B$ representing the fuel gas constant and boiling temperature, respectively. Under those conditions, it is seen that the mass fraction of vapor at the droplet surface is exponentially small during an initial heat-up period corresponding to $T_d < T_B$, during which $\dot{m} = 0$ and all of the thermal power transferred from the gas is dedicated to increasing the temperature of the yet non-vaporizing droplet, with a rate that simplifies to

$$\dot{q}_d = 4\pi\kappa a(T - T_d) \tag{2.16}$$

when variations of the thermal conductivity $\kappa$ in the droplet vicinity are neglected. This heat-up period ends when the liquid temperature reaches values close to the boiling temperature, i.e., $(T_d - T_B)/T_B \sim R_{\text{F}} T_B/L_v \ll 1$, when vaporization starts with values of the vapor mass fraction of order unity at the droplet surface. In this vaporizing period the droplet surface temperature remains equal to the boiling temperature, $T_d = T_B$, so that $\dot{q}_d = 0$, while the vaporization rate is given by

$$\dot{m} = 4\pi a(\kappa/c_p)\lambda, \tag{2.17}$$

where $\lambda$ can be easily computed for small values of $Re_d$ with constant heat conductivity to give the familiar Spalding expression [9]

$$\lambda = \ln\left[1 + \frac{c_p(T - T_B)}{L_v}\right]. \tag{2.18}$$

As previously mentioned, the above formulation is written for droplets with heating and vaporization times much smaller than the inner droplet conduction time, so that the temperature inside the droplet $T_d$ remains uniform, increasing during the heating period from the initial value $T_o$ to the boiling temperature $T_B$, when vaporization begins. In the opposite limit of small fuel conductivity, the temperature inside the droplet remains equal to its initial value $T_o$, with heat conduction affecting only a thin layer of liquid near the droplet surface, across which the temperature increases from $T_o$ to reach the boiling value $T_B$ at the surface. In that case, the time required to heat up the surface layer is very short, so that vaporization is seen to occur inmediately after the droplet enters the hot gas environment. Part of the heat coming from the gas towards the droplet is then used to heat up the liquid, which must be accounted for in this alternative formulation by replacing $\dot{q}_d$ with $c_l(T_B - T_o)\dot{m}$ in (2.7), where $T_d = T_B$ should be used, and also replacing $L_v$ with $L_v + c_l(T_B - T_o)$ in (2.18).

Note also that the expressions given in (2.15)–(2.17) should be modified when $\text{Re}_\text{d}$ increases significantly above unity. For these large values of the droplet Reynolds number, a factor of order $\text{Re}_\text{d}$ should be included in (2.15) and a factor of order $\text{Re}_\text{d}^{1/2}$ should be included in (2.16) and (2.17). In

the sample computations below, a small value of $\mathrm{Re_d}$ will be assumed, and the near-droplet variations of $\mu$, $\kappa$ and $c_p$ will be neglected, thereby enabling the simple expressions (2.15)–(2.18) to be used for the droplet source terms.

## 2.3 The limit of infinitely fast chemical reaction

The solution can be simplified in the Burke-Schumann limit of infinitely fast reaction rate; this can be used, in the first approximation, for the description of flows with fuel-oxidation reaction times much smaller than those associated with convective and diffusive transport and also smaller than the characteristic droplet heating and vaporization times. To illustrate this limit, it is convenient to consider as an approximation the expression

$$\omega_{\mathrm{F}} = \rho B \hat{Y}_{\mathrm{O}} Y_{\mathrm{F}} \exp[-E_a/(R^o T)] \tag{2.19}$$

for the reaction rate (mass of fuel consumed per unit volume per unit time), including a frequency factor $B$ and an activation energy $E_a$, defining a characteristic chemical time for fuel oxidation

$$t_c = B^{-1} \exp[E_a/(R^o T_f)]. \tag{2.20}$$

The characteristic flame temperature

$$T_f = T_A + \frac{q}{c_p(1+S)}, \tag{2.21}$$

is used above in evaluating the temperature-dependent exponential, with $T_A$ denoting the temperature of the air feed stream. Equation (2.19) can be used to express the reaction rates appearing in the conservation equations (2.3)–(2.7), giving for instance

$$\underbrace{\frac{1}{\rho}\mathcal{L}(Y_{\mathrm{F}})}_{Y_{\mathrm{F}}/t_v} = -\underbrace{B\hat{Y}_{\mathrm{O}} Y_{\mathrm{F}} \exp[-E_a/(R^o T)]}_{\hat{Y}_{\mathrm{O}} Y_{\mathrm{F}}/t_c} + \underbrace{n\dot{m}/\rho}_{1/t_v} \tag{2.22}$$

for the fuel balance, where $\mathcal{L}(Y_{\mathrm{F}})$ represents the transport operator appearing on the left-hand side of (2.3). For the discussion, the anticipated orders of magnitude of the different competing phenomena have been indicated below each term, with the rates of accumulation and transport evaluated by assuming that the dominant fluid mechanical times are of the order of the droplet vaporization time. Note that this assumption was also used in (1.5) to evaluate the spray transverse size $L$ from the condition that the diffusion time across the spray $L^2/D_T$ be comparable to the droplet vaporization time.

The Burke-Schumann limit arises in reactive sprays with fuel-oxidation times much smaller than the characteristic vaporization and transport times, or order $t_v$, a condition often satisfied in practical burners whenever complete fuel consumption is to be achieved in the primary combustion region. According to the above order-of-magnitude analysis, in this limit $t_c \ll t_v$ of infinitely large Damköhler

numbers ($t_v/t_c$) the conservation equations for chemical species and energy lead to the condition

$$\hat{Y}_{\mathrm{O}} \cdot Y_{\mathrm{F}} = 0, \tag{2.23}$$

indicating that the fuel and the oxidizer cannot coexist in the first approximation, except within a very thin reaction layer, to be described at leading order in the limit $t_v/t_c \to \infty$ as a sheet $\Sigma_f$, mentioned in the introduction. This flame sheet separates a region $\Omega_{\mathrm{F}}$, where $\hat{Y}_{\mathrm{O}} = 0$, from a region $\Omega_{\mathrm{O}}$, where $Y_{\mathrm{F}} = 0$, whereas at the flame sheet both reactant mass fractions are simultaneously zero. In the solution that appears, the droplets lying in the oxygen-free region $\Omega_{\mathrm{F}}$ vaporize without chemical reaction, generating the fuel vapor that burns at the flame with the oxygen found in $\Omega_{\mathrm{O}}$.

Droplets with sufficient inertia may cross the flame to vaporize in $\Omega_{\mathrm{O}}$. In most applications, typical droplet radii are of the order of a few tenths of microns, much smaller than the characteristic flame thickness of the stoichiometric premixed flame $(D_T t_c)^{1/2}$. Under those conditions, no significant fuel consumption may occur at distances from the droplet of the order of $a$, because the fuel-oxidation time, although much smaller than the droplet vaporization time, is much larger than the characteristic diffusion time around the droplet $a^2/D_T$, as expressed in the inequality

$$a^2/D_T \ll t_c \ll L^2/D_T \sim t_v. \tag{2.24}$$

The fuel generated by droplets vaporizing in $\Omega_{\mathrm{O}}$ must then be consumed in a distributed reaction occuring in the gas phase between droplets. According to the anticipated orders of magnitude displayed in (2.22), the fuel-concentration field in $\Omega_{\mathrm{O}}$ is determined with negligible transport effects by a balance between fuel consumption and vaporization, giving rise to small fuel mass fractions $Y_{\mathrm{F}} \sim t_c/t_v \ll 1$ that can be computed as a correction to the leading-order Burke-Schumann solution $Y_{\mathrm{F}} = 0$. The analysis of this perturbations is addressed below, once the formulation for the leading-order problem is presented.

## 2.4 Leading-order Burke-Schumann solution

As shown by Shvab and Zeldovich, the limit of infinitely fast chemical reaction can be dealt with by eliminating the singular reaction terms through appropriate linear combinations of the conservation equations for energy and species. The procedure is straightforward when the species Lewis numbers are all unity, the case treated in the seminal work of Burke and Schumann [10], but it is somewhat more complicated in the general case $\mathrm{L_F} \neq \mathrm{L_O} \neq 1$. As shown by Liñán for gaseous diffusion flames [4], one needs to consider, together with the regular mixture fraction variable $Z = (SY_{\mathrm{F}} - \hat{Y}_{\mathrm{O}} + 1)/(1+S)$, a generalized mixture fraction variable $\tilde{Z} = (\tilde{S}Y_{\mathrm{F}} - \hat{Y}_{\mathrm{O}} + 1)/(1+\tilde{S})$, where $\tilde{S} = \mathrm{L_O}S/\mathrm{L_F}$, to generate from (2.3) and (2.4) conserved scalars satisfying conservation equations free from the direct effect of the gas-phase reaction. The corresponding conservation equation for spray combustion, found by substracting (2.4) from (2.3) times $S$, takes the form

$$\frac{\partial}{\partial t}(\rho Z) + \nabla \cdot (\rho \mathbf{v} Z) - \frac{1}{\mathrm{L}_m} \nabla \cdot \left(\rho D_T \nabla \tilde{Z}\right) = n\dot{m}, \tag{2.25}$$

where $\mathrm{L}_m = \mathrm{L}_\mathrm{O}(1+S)/(1+\tilde{S})$. According to (2.23), in the limit of infinitely large Damköhler numbers considered here the flame sheet separates a region with no fuel vapor from a region with no oxygen. The flame is located where both vapor fuel $Y_\mathrm{F}$ and oxygen $\hat{Y}_\mathrm{O}$ are simultaneously zero, corresponding to values of the mixture fraction $Z = Z_S = 1/(1+S)$ and $\tilde{Z} = \tilde{Z}_S = 1/(1+\tilde{S})$. The equations

$$\begin{cases} \hat{Y}_\mathrm{O} = 0, \quad Y_\mathrm{F} = (Z - Z_S)/(1 - Z_S) = (\tilde{Z} - \tilde{Z}_S)/(1 - \tilde{Z}_S) & \text{if} \quad Z \geq Z_s \\ Y_\mathrm{F} = 0, \quad \hat{Y}_\mathrm{O} = 1 - Z/Z_S = 1 - \tilde{Z}/\tilde{Z}_S & \text{if} \quad Z \leq Z_s \end{cases} \tag{2.26}$$

therefore link the values of $Z$ and $\tilde{Z}$ everywhere in the flow field, enabling the integration of (2.25) to be performed and providing the mass fractions of reactants in terms of the mixture-fraction variables.

Similarly, by linear combination of (2.4) and (2.7) the chemistry-free conservation equation

$$\frac{\partial}{\partial t}(\rho H) + \nabla\cdot(\rho \mathbf{v} H) - \nabla\cdot\left(\rho D_T \nabla \tilde{H}\right) = \\ - n\left\{\dot{m}\left[q/S + L_v - c_p\left(T_B - T_A\right)\right] + \dot{q}_d\right\} \tag{2.27}$$

can be derived in terms of the total enthalpy, $H = c_p(T - T_A) + (\hat{Y}_\mathrm{O} - 1)q/S$ and the modified total enthalpy, $\tilde{H} = c_p(T - T_A) + (\hat{Y}_\mathrm{O} - 1)q/(S\mathrm{L}_\mathrm{O})$, where $T_A$ has been used to denote the temperature of the air in its feed stream. In writing (2.27), the droplet temperature $T_d$ has been replaced by the boiling temperature $T_B$, as corresponds to the limit $L_v/(R_F T_B) \gg 1$ discussed above. The integration of (2.27) requires use of the expressions

$$\begin{cases} c_p(T - T_A) = H + q/S = \tilde{H} + q/(S\mathrm{L}_\mathrm{O}) & \text{if} \quad Z \geq Z_s \\ c_p(T - T_A) = H + (Z/Z_S)(q/S) = \tilde{H} + (Z/Z_S)q/(S\mathrm{L}_\mathrm{O}) & \text{if} \quad Z \leq Z_s \end{cases} \tag{2.28}$$

relating $H$ and $\tilde{H}$ on both sides of the flame and enabling the temperature to be computed from the coupling-function variables. An alternative to (2.27), free from the vaporization terms, can be derived by further combining (2.25) and (2.27) to yield

$$\frac{\partial}{\partial t}(\rho H') + \nabla\cdot(\rho \mathbf{v} H') - \nabla\cdot\left(\rho D_T \nabla \tilde{H}'\right) = -n\dot{q}_d, \tag{2.29}$$

where $H' = H + Z[q/S + L_v + c_p(T_A - T_B)]$ and $\tilde{H}' = \tilde{H} + \tilde{Z}[q/S + L_v + c_p(T_A - T_B)]$. Also, conservation equations that determine the product concentrations can be obtained from (2.3)–(2.6) to give

$$\frac{\partial\left(\rho P_{\mathrm{CO_2}}\right)}{\partial t} + \nabla\cdot\left(\rho \mathbf{v} P_{\mathrm{CO_2}}\right) - \nabla\cdot\left(\rho D_T \nabla \tilde{P}_{\mathrm{CO_2}}\right) = 0 \tag{2.30}$$

and

$$\frac{\partial\left(\rho P_{\mathrm{H_2O}}\right)}{\partial t} + \nabla\cdot\left(\rho \mathbf{v} P_{\mathrm{H_2O}}\right) - \nabla\cdot\left(\rho D_T \nabla \tilde{P}_{\mathrm{H_2O}}\right) = 0 \tag{2.31}$$

where $P_{\mathrm{CO_2}} = Y_{\mathrm{CO_2}} + (\hat{Y}_\mathrm{O} - 1)s_{\mathrm{CO_2}}/S + Z s_{\mathrm{CO_2}}/S$, $\tilde{P} = Y_{\mathrm{CO_2}}/\mathrm{L}_{\mathrm{CO_2}} + (\hat{Y}_\mathrm{O} - 1)s_{\mathrm{CO_2}}/(S\mathrm{L}_\mathrm{O}) + \tilde{Z} s_{\mathrm{CO_2}}/(SL_m)$, $P_{\mathrm{H_2O}} = Y_{\mathrm{H_2O}} + (\hat{Y}_\mathrm{O} - 1)s_{\mathrm{H_2O}}/S + Z s_{\mathrm{H_2O}}/S$, and $\tilde{P} = Y_{\mathrm{H_2O}}/\mathrm{L}_{\mathrm{H_2O}} + (\hat{Y}_\mathrm{O} - 1)s_{\mathrm{H_2O}}/(S\mathrm{L}_\mathrm{O}) + \tilde{Z} s_{\mathrm{H_2O}}/(S\mathrm{L}_m)$

These results complete the formulation of the leading-order problem for Lewis numbers different from unity by extending the previous gaseous-fuel formulation to liquid-fuel problems.

## 2.5 Distributed air-side fuel oxidation

As previously mentioned, small fuel mass fractions of order $Y_{\text{F}} \sim t_c/t_v \ll 1$ may appear in $\Omega_{\text{O}}$ as a result of droplet vaporization when the droplets have sufficient inertia to cross the flame. The reaction occurs in a distributed manner, with negligible effects of fuel transport, as can be anticipated from the order-of-magnitude analysis (2.22). Equating the fuel-comsumption rate by chemical reaction and the fuel-generation rate by droplet vaporization yields in the first aproximation

$$Y_{\text{F}} = \frac{4\pi}{B}\frac{aD_T n}{\hat{Y}_{\text{O}}}\exp[E_a/(R^o T)]\ln\left[1+\frac{c_p(T-T_B)}{L_v}\right] \tag{2.32}$$

as an explicit expression for the distribution of the fuel mass fraction, where the values of $a$, $D_T$, $n$, $\hat{Y}_{\text{O}}$, and $T$ are to be evaluated from the leading-order Burke-Schumann solution. The accuracy of the above prediction is subject to the condition that the chemistry remains sufficiently fast for the transport rate to be negligible in (2.22). Because of the temperature dependence of the reaction rate, in regions of lower temperature the chemical reaction becomes slower. The associated fuel-consumption time becomes comparable to the vaporization time when the temperature decreases to values of the order of a critical crossover temperature, $T_{cc}$, such that

$$\exp\left[\frac{E_a}{R^o}\left(\frac{1}{T_f}-\frac{1}{T_{cc}}\right)\right] \sim \frac{t_c}{t_v}. \tag{2.33}$$

In regions away from the flame where $T \sim T_{cc}$, transport effects enter to modify the analytic prediction (2.32), with larger corrections expected to appear at increasing distances from the flame. If the nondimensional activation energy $E_a/(R^o T_{cc})$ is large, then fuel consumption freezes as soon as the temperature falls below $T_{cc}$. When this occurs, the fuel mass fraction is determined by a balance between transport and vaporization. Consideration of fuel transport in cold regions with $T < T_{cc}$ would be needed in particular to determine emissions of unburnt hydrocarbons in liquid-fueled combustors.

The expression (2.32) applies specifically to fuels with oxidation chemistry represented by the idealized one-step irreversible reaction (2.8) with rate (2.19). It is however straightforward to extend the result to more general chemistry descriptions. Although the detailed chemistry of high alkanes typically involves a few thousand elementary reactions between a few hundred reactive species, studies of nonpremixed flames have demonstrated that most of the chemical intermediates are in steady state, so that reduced chemical-kinetic descriptions with just a few overall steps provide sufficient accuracy for most purposes. For the simplest hydrocarbons, combustion can be described by introducing steady-state approximations for all but three chemical intermediates, namely, H, CO, and $H_2$. For a general hydrocarbon $C_xH_y$, the resulting reduced mechanism can be expressed in the general form

[11, 12]

$$\begin{aligned} C_xH_y + xH_2O &\xrightarrow{F} xCO + (x + y/2)H_2, \\ 3H_2 + O_2 &\overset{B}{\rightleftharpoons} 2H_2O + 2H, \\ H + H &\xrightarrow{R} H_2, \\ CO + \frac{1}{2}O_2 &\overset{CO}{\rightleftharpoons} CO_2, \end{aligned}$$

with corresponding rates (moles per unit volume per unit time) of fuel consumption, chain branching, chain recombination and CO oxidation given by $w_F$, $w_B$, $w_R$, and $w_{CO}$, respectively. For this reduced description, conservation equations can be written for the fuel and for the different intermediates according to

$$\begin{aligned} \mathcal{L}(Y_F) &= -M_F w_F + n\dot{m}, \\ \mathcal{L}(Y_{CO}) &= M_{CO}(x w_F - w_{CO}), \\ \mathcal{L}(Y_{H_2}) &= M_{H_2}[(x + y/2)w_F - 3w_B + w_R], \\ \mathcal{L}(Y_H) &= M_H(2w_B - 2w_R). \end{aligned}$$

As in (2.22), the symbol $\mathcal{L}$ is used here to represent the transport differential operator for each chemical species. At temperatures of the order of $T_f$, the chemical times associated with the four overall reactions are sufficiently large for the condition $t_c \ll t_v$ to hold in $\Omega_O$, so that the transport terms can be neglected in the first approximation in the above equations, reducing the computation of the concentrations of $C_xH_y$, CO, $H_2$, and H to the solution of the reduced fuel conservation equation $M_F w_F = n\dot{m}$ along with the three steady-state expressions for the intermediates $x w_F = w_{CO}$, $(x + y/2)w_F + w_R = 3w_B$, and $w_B = w_R$. In the solution, the concentrations of $O_2$, $H_2O$, $CO_2$, the temperature, the number of droplets per unit volume $n$, and their radius $a$ are to be evaluated from the leading-order Burke-Schumann solution.

Note that descriptions seeking increased accuracy should account for the fact that the rate of CO oxidation is typically smaller than that of the other chemical processes [13], so that the steady-state expression for CO fails before those of H and $H_2$ as the temperature drops away from the flame. As a result, in computations of CO emissions from spray burners, the CO transport should be incorporated in its conservation equation, to be integrated with use made of the steady-state expressions for H and $H_2$ and the consumption-vaporization balance for the fuel.

## 2.6 Conclusions

In this chapter a general formulation for the combustion of dilute sprays in the fast-chemistry limit has been derived. An efficient way to account for effects of Lewis numbers different from unity, previously developed for purely gaseous systems, was extended so that it can be used in spray combustion. That extension leads to the explicit appearance of source terms in conservation equations for gaseous and spray continua, which account for the mutual interactions between the gaseous and condensed phases.

# References

[1] J. Reveillon, L. Vervisch, Analysis of weakly turbulent dilute-spray flames and spray combustion regimes, J. Fluid Mech. 537 (2005) 317–347.

[2] P. Moin, S. Apte, Large-eddy simulation of realistic gas turbine combustors, AIAA Journal 44 (2006) 698–708.

[3] K. Luo, H. Pitsch, M. G. Pai, O. Desjardin, Direct numerical simulations and analysis of three-dimensional n-heptane spray flames in a model swirl combustor, Proc. Comb. Inst. 89 (2011) 1447–1460.

[4] A. Liñán, The structure of diffusion flames, in: M. Onofri, A. Tesei (Eds.), Fluid dynamical aspects of combustion theory, Longman Scientific Technical Essex, 1991, pp. 11–19.

[5] A. Bermúdez, J. L. Ferrín, A. Liñán, The modelling of the generation of volatiles, $H_2$ and CO, and their simultaneous diffusion controlled oxidation, in pulverized coal furnaces, Combus. Theor. Modell. 11 (2007) 949–976.

[6] A. Bermúdez, J. Ferrín, A. Liñán, L. Saavedra, Numerical simulation of group combustion of pulverized coal, Comb. Flame 158 (2011) 1852–1865.

[7] S. Sadhal, P. Ayyaswamy, Flow past a liquid drop with large non-uniform velocity, J. Fluid Mech. 133 (1983) 65–81.

[8] A. Liñán, Theory of droplet vaporization and combustion, in: R. Borghi, P. Clavin, A. Liñán, P. Pelcé, G. I. e. Sivashinsky (Eds.), Modélisation des phénoménes de combustion, Editions Eyrolles, 1985, pp. 73–103.

[9] G. A. Godsave, Studies of the combustion of drops in a fuel spray – the burning of single drops of fuel, Proc. Combust. Inst 4 (1953) 818–830.

[10] S. Burke, T. Schumann, Diffusion flames, Indust. Eng. Chem. 20 (1928) 998–1009.

[11] W. Sirignano, Fluid dynamics and transport of droplets and sprays, Cambridge University Press, Cambridge, UK., 1999.

[12] F. Williams, The role of theory in combustion science, Proc. Combust. Inst. 24 (1992) 1–17.

[13] A. L. Sánchez, A. Lépinette, M. Bollig, A. . Liñán, B. Lázaro, The reduced kinetic description of lean premixed combustion, Combust. Flame 123 (2000) 436–464.

CHAPTER

**THREE**

# Sheath vaporization of a fuel-spray jet

## 3.1 Introduction

The two-continua formulation presented in the previous chapter will be used now to analyze the group vaporization of a monodisperse fuel-spray jet discharging into a hot coflowing gaseous stream. The analysis is based on asymptotic and analytic methods rather than on detailed numerical simulations, because even though the latter can include many phenomena, the former are better suited for isolating the most important effects, thereby increasing understanding of the underlying physics significantly. In addition, they often can yield formulas that are readily applied to calculate quantities of interest in applications.

To focus more directly on the group vaporization process, a simple laminar configuration including a central monodisperse fuel-spray jet discharging with a high Reynolds number into a surrounding hot coflow, sketched in figure 3.1, is selected for the study, the objective being that of developing new understanding, which is also sought in recent experimental studies involving laminar sprays [1–3]. Clearly, given the simplicity of the flow considered, the results cannot be expected to be directly applicable to realistic configurations such as transient diesel sprays, supercritical conditions or complex turbulent flows in gas turbines with potential acoustic amplification of pressure oscillations, but can help in developing ideas for these applications. For instance, key controlling parameters will be identified and their influence on the spray structure will be described both numerically and analytically. Particular attention will be given to the sheath-vaporization regime, previously analysed in [4] for the spherical droplet cloud, with droplet vaporization occurring only in a thin layer surrounding the spray, whose location will be found as a free boundary in a parabolic problem that is solved by numerical integration in the distinguished regime $\alpha_c \sim O(1)$, with $\alpha_c$ representing the mass of liquid fuel per unit mass of gas in the spray stream, as defined above in (1.1). The jet configuration considered here has been subject to a limited number of theoretical investigations [5, 6]. Instead, most of the initial theoretical workers considered vaporization [4] or combustion [7–9] of a spherical droplet cloud, with the objective of gaining insight into the underlying competing physical phenomena rather than evaluating a specific practical application. The jet problem investigated below, although still highly simplified, provide information of more direct relevance for combustor performance, such as penetration distances.

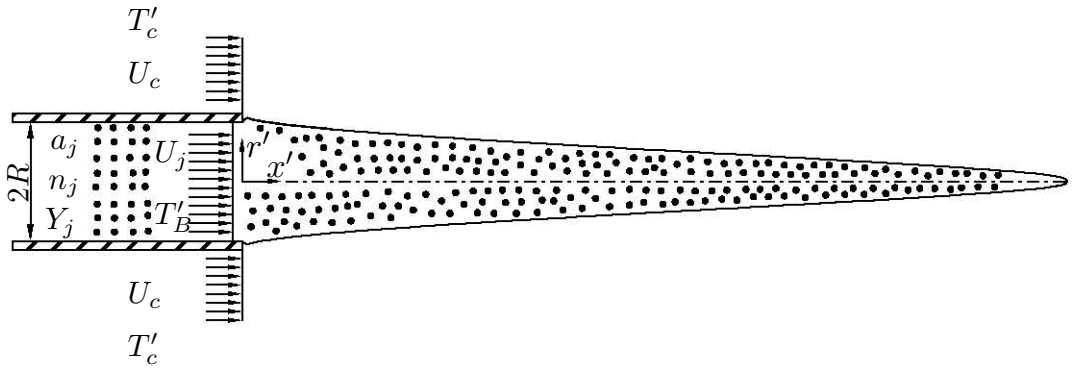


**Figure 3.1:** Vaporization of a monodisperse spray.

## 3.2 Problem statement

The jet spray includes the interaction region between the round spray flowing out of the injector and the hot coflowing stream at temperature $T_c'$ larger than that of the injected jet, $T_j'$. The velocity profiles in the jet and the coflow are assumed to be uniform, with values given respectively by $U_j$ and $U_c$. The spray is assumed to be monodisperse, with the uniform values $a_j$ and $n_j$ of the droplet radius and the droplet number density at the jet exit. Furthermore, the injector is assumed to be sufficiently long for the mixture to be in saturated equilibrium at the jet exit. Thus, the temperature $T_j'$ and initial fuel mass fraction $Y_j$ in the jet stream can be related by the Clausius Clapeyron equation

$$Y_j = \frac{W_{\mathrm{F}}}{W_j} \exp[L_v/(R_{\mathrm{F}} T_B') - L_v/(R_{\mathrm{F}} T_j')], \tag{3.1}$$

where $T_B'$ is the boiling temperature, $L_v$ is the specific latent heat of vaporization, $R_{\mathrm{F}} = R^o/W_{\mathrm{F}}$ is the gas constant of the fuel, with $R^o$ representing the universal gas constant, and $W_{\mathrm{F}}$ and $W_j$ are the molecular weight of the fuel and the jet carrier gas mixture, respectively. It is assumed that, as often occurs in applications, $L_v/(R_{\mathrm{F}} T_B') \gg 1$, which implies that, at equilibrium, the departures of $T_j'$ from the boiling temperature $T_B'$ are of order $T_j' - T_B' \sim [L_v/(R_{\mathrm{F}} T_B')]^{-1} T_B' \ll T_B'$, and can be consequently neglected in the first approximation.

We assume in our analysis that the spray is dilute (in the sense that the volume fraction of the liquid is small, even though we consider the liquid mass per unit volume to be comparable with or larger than that of the gas) and that the spray contains many droplets, so that the inequalities given in (1.6) are satisfied. For the monodisperse laminar spray considered here, the liquid phase can be treated as a continuum, as indicated in section 2.1, a convenient approximation for the analytical work attempted below. The variables describing the liquid phase are the droplet radius $a'$, droplet number density $n'$ and droplet axial and radial velocity components $u_d'$ and $v_d'$, in this continuum description that applies in the limit $R \gg l_d$, while the gas phase is characterized by its density and temperature $\rho'$ and $T'$, velocity components $u'$ and $v'$ and fuel mass fraction $Y$.

In the formulation, we shall further assume that the jet Reynolds number $\mathrm{Re_j} = \rho_j U_j R/\mu$, where $\rho_j$ is the gas density at the jet exit and $\mu$ is the viscosity of the gas mixture, is large compared with

unity for the flow to be slender, and yet not so large to ensure that the motion remains laminar and steady. In that case, the boundary-layer form of the axisymmetric conservation equations suffices to describe, with relative errors of order $\mathrm{Re_j}^{-2}$, the resulting slender flow solution in terms of the axial and radial coordinates $x'$ and $r'$. The description of the gas phase reduces to the integration of the conservation equations for mass (2.1), momentum (2.2), species (2.3) and energy (2.7) in the axisymmetric boundary-layer form and assuming $\omega_f = 0$. These equations, supplemented with the near-isobaric form of the equation of state (2.9), are to be integrated with initial conditions at $x' = 0$, corresponding to the spray and coflow properties at the exit plane, and boundary conditions at $r' = 0$ and as $r' \to \infty$ for $x' > 0$. Numerical integrations of the corresponding parabolic problem for a selected number of cases were reported in [6].

## 3.3 Characteristic time scales and controlling parameters

An order-of-magnitude analysis of the different competing physical phenomena leads to useful estimates for the three characteristic times that are involved in the spray vaporization process. Thus, comparing convection and transverse diffusion in the gas-phase conservation equations leads to

$$t_{\mathrm{D}} = R^2/D_{T_j} \tag{3.2}$$

as an estimate for the diffusion time across the jet, with $D_{T_j} = \kappa/(\rho_j c_p)$ representing the thermal diffusivity of the gas at the spray exit. This time is equal to the residence time in the region of jet development, and typically differs from the droplet lifetime

$$t_a = \frac{\rho_l a_j^2}{3\rho_j D_{T_j}}, \tag{3.3}$$

obtained by dividing the initial droplet mass $(4\pi/3)a_j^3\rho_l$, where $\rho_l$ denotes the liquid fuel density, by the characteristic value of the vaporization rate $4\pi a_j(\kappa/c_p)$, obtained from (2.17) with a unity factor replacing the logarithmic term, as is appropriate when the Spalding number is of order unity. Note that, except for an irrelevant factor $2/(3\mathrm{Pr})$, where Pr is the Prandtl number of the gas phase, the same estimate (3.3) is obtained for the characteristic time of droplet acceleration, as can be seen by equating the orders of magnitude of droplet acceleration $\rho_l(4/3)\pi a_j^3 U_j/t_a$ and the characteristic value of the drag force $6\pi\mu a_j U_j$, obtained from (2.15).

The time scale given in (3.3) characterizes the vaporization of each individual droplet. The collective effect of spray vaporization on the density, velocity, temperature, and fuel-vapour evolution in the jet is however measured by a different time scale, a spray-interaction time,

$$t_s = \frac{1}{4\pi a_j n_j D_{T_j}}, \tag{3.4}$$

obtained as the ratio of the characteristic jet density $\rho_j$ to the volume rate of mass production through vaporization $4\pi a_j n_j \kappa/c_p$ (fuel mass per unit volume per unit time), the latter being the product of the characteristic value of the vaporization rate $4\pi a_j \kappa/c_p$ and the initial number of droplets per unit

volume $n_j$. The scale given in (3.4) therefore corresponds to the characteristic time required for droplet vaporization to change appreciably – i.e. by a relative amount of order unity – the value of the gas density in the jet, as can also be obtained by comparing the convective term with the droplet source term in the gas-phase continuity equation. Similarly, the comparison of the convective and vaporization terms in the momentum, energy and fuel conservation equations also yields (3.4) as the characteristic time required for droplet vaporization to change significantly the values of the gas velocity, temperature and fuel mass fraction in the jet, respectively.

The two primary parameters that control the spray solution are obtained as the ratios of the above characteristic times. The first relevant parameter is the mass of liquid fuel per unit mass of gas in the spray stream

$$\alpha_c = \frac{(4\pi/3)a_j^3 n_j \rho_l}{\rho_j}, \tag{3.5}$$

corresponding to the definition given above in (1.1) with $a_o = a_j$, $n_c = n_j$ and $\rho_c = \rho_j$, which is also equal to the characteristic time ratio $\alpha_c = t_a/t_s$. This parameter, measuring the dilution of the spray, will be taken as an order unity magnitude in the following development, as corresponds to spray configurations with characteristic values of the average distance between neighbouring droplets $l_d = n_j^{-1/3}$ of order $l_d \sim (\rho_l/\rho_j)^{1/3} a_j \sim 10 a_j$. Separate consideration will be given to the limiting cases $\alpha_c \gg 1$ and $\alpha_c \ll 1$, the latter being of interest in combustion applications, where small values of $\alpha_c$ of the order of the stoichiometric mixture fraction are often encountered. Note that in the limit $\alpha_c \gg 1$ of relatively dense sprays, the condition $l_d \gg a_j$ introduces an upper limit $\alpha_c \ll \rho_l/\rho_j$, so that the spray remains sufficiently dilute for the formulation to remain valid.

The second controlling parameter is the ratio of the characteristic time of jet evolution due to spray vaporization $t_s$ to the diffusion time $t_{\text{D}}$:

$$\varepsilon = \frac{t_s}{t_{\text{D}}} = \frac{1}{4\pi a_j n_j R^2}. \tag{3.6}$$

In terms of the three characteristic scales involved in (1.6), this ratio can be seen to be of order

$$\varepsilon \sim \left(\frac{l_d}{R}\right)^2 \left(\frac{l_d}{a_j}\right). \tag{3.7}$$

With $l_d/a_j$ typically being a moderately large quantity of order $(\rho_l/\rho_j)^{1/3} \simeq 10$ for $\alpha_c \sim O(1)$, the resulting value of $\varepsilon$ depends on $l_d/R$. Small values of $\varepsilon$ are expected to appear in general in connection with the vaporization of sprays with multiple droplets, that is, sufficiently small values of $l_d/R$. On the other hand, in view of (3.7), it is clear that values of $\varepsilon$ of order unity or larger will be found only under conditions of extreme dilution, not often encountered in applications. Therefore, because of its expected wide range of applicability, the development of a deeper understanding of the limit $\varepsilon \ll 1$ is clearly worthwhile.

The parameter $\varepsilon$ was used previously as a small quantity for the asymptotic analysis of droplet cloud vaporization [4] and, as discussed in [9], controls the group combustion characteristics in

reactive configurations. In many practical applications, the parameter $\varepsilon$ takes on small values, causing vaporization to occur in a sheath or vaporization front that separates the spray, in saturated equilibrium, from the surrounding droplet-free hot gas, with the flame standing outside the spray in combustion configurations. This limit of sheath vaporization, analysed in [4] for a spherical droplet cloud, will be investigated here for the axisymmetric vaporizing jet spray.

Note that as an alternative to $\varepsilon$ one could employ in the analysis the characteristic Stokes number of the problem $\mathrm{St} = 2/(3\mathrm{Pr})(t_a/t_{\mathrm{D}})$, which can be expressed as $\mathrm{St} = 2\alpha_c\varepsilon/(3\mathrm{Pr})$. The results to be obtained if St replaces $\varepsilon$, including all relevant asymptotic limits, would be equivalent to those encountered with use made of $\varepsilon$. In particular, with $\alpha_c \sim O(1)$, the limit of sheath vaporization would arise in this alternative development for $\mathrm{St} \ll 1$. Since $\varepsilon$ was preferred by previous investigators [4, 9] we choose to address the spray problem in terms of this parameter.

## 3.4 Dimensionless formulation

To nondimensionalize the problem, the characteristic diffusion time $t_{\mathrm{D}}$ will be used to construct scales for the streamwise length, $U_j t_{\mathrm{D}}$, and for the gas and droplet radial velocities, $R/t_{\mathrm{D}} = D_{T_j}/R$. Furthermore, the radial distance will be scaled with $R$, whereas the droplet and gas axial velocity components, the droplet radius and number density, and the gas temperature and density will be scaled with their values at the spray exit. With these scales, the complete set of dimensionless variables is given by $x = x'/(U_j t_{\mathrm{D}})$, $r = r'/R$, $u = u'/U_j$, $u_d = u'_d/U_j$, $v = v'/(R/t_{\mathrm{D}})$, $v_d = v'_d/(R/t_{\mathrm{D}})$, $a = a'/a_j$, $n = n'/n_j$, $T = T'/T'_j$ and $\rho = \rho'/\rho_j$. The corresponding dimensionless form of the gas-phase equations is

$$\frac{\partial}{\partial x}(\rho u) + \frac{1}{r}\frac{\partial}{\partial r}(\rho r v) = \frac{na}{\varepsilon}\ln\left[1 + \frac{(T-1)}{\beta}\right], \tag{3.8}$$

$$\frac{\partial}{\partial x}\left(\rho u^2\right) + \frac{1}{r}\frac{\partial}{\partial r}(\rho r v u) - \frac{\mathrm{Pr}}{r}\frac{\partial}{\partial r}\left(r\frac{\partial u}{\partial r}\right) = \frac{nau_d}{\varepsilon}\ln\left[1 + \frac{(T-1)}{\beta}\right] + +\frac{3}{2}\frac{\mathrm{Pr}}{\varepsilon}(u_d - u)na, \tag{3.9}$$

$$\frac{\partial}{\partial x}(\rho u T) + \frac{1}{r}\frac{\partial}{\partial r}(\rho r v T) - \frac{1}{r}\frac{\partial}{\partial r}\left(r\frac{\partial T}{\partial r}\right) = -\frac{na}{\varepsilon}(\beta - 1)\ln\left[1 + \frac{(T-1)}{\beta}\right], \tag{3.10}$$

$$\frac{\partial}{\partial x}(\rho u Y) + \frac{1}{r}\frac{\partial}{\partial r}(\rho r v Y) - \frac{1}{\mathrm{Lr}}\frac{\partial}{\partial r}\left(r\frac{\partial Y}{\partial r}\right) = \frac{na}{\varepsilon}\ln\left[1 + \frac{(T-1)}{\beta}\right], \tag{3.11}$$

while the equations for the liquid phase become

$$\frac{\partial}{\partial x}(n u_d) + \frac{1}{r}\frac{\partial}{\partial r}(n r v_d) = 0, \tag{3.12}$$

$$u_d\frac{\partial a^3}{\partial x} + v_d\frac{\partial a^3}{\partial r} = -\frac{a}{\varepsilon\alpha_c}\ln\left[1 + \frac{(T-1)}{\beta}\right], \tag{3.13}$$

$$u_d\frac{\partial u_d}{\partial x} + v_d\frac{\partial u_d}{\partial r} = \frac{3\mathrm{Pr}}{2\varepsilon\alpha_c}\frac{u - u_d}{a^2}, \tag{3.14}$$

$$u_d\frac{\partial v_d}{\partial x} + v_d\frac{\partial v_d}{\partial r} = \frac{3\mathrm{Pr}}{2\varepsilon\alpha_c}\frac{v - v_d}{a^2}. \tag{3.15}$$

The problem is subject to the initial and boundary conditions

$$x = 0 : \begin{cases} r < 1 : & u = T = n = a = u_d = 1, Y = Y_j, v_d = 0 \\ r > 1 : & u = u_c, \quad T = T_c, \quad Y = 0, \end{cases} \tag{3.16}$$

and

$$x > 0 : \begin{cases} r = 0 : & v = \partial u/\partial r = \partial T/\partial r = \partial Y/\partial r = 0 \\ r \to \infty : & u = u_c, \quad T = T_c, \quad Y = 0. \end{cases} \tag{3.17}$$

The above equations must be supplemented with the dimensionless form of the equation of state. The description is simplified when changes in mean molecular weight of the gas mixture are neglected, thereby reducing the equation of state to

$$\rho T = 1. \tag{3.18}$$

We shall adopt this simplifying approximation in the following description. Nevertheless, quantitative departures, arising from variations in mean molecular weight in vaporization processes of typical liquid fuels, are worth investigating in the future.

Sources of mass, momentum and energy appear in the above equations associated with the drag force acting on the droplets and their vaporization rate, as given by (2.15) and (2.17). Linear combinations can be used to derive source-free equations. For instance, using (3.9) and (3.12) (3.14) provides the spray momentum equation

$$\frac{\partial}{\partial x}\left(\rho u^2 + \alpha_c n a^3 u_d^2\right) + \frac{1}{r}\frac{\partial}{\partial r}\left(\rho r v u + \alpha_c n a^3 r v_d u_d\right) - \frac{\mathrm{Pr}}{r}\frac{\partial}{\partial r}\left(r\frac{\partial u}{\partial r}\right) = 0, \tag{3.19}$$

which can be integrated radially across the jet with the boundary conditions indicated above to provide the integral constraint

$$\int_0^\infty r[\rho u(u - u_c) + \alpha_c n a^3 u_d(u_d - u_c)]\mathrm{d}r = (1 - u_c)(\alpha_c + 1)/2, \tag{3.20}$$

associated with the conservation of momentum flux. Source-free spray conservation equations can also be derived for energy and fuel mass, leading to two additional integral constraints that were used, together with (3.20), in monitoring the accuracy of the numerical integrations of (3.8)-(3.18).

As can be seen, besides $\varepsilon$, $\alpha_c$ and the Prandtl and Lewis numbers, $\mathrm{Pr} = \mu c_p/\kappa$ and $\mathrm{L} = \kappa/(\rho_j c_p D_{T_j})$, respectively, there exist three additional dimensionless parameters in the formulation, namely the dimensionless latent heat of vaporization $\beta = L_v/(c_p T_B')$ and the coflow to spray temperature and velocity ratios $T_c = T_c'/T_B'$ and $u_c = U_c/U_j$. The value $\beta = 0.36$, corresponding to octane [4], is employed for the latent heat of vaporization in the computations below, which consider different values of $T_c - 1$ and $u_c$. The computations include, in particular, jets discharging into a stagnant atmosphere ($u_c = 0$) and also coflow velocities equal to the spray velocity ($u_c = 1$), the latter being particularly simple, in that the solution for the axial velocity components reduces to $u = u_d = 1$ everywhere in the

flow field, thereby facilitating the computations.

## 3.5 Sample numerical results

Figures 3.2–3.6 correspond to numerical integrations of (3.8)–(3.18) for L = 1, Pr = 0.7, $\beta = 0.36$, $T_c = 2.15$, $Y_j = 0.2$, $u_c = 0$, and different values of $\alpha_c$ and $\varepsilon$, including dilute ($\alpha_c = 0.1$) and dense ($\alpha_c = 20$) sprays. The numerical scheme employed in the integrations is described in appendix A. Results obtained in the sheath-vaporization limit $\varepsilon = 0$, to be discussed later, are also provided in figures 3.3–3.6, with the details of the associated numerical method also presented in appendix A.

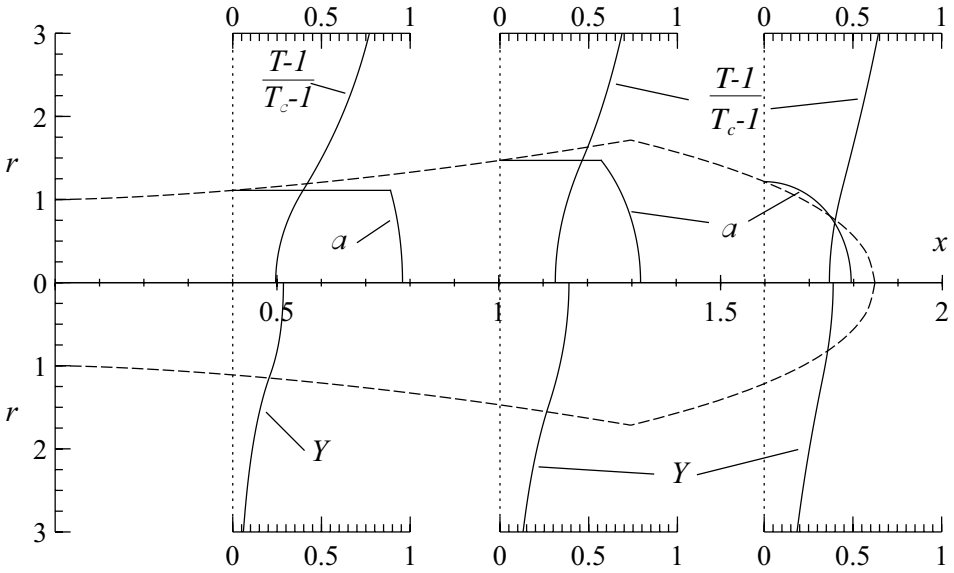


**Figure 3.2:** Profiles of temperature, droplet radius and fuel mass fraction across the vaporizing jet as obtained by integration of (3.8)-(3.18) for $u_c = 0$, L = 1, $Y_j = 0.2$, Pr = 0.7, $\beta = 0.36$, $T_c = 2.15$, $\alpha_c = 1$ and $\varepsilon = 1$; the dashed line indicates the outer boundary of the spray.

Figure 3.2 shows profiles of temperature, droplet radius and fuel mass fraction across the jet spray at three different axial locations. As can be seen, for the case $\varepsilon = 1$ vaporization occurs in a distributed manner. In particular, although the vaporization is more pronounced at the edge of the spray, nonnegligible vaporization of the droplets located along the axis can be noticed already at $x = 0.4$. As a result, the fuel mass fraction increases from its initial value $Y_j = 0.2$, giving profiles that peak at the axis. Also of interest is that heat transfer from the hot coflow increases the temperature within the spray to values significantly larger than the boiling temperature $T = 1$.

Also shown in figure 3.2 is the outer boundary of the spray, which coincides initially with the outermost droplet trajectory. The radius of this boundary droplet decreases, however, downstream from the injector rim, as the droplet vaporizes in contact with the high-temperature coflow. This droplet is completely consumed at a finite distance from the injector $x \simeq 1.3$, so that farther downstream the spray boundary is defined as the location where $a = 0$, corresponding to vaporizing droplets located initially within the jet away from the injector edge.

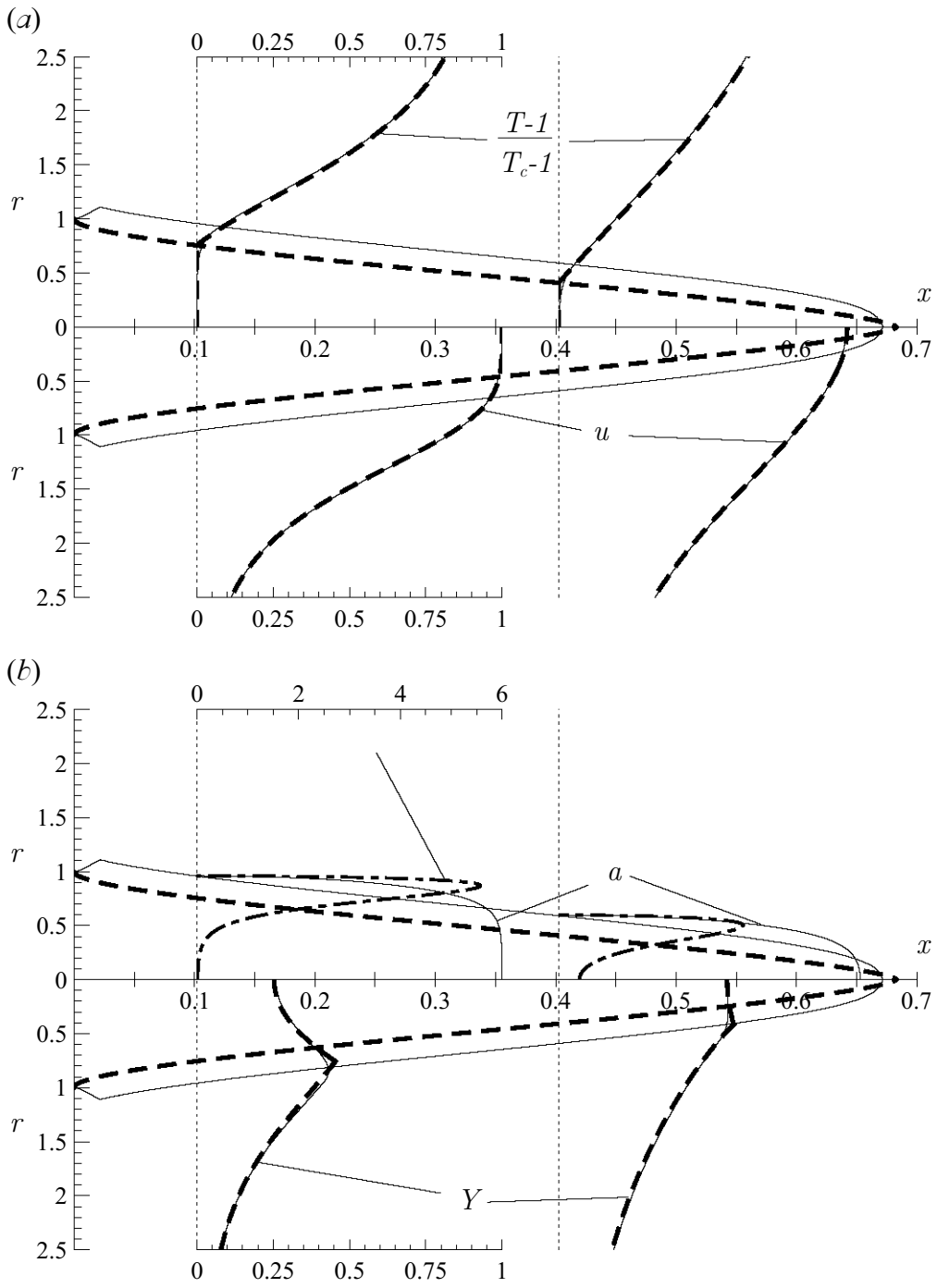


**Figure 3.3:** $(a, b)$ The vaporizing jet as obtained by integration of (3.8)–(3.18) for $u_c = 0$, L = 1, $Y_j = 0.2$, Pr = 0.7, $\beta = 0.36$, $T_c = 2.15$, $\alpha_c = 1$ and $\varepsilon = 0.01$ (solid lines) along with results obtained in the sheath-vaporization limit $\varepsilon = 0$ (dashed lines); the dot-dashed curves represent the radial profiles of the rescaled mass vaporization rate $na \ln[1 + (T - 1)/\beta]/\varepsilon$. The scales are indicated for the profiles at the first axial location, with a different scale used for the mass vaporization rate.

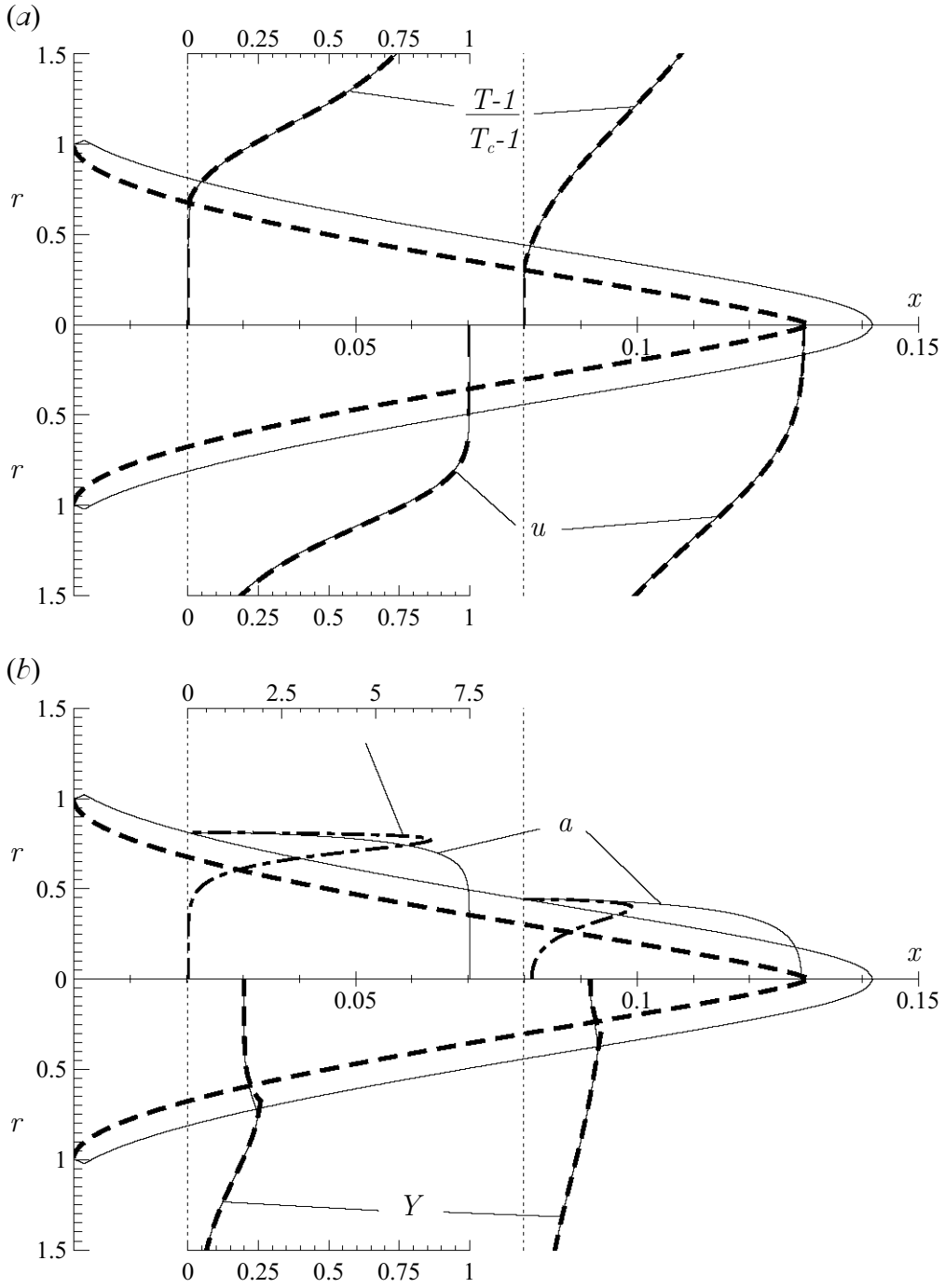


**Figure 3.4:** $(a, b)$ The vaporizing jet as obtained by integration of (3.8)–(3.18) for $u_c = 0$, L $= 1$, $Y_j = 0.2$, Pr $= 0.7$, $\beta = 0.36$, $T_c = 2.15$, $\alpha_c = 0.1$ and $\varepsilon = 0.01$ (solid lines) along with results obtained in the sheath-vaporization limit $\varepsilon = 0$ (dashed lines); the dot-dashed curves represent the radial profiles of the rescaled mass vaporization rate $na \ln[1 + (T - 1)/\beta]/\varepsilon$. The scales are indicated for the profiles at the first axial location, with a different scale used for the mass vaporization rate.

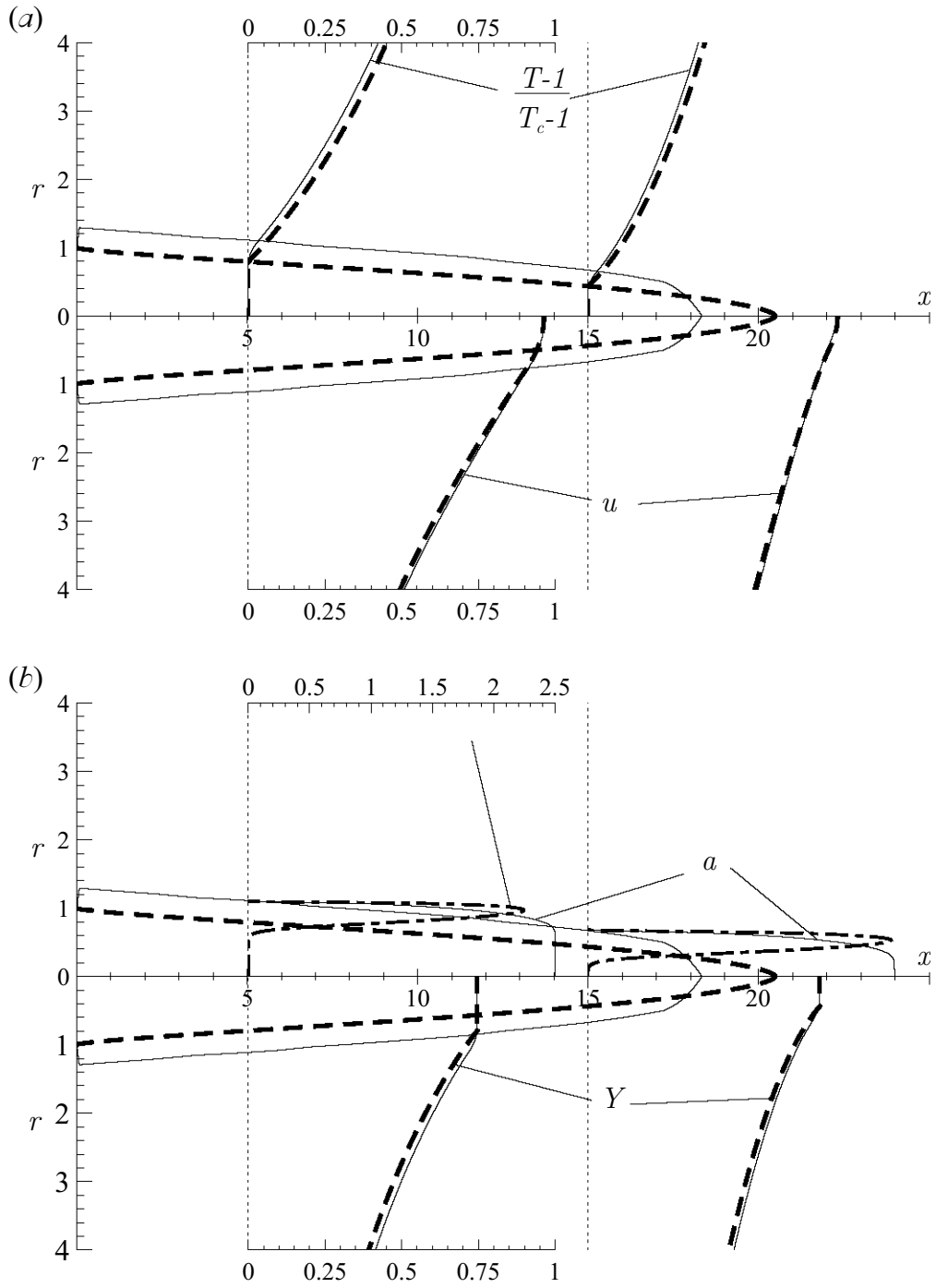


**Figure 3.5:** $(a, b)$ The vaporizing jet as obtained by integration of (3.8)–(3.18) for $u_c = 0$, L $= 1$, $Y_j = 0.2$, Pr $= 0.7$, $\beta = 0.36$, $T_c = 2.15$, $\alpha_c = 20$ and $\varepsilon = 10^{-3}$ (solid lines) along with results obtained in the sheath-vaporization limit $\varepsilon = 0$ (dashed lines); the dot-dashed curves represent the radial profiles of the rescaled mass vaporization rate $na \ln[1 + (T - 1)/\beta]/\varepsilon$. The scales are indicated for the profiles at the first axial location, with a different scale used for the mass vaporization rate.

The plots in 3.3–3.5 show profiles of temperature, fuel mass fraction, gas axial velocity, droplet radius, and mass vaporization rate at two different axial locations. For all three cases considered, corresponding to relatively small values of $\varepsilon$, the solution shows a structure not present in figure 3.2. The distinct flow structure that emerges includes a thin vaporization layer, where the vaporization rate is concentrated and the fuel-vapour mass fraction reaches its peak value, separating an outer nonvaporizing region with $a = 0$ from an inner equilibrium region, where the temperature, velocity and droplet radius remain approximately equal to their injector values $T = u = a = 1$. This sheath-vaporization regime, identified in [4] when dealing with the vaporization of a spherical fuel-droplet cloud, will be further considered in the following section for the analysis of the jet structure.

Figures 3.3–3.5 also show the outer boundary of the spray, which increases with $\alpha_c$, as may be seen from the different $x$ scales in the figures. The evolution of the corresponding spray shape for decreasing values of $\varepsilon$ and two different coflow velocities is shown in figure 3.6. The downstream distance for vaporization of the boundary droplet leaving the injector rim is proportional to the initial jet velocity $U_j$ times the vaporization time of a single droplet $t_a$. With the scales selected here, this distance becomes proportional to $\varepsilon\alpha_c$ when expressed in dimensionless form, as can be inferred from (3.13). Therefore, as $\varepsilon$ decreases for a given value of $\alpha_c$, the corresponding vaporization distance for the boundary droplet also decreases, a result seen in the plots of figure 3.6.

The downstream position where the droplet located initially at the axis vaporizes completely, which is the location where the boundary of the spray intersects the axis, defines the spray penetration distance $x_v$. This is seen in figures 3.3–3.6 to depend on the spray dilution through the liquid-to-gas spray mass ratio $\alpha_c$. Dilute sprays corresponding to $\alpha_c \ll 1$ vaporize at a short distance from the exit plane, whereas dense sprays with $\alpha_c \gg 1$ penetrate farther. The rough estimate

$$x_v = \frac{\alpha_c}{2(T_c - 1)/\beta} \tag{3.21}$$

for the dependence of $x_v$ on $\alpha_c$ follows from equating the total heat provided by the coflow per unit time, which can be estimated as the product of the characteristic radial heat flux $\kappa(T_c' - T_B')/R$ and the spray lateral surface $2\pi R x_v'$, to the amount of heat needed per unit time to vaporize the droplets, obtained as the product of the liquid mass flow rate $\pi R^2 U_j n_j (4/3)\pi a_j^3 \rho_l$ and the latent heat of vaporization $L_v$. As seen below, for very long and very short sprays, corresponding to the two limiting cases $\alpha_c \gg 1$ and $\alpha_c \ll 1$, the radial heat flux is modified, so that the analytical expressions that are obtained for the penetration distance in the sheath-vaporization limit $\varepsilon = 0$, given later in (3.64) and (3.80), exhibit dependences on parameters that differ from those displayed in (3.21).

## 3.6 The sheath-vaporization limit

The appearance of the sheath-vaporization regime for small values of $\varepsilon$, clearly apparent in the numerical results shown in figures 3.3–3.5, can be anticipated by observing that in the limit $\varepsilon \to 0$ the solution of (3.8)–(3.11) –or that of (3.13)– leads to $a \ln[1 + (T - 1)/\beta] = 0$, indicating the existence of a thin vaporization front located at $r = r_v(x)$ separating an outer region for $r > r_v$ where no droplets are found ($a = 0$) and an inner region for $r < r_v$ where the temperature remains equal to the boiling

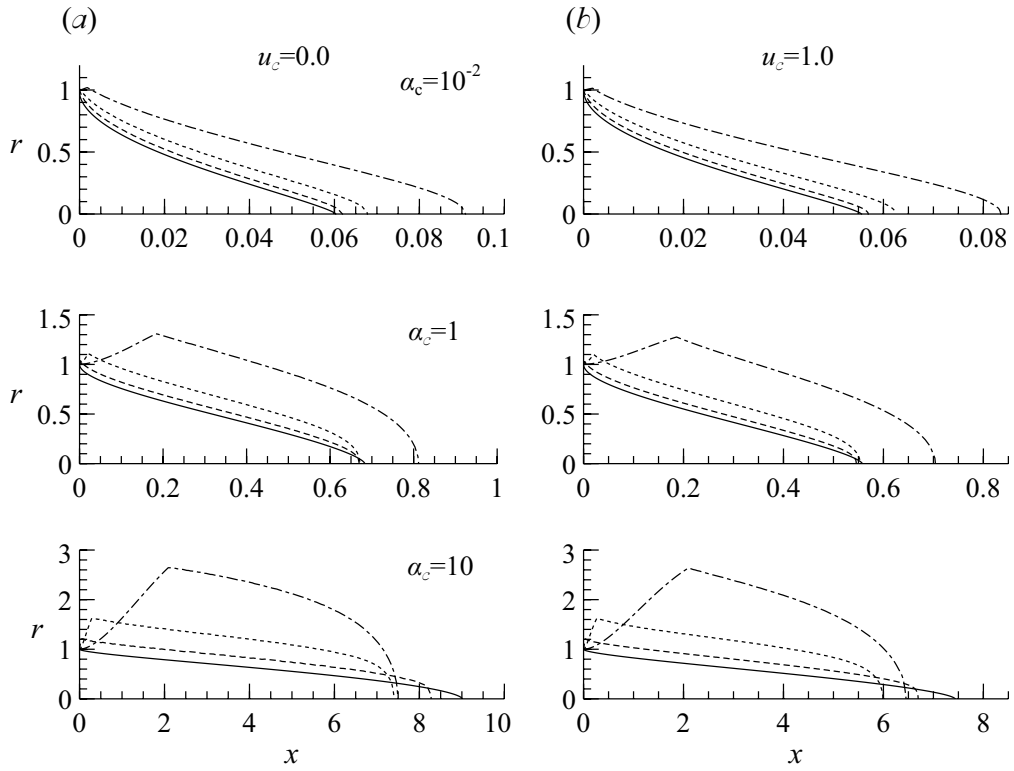


**Figure 3.6:** $(a, b)$ The boundary of the liquid phase where $a = 0$ obtained by integration of (3.8)–(3.18) for L = 1, Pr = 0.7, $\beta = 0.36$, and $T_c = 2.15$ for three different values of $\alpha_c$ and for $\varepsilon = 10^{-1}$ (dash-dotted line), $\varepsilon = 10^{-2}$ (dotted line) and $\varepsilon = 10^{-3}$ (dashed line). The solid line represents the vaporization-layer location $r_v(x)$ obtained in the limit $\varepsilon = 0$.

temperature in the first approximation ($T = 1$). Droplets vaporize only within the thin vaporization layer, of characteristic thickness $\varepsilon^{1/2}$, which appears as a localized sink of energy and source of mass, causing the profiles of $T$ and $Y$ to show a discontinuous radial gradient at $r = r_v$, with $Y$ reaching its peak value $Y_v$ there. Since $T - 1 \sim \varepsilon^{1/2}$ in the vaporization layer, with both $n$ and $a$ remaining of order unity, the resulting dimensionless mass vaporization rate $na\ln[1 + (T - 1)/\beta]/\varepsilon$ becomes of order $\varepsilon^{-1/2}$, as can be observed in the plots of figures 3.3–3.5. Because of the concentrated mass release, the droplet and gas radial velocity components, $v_d$ and $v$, which are equal in the first approximation as can be seen from (3.15) in the limit $\varepsilon \to 0$, exhibit a jump across the vaporization layer. The axial velocity components $u$ and $u_d$ are also almost equal, as follows from (3.14) with $\varepsilon \ll 1$. Vaporization does not result in a net axial momentum exchange between the liquid and gas phases, so that the values of $u$ and $u_d$ and those of their radial gradients are equal on both sides of the vaporization front.

The leading-order asymptotic analysis in the limit $\varepsilon \to 0$ leads to a free-boundary problem in which $r_v(x)$ is to be determined as part of a nonlinear parabolic problem. In the notation employed, the flow properties at the vaporization front will be denoted by the subscript $v$, with the $+$ and $-$ signs used to refer to the outer and inner sides when, as occurs for instance with the radial velocity and with the temperature gradient, there is a leading-order change across the front caused by vaporization.

### 3.6.1 The outer non-vaporizing streams

As previously anticipated, for $r > r_v$ the solution of (3.13) in the limit $\varepsilon = 0$ yields $a = 0$, thereby reducing the solution for the gas phase to the integration of

$$\frac{\partial}{\partial x}(\rho u) + \frac{1}{r}\frac{\partial}{\partial r}(\rho r v) = 0, \tag{3.22}$$

$$\frac{\partial}{\partial x}\left(\rho u^2\right) + \frac{1}{r}\frac{\partial}{\partial r}(\rho r v u) - \frac{\mathrm{Pr}}{r}\frac{\partial}{\partial r}\left(r\frac{\partial u}{\partial r}\right) = 0, \tag{3.23}$$

$$\frac{\partial}{\partial x}(\rho u T) + \frac{1}{r}\frac{\partial}{\partial r}(\rho r v T) - \frac{1}{r}\frac{\partial}{\partial r}\left(r\frac{\partial T}{\partial r}\right) = 0, \tag{3.24}$$

$$\frac{\partial}{\partial x}(\rho u Y) + \frac{1}{r}\frac{\partial}{\partial r}(\rho r v Y) - \frac{1}{\mathrm{L}r}\frac{\partial}{\partial r}\left(r\frac{\partial Y}{\partial r}\right) = 0. \tag{3.25}$$

For $r < r_v$, on the other hand, $T = 1$ and, therefore, $\rho = 1$ according to (3.18), so that (3.8) reduces to

$$\frac{\partial u}{\partial x} + \frac{1}{r}\frac{\partial}{\partial r}(r v) = 0. \tag{3.26}$$

In the absence of vaporization, the radius of each droplet remains unperturbed, as can be seen by inspection of (3.13), so that $a = 1$ for $r < r_v$. Furthermore, observation of (3.14) and (3.15) indicates that $u - u_d \sim v - v_d \sim O(\varepsilon)$, so that, in the first approximation one may use $u_d = u$ and $v_d = v$. When this condition is used along with (3.26) in (3.12) the equation $u_d \partial n/\partial x + v_d \partial n/\partial r = 0$ is obtained, which yields $n = 1$ for $r < r_v$ upon integration along the droplets trajectories. The small differences $u - u_d \sim \varepsilon$ are sufficiently large for the Stokes force to be nonnegligible in (3.9) and (3.14). To avoid the presence of the resulting singular term, the leading-order results $T = 1$, $a = 1$, $n = 1$, $u_d = u$, and

$v_d = v$ are used in the spray momentum equation (3.19) to give the alternative equation

$$u\frac{\partial u}{\partial x} + v\frac{\partial u}{\partial r} - \frac{\mathrm{Pr}}{1+\alpha_c}\frac{1}{r}\frac{\partial}{\partial r}\left(r\frac{\partial u}{\partial r}\right) = 0, \tag{3.27}$$

for the computation of $u = u_d$ for $r < r_v$. Finally, the fuel conservation equation reduces with $\rho = 1$ to

$$\frac{\partial}{\partial x}(uY) + \frac{1}{r}\frac{\partial}{\partial r}(rvY) - \frac{1}{\mathrm{Lr}}\frac{\partial}{\partial r}\left(r\frac{\partial Y}{\partial r}\right) = 0, \tag{3.28}$$

which completes the set of equations in the outer nonvaporizing streams.

### 3.6.2 The vaporization layer

The study of the self-similar inner structure of the vaporization layer provides a set of boundary conditions at $r = r_v$ to be used in integrating (3.22)–(3.28). Across this layer, of characteristic thickness $\varepsilon^{1/2}$, the values of $T$, $u$, and $Y$ only change by a small amount of order $\varepsilon^{1/2}$ from their order-unity values $T = 1$, $u = u_v$ and $Y = Y_v$, respectively, whereas $v$, $a$ and $n$ experience changes of order unity. The relative velocity components $u - u_d \sim \varepsilon$ and $v - v_d \sim \varepsilon^{1/2}$ are sufficiently small for (3.14) and (3.15) to be replaced at leading order by $u = u_d$ and $v = v_d$. The solution can be determined by rewriting (3.8)–(3.13) in terms of the rescaled radial coordinate $\xi = (r - r_v)/\varepsilon^{1/2}$ and the rescaled variables $\theta = (T-1)/\varepsilon^{1/2}$, $U = (u - u_v)/\varepsilon^{1/2}$ and $\phi = (Y - Y_v)/\varepsilon^{1/2}$. In the formulation, the subscript $\xi$ denotes differentiation with respect to this variable.

The development begins by integrating once $-u_v(\mathrm{d}r_v/\mathrm{d}x)n_\xi + (nv)_\xi = 0$, corresponding to the reduced form of (3.12), with boundary conditions $n = 1$ and $v = v_-$ on the spray side (i.e., as $\xi \to -\infty$) to give

$$n\left(v - u_v\frac{\mathrm{d}r_v}{\mathrm{d}x}\right) = v_- - u_v\frac{\mathrm{d}r_v}{\mathrm{d}x}. \tag{3.29}$$

Introduction of the rescaled variables into (3.8) and (3.13) gives

$$\alpha_c\left(u_v\frac{\mathrm{d}r_v}{\mathrm{d}x} - v_-\right)(a^3)_\xi = v_\xi = \frac{na\theta}{\beta}, \tag{3.30}$$

where (3.29) has been employed to express the factor multiplying $(a^3)_\xi$ in a form independent of $\xi$. Equation (3.30) can be used in (3.10) and (3.11) to give

$$\frac{\theta_{\xi\xi}}{\beta} = -\frac{\phi_{\xi\xi}}{\mathrm{L}(1-Y_v)} = \frac{na\theta}{\beta}, \tag{3.31}$$

and in (3.9) to give

$$U_{\xi\xi} = 0. \tag{3.32}$$

First integrations of (3.30), (3.31) and (3.32) with boundary conditions as

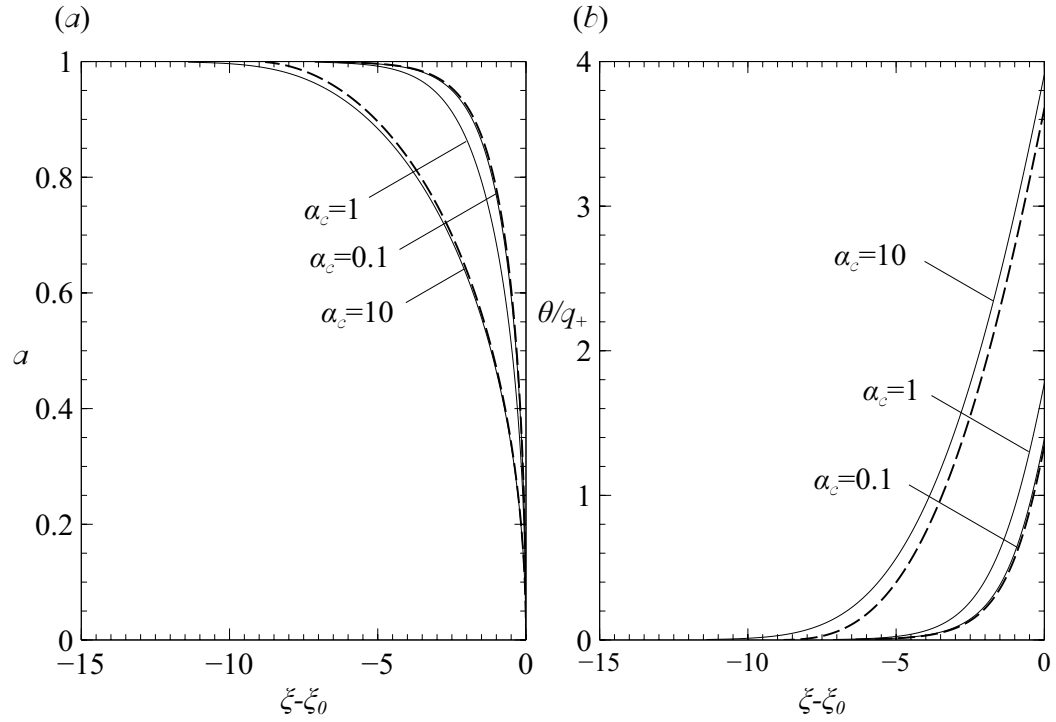


**Figure 3.7:** $(a, b)$ The vaporization layer as obtained by integration of (3.40) and (3.39) for different values of $\alpha_c$, (solid lines) along with results obtained for dense sprays (dashed lines) and diluted sprays (dashed lines)

$\xi \to -\infty$ give

$$-\alpha_c \left( u_v \frac{\mathrm{d}r_v}{\mathrm{d}x} - v_- \right) (1 - a^3) = v - v_- = \frac{\theta_\xi}{\beta} = -\frac{\phi_\xi - (\phi_\xi)_-}{\mathrm{L}(1 - Y_v)} \tag{3.33}$$

and $U_\xi = (U_\xi)_-$. Evaluating these expressions as $\xi \to +\infty$ provides the jump conditions across the vaporization layer

$$-\alpha_c \left( u_v \frac{\mathrm{d}r_v}{\mathrm{d}x} - v_- \right) = v_+ - v_- = \frac{1}{\beta} \left( \frac{\partial T}{\partial r} \right)_+ = -\frac{\left(\frac{\partial Y}{\partial r}\right)_+ - \left(\frac{\partial Y}{\partial r}\right)_-}{\mathrm{L}(1 - Y_v)} \tag{3.34}$$

and

$$\left( \frac{\partial u}{\partial r} \right)_+ = \left( \frac{\partial u}{\partial r} \right)_- , \tag{3.35}$$

which have been written in terms of the original spray variables.

The jump conditions given above in (3.34) and (3.35) are needed for the integration of the outer equations given in (3.22)–(3.28). No additional details are necessary at the leading order considered here. Nevertheless, for completeness of the presentation, we give below the detailed solution for $n$, $a$ and $\theta$ across the vaporization layer. The first equation in (3.33) can be employed together with (3.29)

to write

$$n = \frac{1}{1+\alpha_c(1-a^3)}, \tag{3.36}$$

which can be evaluated with $a = 0$ to determine the value of the droplet number density on the outer side of the vaporization layer, a function of the dilution given by $n_+ = (1+\alpha_c)^{-1}$. On the other hand, according to (3.31), the temperature variation across the vaporization layer can be computed from

$$\theta_{\xi\xi} = na\theta \begin{cases} \theta(-\infty) = 0, \\ \theta(+\infty) = q_+\xi, \end{cases} \tag{3.37}$$

where the heat flux $q_+ = (\partial T/\partial r)_+$ is to be determined as part of the integration of the outer problem. To facilitate the computation, the expression for the temperature gradient $\theta_\xi = q_+(1-a^3)$, given in (3.33), can be used together with (3.36) to rewrite (3.37) in the form

$$\theta\frac{\mathrm{d}\theta}{\mathrm{d}a} = -3q_+^2 a(1-a^3)[1+\alpha_c(1-a^3)], \tag{3.38}$$

which leads to

$$\theta/q_+ = \sqrt{6}\left[\frac{3}{10} - \frac{a^2}{2} + \frac{a^5}{5} + \alpha_c\left(\frac{9}{40} - \frac{a^2}{2} - \frac{a^8}{8} + \frac{2a^5}{5}\right)\right]^{1/2} \tag{3.39}$$

upon integration with boundary condition $\theta = 0$ when $a = 1$. Evaluating (3.39) with $a = 0$ provides $\theta_0 = 3q_+[(4+3\alpha_c)/20]^{1/2}$ for the value of the temperature increase at the inner-layer location $\xi = \xi_0 = 3[(4+3\alpha_c)/20]^{1/2}$, where $a = 0$. For $\xi > \xi_0$, the temperature is simply given by $\theta = q_+\xi$, as follows from integrating (3.37) with $a = 0$, whereas for $\xi < \xi_0$ the temperature is determined through (3.39) in terms of the droplet-radius distribution,

$$\xi_0 - \xi = \int_0^a \frac{3a[1+\alpha_c(1-a^3)]}{\theta/q_+}\mathrm{d}a, \tag{3.40}$$

obtained from $\theta_\xi = q_+(1-a^3)$, with the function (3.39) used to express the denominator in the above integral as a function of $a$. The expressions of the integral (3.39) and the droplet radius distribution (3.40) are simplified for dense and diluted sprays. In particular for dense sprays, the temperature distribution simplifies to yield

$$\Theta/q_+ = \sqrt{6}\left(\frac{9}{40} - \frac{a^2}{2} - \frac{a^8}{8} + \frac{2a^5}{5}\right)^{1/2}, \tag{3.41}$$

where $\Theta = \theta/\sqrt{\alpha_c}$ represents the rescaled temperature across the vaporization. Similarly, the location of the inner-layer is also simplfied, providing

$\Xi_0 = \xi_0/\alpha_c^{1/2} = 3(3/20)^{1/2}$, and the droplet radius distribution is obtained integrating

$$\Xi_0 - \Xi = \int_0^a \frac{3a\left(1-a^3\right)}{\Theta/q_+}\mathrm{d}a. \tag{3.42}$$

The description of the vaporization layer for diluted sprays is facilitated neglecting the terms of order $\alpha_c$ in (3.39) and (3.40), providing

$$\theta/q_+ = \sqrt{6}\left(\frac{3}{10} - \frac{a^2}{2} + \frac{a^5}{5}\right)^{1/2}, \tag{3.43}$$

and

$$\xi_0 - \xi = \int_0^a \frac{3a}{\theta/q_+}\mathrm{d}a, \tag{3.44}$$

for the temperature and droplet radius distribution respectively, where $\xi_0 = 3/\sqrt{5}$ represents the asymptotic inner-layer location for diluted sprays. The asymptotic behaviours (3.41)–(3.42) and (3.43)–(3.44) are plotted in figure 3.7, comparing favourably with the droplet radius and temperature profiles obtained integrating (3.39) and (3.40)

### 3.6.3 Mixing layer near the injector rim

Initial conditions for the integration of (3.22)–(3.28) follow from investigating the near-injector region, an analysis presented below. For $x$ in the range $\alpha_c\varepsilon \ll x \ll 1$ the vaporization front has already developed, but remains embedded in the mixing layer that separates the jet and the coflow, whose thickness increases downstream from the injector rim proportional to the square root of the streamwise distance. The analysis of this region employes the local coordinate $\eta = (r-1)/\sqrt{x}$ and the mixture fraction $\psi = \sqrt{x}F(\eta)$, defined such that the rescaled front location is given by $\eta_v = (r_v - 1)/\sqrt{x}$ while the velocity components can be expressed in the form $u = TF_\eta$ and $V = \sqrt{x}v = T(\eta F_\eta - F)/2$, where the subscript $\eta$ indicates differentiation with respect to this similarity coordinate. Introducing these variables into (3.23) and (3.24) gives

$$(TF_\eta)_{\eta\eta} + \frac{1}{2\mathrm{Pr}}F(TF_\eta)_\eta = 0, \tag{3.45}$$

$$T_{\eta\eta} + \frac{1}{2}FT_\eta = 0, \tag{3.46}$$

whereas (3.27) yields

$$F_{\eta\eta\eta} + \frac{1+\alpha_c}{2\mathrm{Pr}}FF_{\eta\eta} = 0, \tag{3.47}$$

and the fuel mass fraction satisfies

$$Y_{\eta\eta} + \frac{1}{2\mathrm{L}}FY_\eta = 0. \tag{3.48}$$

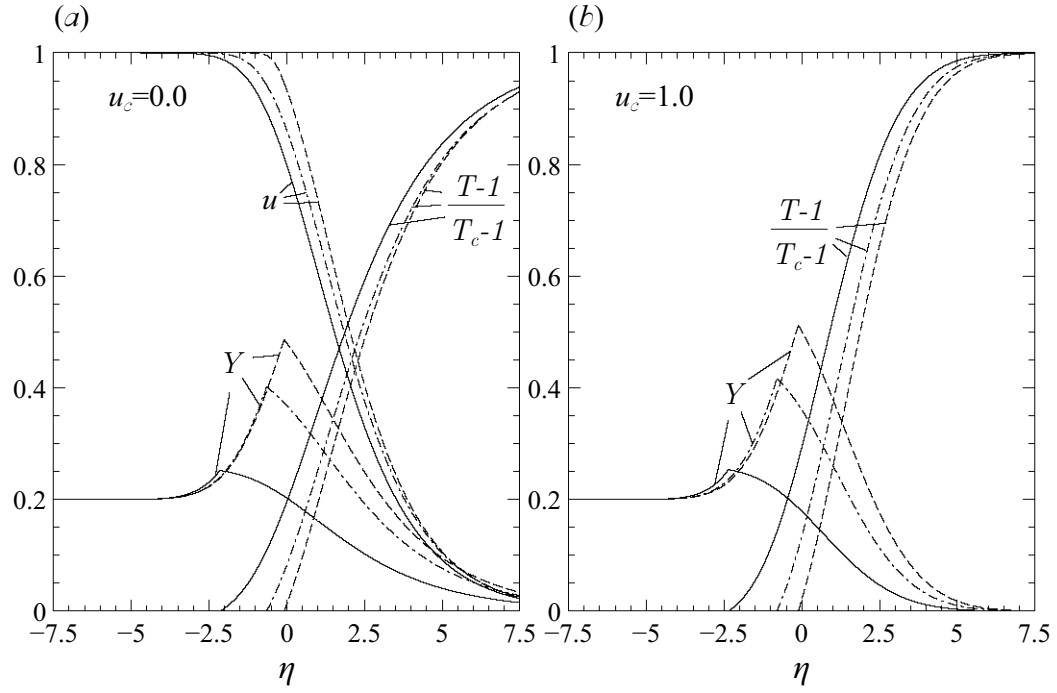


**Figure 3.8:** $(a, b)$ Profiles of temperature, fuel mass fraction and axial velocity in the mixing layer as obtained for $\beta = 0.36$, $T_c = 2.15$, Pr $= 0.7$, L $= 1$, $Y_j = 0.2$ and $\alpha_c = 10^{-1}$ (solid line), $\alpha_c = 1$ (dash-dotted line) and $\alpha_c = 10$ (dashed line); with $u_c = 1$ the solution for the axial velocity reduces to $u = 1$ and is not shown in the figure.

The solution involves integration of (3.45), (3.46) and (3.48) for $\eta > \eta_v$ with boundary conditions $F_\eta - u_c/T_c = T - T_c = Y = 0$ as $\eta \to \infty$ and $T - 1 = F_\eta - u_v = Y - Y_v = 0$ at $\eta = \eta_v$, and of (3.47) and (3.48) for $\eta < \eta_v$ with boundary conditions $F - \eta = Y - Y_j = 0$ as $\eta \to -\infty$ and $F_\eta - u_v = Y - Y_v = 0$ at $\eta = \eta_v$. The additional conditions

$$-\frac{\alpha_c}{2}F_- = \frac{1}{2}(F_- - F_+) = \frac{1}{\beta}(T_\eta)_+ = \frac{(Y_\eta)_- - (Y_\eta)_+}{\mathrm{L}(1 - Y_v)}, \tag{3.49}$$

$$(T_\eta F_\eta + F_{\eta\eta})_+ - (F_{\eta\eta})_- = 0, \tag{3.50}$$

at $\eta = \eta_v$, corresponding respectively to (3.34) and (3.35), serve to close the problem. For given values of $\beta$, $\alpha_c$, $T_c$ and $Y_j$, the integration provides the temperature, velocity and fuel mass fraction across the mixing layer, including the vaporization-layer values $u_v$, $Y_v$, and $\eta_v$. Sample profiles are shown in figure 3.8 for $u_c = 0$ and $u_c = 1$. The dependence of $\eta_v$ with $\alpha_c$ for different values of $T_c$ and $u_c$ is shown in figure 3.9. As can be seen, the location of the vaporization layer depends on the value of $\alpha_c$. The two limiting cases of very dense and very dilute sprays are addressed below.

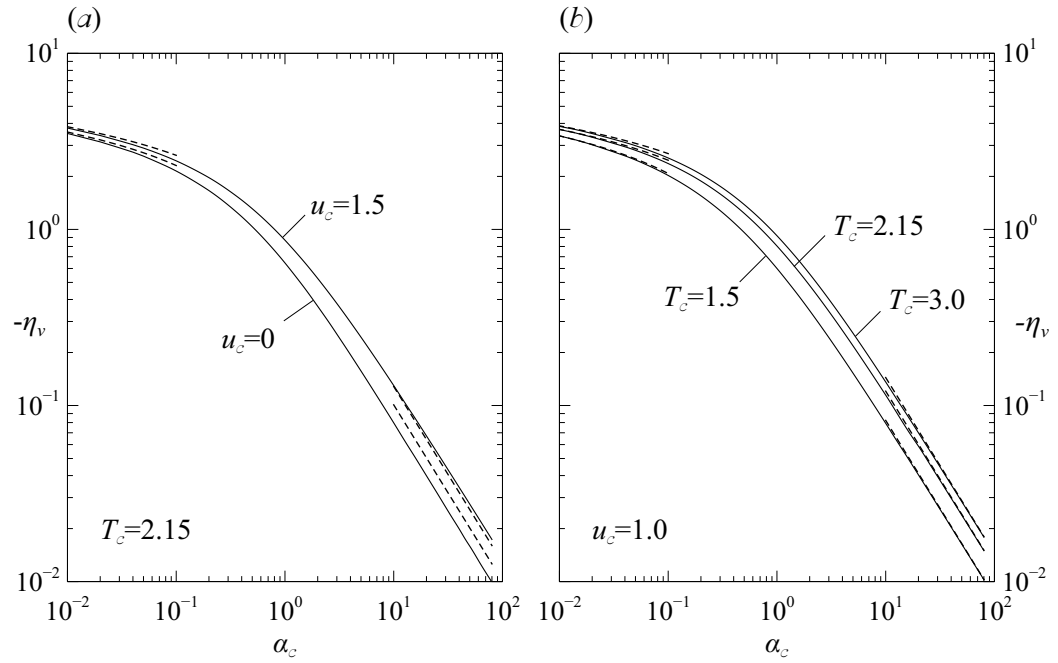


**Figure 3.9:** $(a, b)$ The variation of $\eta_v$ as a function of $\alpha_c$ for $\beta = 0.36$, $\mathrm{Pr} = 0.7$, and different values of $T_c$ and $u_c$. The dashed lines represent the asymptotic behaviours for $\alpha_c \ll 1$ and $\alpha_c \gg 1$.

## 3.7 Sheath-vaporization results

The solution for the jet in the sheath-vaporization regime can be determined by integration of (3.22)–(3.25) with boundary conditions $u - u_c = T - T_c = Y = 0$ as $r \to \infty$ and $u - u_v = T - 1 = Y - Y_v = 0$ as $r \to r_v$ and of (3.26)–(3.28) with boundary conditions $v = \partial u/\partial r = \partial Y/\partial r = 0$ at $r = 0$ and $u - u_v = Y - Y_v = 0$ as $r \to r_v$. Initial conditions correspond to the self-similar solutions identified above at $x \ll 1$. The two problems are coupled through the additional constraints (3.34) and (3.35). The solution determines in particular the boundary values $u_v(x)$, $Y_v(x)$, $v_+(x)$ and $v_-(x)$ along with the evolution of the vaporization front $r_v(x)$ from its initial location $r_v(0) = 1$.

Figures 3.3–3.5 show by dashed curves the profiles of temperature, axial velocity, droplet radius, and fuel mass fraction determined in the sheath-vaporization limit. As can be seen, the agreement with the results of numerical integrations of the original spray equations for small values of $\varepsilon$ is excellent. The location of the vaporization front $r_v(x)$ is also shown in these figures, and also in figure 3.6, where it can be clearly seen that the spray boundary computed for decreasing values of $\varepsilon$ approaches the vaporization front of the sheath-vaporization limit, with departures appearing at small distances $x \sim \varepsilon\alpha_c$, in the initial region where the vaporization front is forming.

Of particular interest in applications is the downstream distance of spray penetration $x'_v$ before complete vaporization is achieved. In the sheath-vaporization limit, this penetration distance corresponds to the downstream location $x_v$ at which the vaporization front $r_v(x)$ reaches the axis, i.e. $r_v(x_v) = 0$. The variation of this distance with $\alpha_c$ is compared in figure 3.10 with results of numerical integrations of the original problem (3.8)–(3.18) for

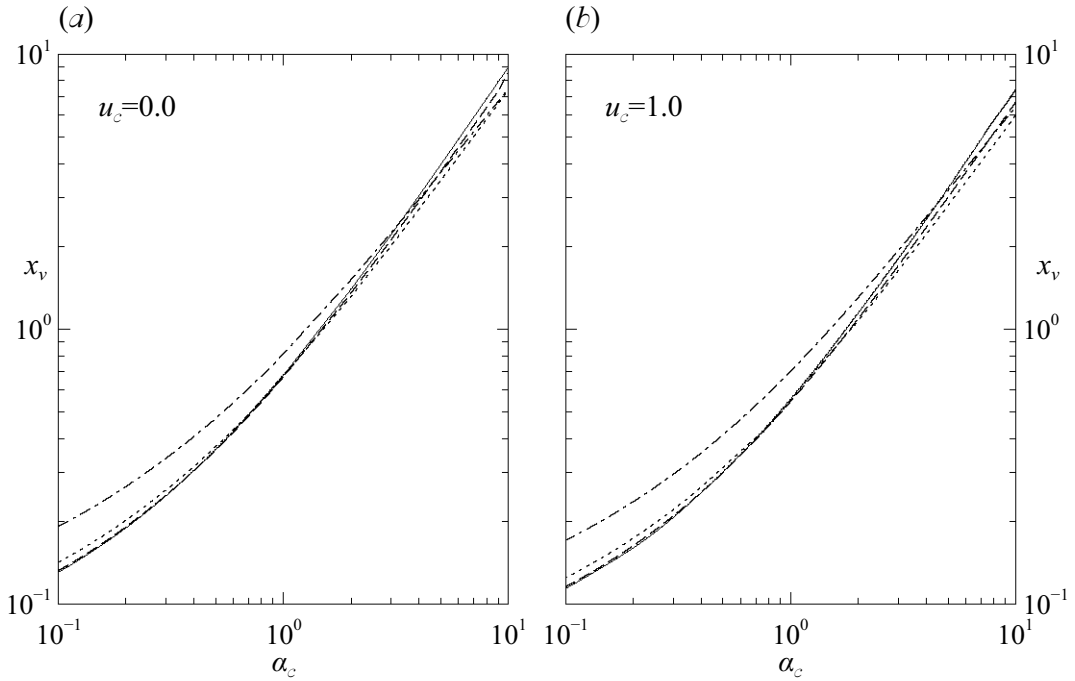


**Figure 3.10:** $(a, b)$ The spray penetration distance obtained with $T_c = 2.15$, $\beta = 0.36$ and $\mathrm{Pr} = 0.7$ by integration of (3.8)–(3.18) for $\varepsilon = 10^{-1}$ (dash-dotted line), $\varepsilon = 10^{-2}$ (dotted line) and $\varepsilon = 10^{-3}$ (dashed line) compared with the vaporization distance obtained in the limit $\varepsilon \to 0$ (solid line).

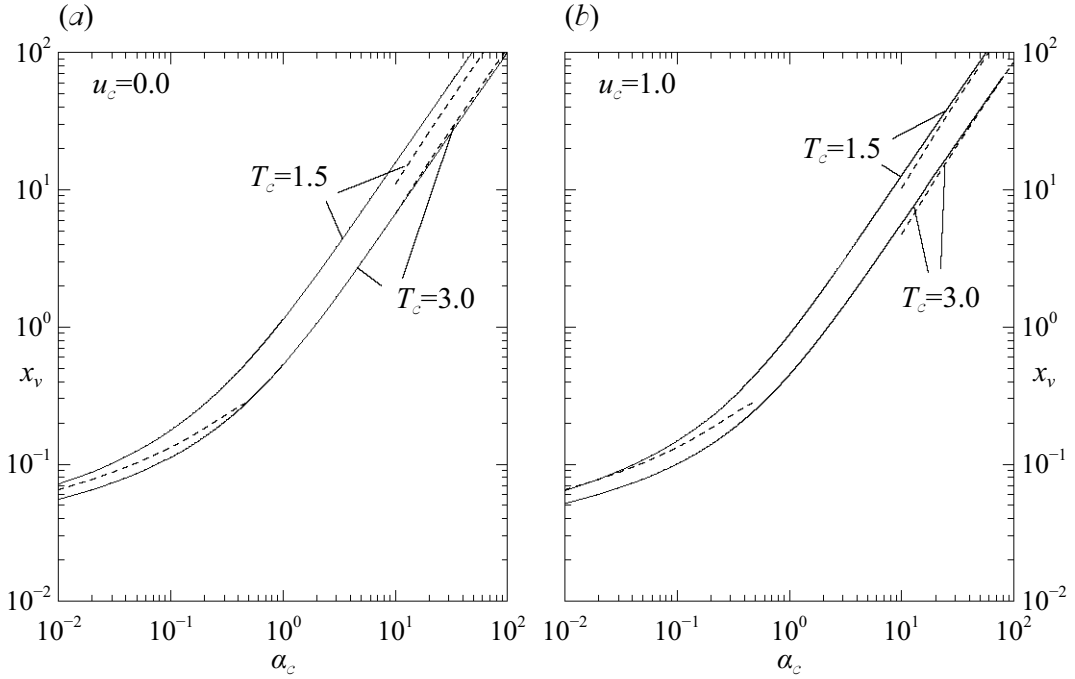


**Figure 3.11:** $(a, b)$ The spray penetration distance $x_v$ obtained in the limit $\varepsilon \to 0$ with $\beta = 0.36$ and $\mathrm{Pr} = 0.7$ for two different values of $T_c$ and $u_c$. The asymptotic leading-order predictions given for $\alpha_c \ll 1$ in (3.80) and for $\alpha_c \gg 1$ in (3.64) are also plotted as dashed curves, with the characteristic distance $\delta$ in the latter being computed from (3.57) for $u_c = 1$ and from (3.65) for $u_c = 0$.

three values of $\varepsilon$ and two different coflow velocities. As expected, the sheath-vaporization limit correctly predicts the penetration distance of sprays with $\varepsilon \ll 1$, with relative errors being typically small (e.g. of the order of 20% for $\alpha_c \sim O(1)$ and $\varepsilon = 0.1$). Values of $x_v$ obtained with the sheath-vaporization reduced problem for different coflow conditions are shown in figure 3.11, where the dashed lines represent the asymptotic predictions to be obtained below for dense and dilute sprays. As expected, vaporization is enhanced for larger values of the coflow temperature, so that the value of $x_v$ decreases for increasing values of $T_c$ for both $u_c = 0$ and $u_c = 1$.

## 3.8 The limit $\alpha_c \gg 1$

For sufficiently dense sprays with $\alpha_c \gg 1$, the vaporization front moves slowly, causing the resulting penetration distance to become much larger than the characteristic distance of jet development. The mixing layer between the emerging jet and the surrounding gas will be considered first, after which the subsequent development of the jet will be addressed.

### 3.8.1 Mixing-layer solution

Initially, the front is embedded in the mixing layer that departs from the injector rim, investigated above in section 3.6.3. In this limiting case, the solution of (3.47) for $\eta < \eta_v$ is in the first approximation $F = \eta$, except in a thin layer $\eta \sim O(\alpha_c^{-1/2})$ that need not be solved to obtain the solution for $\eta > \eta_v$, which is found by integrating (3.45) and (3.46) with boundary conditions $F_\eta - u_c/T_c = T - T_c = 0$ at $\eta \to \infty$ and $F/2 = -T_\eta/\beta$ and $T - 1 = F_\eta - 1 = 0$ at $\eta = 0$. The resulting value of $F(0) = F_+$ can be used in the first equation of (3.49) to obtain the vaporization-layer location according to

$$\eta_v = \alpha_c^{-1} F_+, \tag{3.51}$$

where the constant $F_+$ takes for $\beta = 0.36$ and $T_c = (1.5, 2.15, 3.0)$ the values $F_+ = (-0.6572, -1.0084, -1.2455)$ and $F_+ = (-0.8228, -1.2062, -1.4408)$ for $u_c = 0$ and $u_c = 1$, respectively. On the other hand, the second derivative $F_{\eta\eta}(0) = (F_{\eta\eta})_+$ can be used in (3.50) to obtain $(F_{\eta\eta})_- = (F_{\eta\eta})_+ - \beta F_+/2$, which in turn determines from (3.47) the small departures

$$F - \eta = (\sqrt{\pi}/2)(F_{\eta\eta})_- \alpha_c^{-1} \mathrm{i}^1\mathrm{erfc}[-\alpha_c^{1/2}\eta/(2\sqrt{\mathrm{Pr}})] \tag{3.52}$$

of the stream function for $\eta < \eta_v$, where $\mathrm{i}^1\mathrm{erfc}$ is the first integral of the error function. The prediction for the initial front location given in (3.51) is found to be very accurate, as can be seen in the comparisons of figure 3.9.

### 3.8.2 Leading-order analysis

The vaporization front continues to move slowly as the jet develops, with most of the spray vaporization occurring for $x \sim \delta \gg 1$, where $\delta(\alpha_c)$ is to be determined as part of the asymptotic analysis for $\alpha_c \gg 1$. The terms involving axial derivatives in (3.22)–(3.28) are of order $\delta^{-1}$, as is apparent when the rescaled

coordinate $X = x/\delta$ is introduced. If the corresponding term is neglected in (3.26), integration with boundary condition $v = 0$ at $r = 0$ yields $v = 0$ for $0 < r < r_v$, which can be used in integrating (3.27) and (3.28), also with axial convection neglected, to give the uniform profiles $u = u_v$ and $Y = Y_v$ for $r < r_v$. Note that, across the spray, the departures of $v$ and $Y - Y_v$ from their leading-order values $v = 0$ and $Y = Y_v$ can be expected to be of order $\delta^{-1}$, which is the relative error associated with the axial derivative that has been neglected in integrating (3.26) and (3.28). However, because of the small factor $1/(1 + \alpha_c)$ affecting the viscous force in (3.27), axial-velocity variations $u - u_v$ in this region are much larger, of order $\alpha_c/\delta$, leading to a radial velocity gradient at the vaporization front given by

$$\mathrm{Pr}\left(\frac{\partial u}{\partial r}\right)_- = \frac{\alpha_c}{\delta}\frac{1}{2} r_v u_v \dot{u}_v, \tag{3.53}$$

as can be seen by integrating once (3.27) for $u - u_v \ll 1$. Here, the dot will be used to denote differentiation with respect to the rescaled axial coordinate $X$, so that, for instance, $\dot{u}_v = \mathrm{d}u_v/\mathrm{d}X$ in the above equation. The quasi-steady profiles obtained for $r > r_v$ by neglecting axial convection in (3.22)–(3.25) provide the solution at distances $r - r_v \sim O(1)$ with small errors of order $\delta^{-1}$. Integration of (3.22) gives $\rho r v = -(\alpha_c/\delta) u_v r_v \dot{r}_v$, with the first equation in (3.34) with $v_- = 0$ employed to evaluate the constant value of the radial mass flux. Using this result in integrating (3.24) with boundary conditions $T = 1$ and $(\partial T/\partial r)_+ = -\beta(\alpha_c/\delta) u_v \dot{r}_v$ at $r = r_v$ yields

$$T = \beta (r/r_v)^{-(\alpha_c/\delta) u_v r_v \dot{r}_v} - \beta + 1, \tag{3.54}$$

whereas, at the same level of approximation, integration of (3.23) and (3.25) gives

$$\frac{\alpha_c}{\delta} u_v \dot{r}_v (u - u_v) = -\mathrm{Pr}\left(\frac{\partial u}{\partial r}\right)_+ \left[\left(1 + \frac{T-1}{\beta}\right)^{1/\mathrm{Pr}} - 1\right] \tag{3.55}$$

and

$$Y = 1 - (1 - Y_v)\left(1 + \frac{T-1}{\beta}\right)^{\mathrm{L}} \tag{3.56}$$

when the boundary conditions $u = u_v$ and $\partial u/\partial r = (\partial u/\partial r)_+$ and $Y = Y_v$ and $\partial Y/\partial r = (\alpha_c/\delta) u_c \mathrm{L}(1 - Y_v)\dot{r}_v$ are employed, the latter determined from (3.34) with $(\partial Y/\partial r)_- = 0$.

The equations that determine $r_v(X)$, $u_v(X)$ and $Y_v(X)$ are obtained by matching the quasisteady profiles (3.54), (3.55) and (3.56) with those found in the far-field region, where the effect of axial convection can no longer be neglected in (3.22)–(3.25). For non-zero values of $u_c$, this region corresponds to radial distances of order $r \sim \sqrt{\delta}$, as follows from a simple convection diffusion balance in (3.23)–(3.25). Therefore, matching at leading order requires that $T - T_c$, $u - u_c$ and $Y$ all be small at radial distances of order $r \sim \sqrt{\delta}$. When this condition is used in (3.54), the scaling law

$$\alpha_c \ln(\delta)/\delta = 1 \tag{3.57}$$

follows, along with the leading-order result

$$u_v r_v \dot{r}_v = -2 \ln \alpha_c, \tag{3.58}$$

where

$$\Lambda = 1 + \frac{T_c - 1}{\beta}. \tag{3.59}$$

At the same level of approximation, (3.55) and (3.56) lead to

$$2(u_v - u_c)\dot{r}_v = (\Lambda^{1/\mathrm{Pr}} - 1) r_v \dot{u}_v \tag{3.60}$$

and

$$Y_v = 1 - \Lambda^{-\mathrm{L}}, \tag{3.61}$$

with (3.53) used to evaluate $(\partial u/\partial r)_+ = (\partial u/\partial r)_-$ in deriving (3.60) from (3.55). Straightforward integration of (3.60) with $r_v = 1$ when $u_v = 1$ gives

$$u_v = u_c + (1 - u_c)(r_v^2)^{1/(\Lambda^{1/\mathrm{Pr}} - 1)}, \tag{3.62}$$

which can be substituted into (3.58) to provide an evolution equation for $r_v(X)$, finally yielding

$$4X \ln \Lambda = u_c(1 - r_v^2) + (1 - \Lambda^{-1/\mathrm{Pr}})(1 - u_c)[1 - (r_v^2)^{1/(1 - \Lambda^{-1/\mathrm{Pr}})}] \tag{3.63}$$

upon integration with initial condition $r_v = 1$ at $X = 0$. The rescaled penetration distance $X_v = [1 + (u_c - 1)\Lambda^{-1/\mathrm{Pr}}]/(4 \ln \Lambda)$ follows from setting $r_v = 0$ in the above equation. At leading order, the asymptotic analysis therefore gives

$$x_v = \frac{\delta[1 + (u_c - 1)\Lambda^{-1/\mathrm{Pr}}]}{4 \ln \Lambda}, \tag{3.64}$$

as a prediction for the penetration distance when $u_c \neq 0$, with $\Lambda$ given in (3.59) in terms of $T_c$ and $\beta$ and $\delta \simeq \alpha_c \ln \alpha_c$ determined from (3.57) for a given value of $\alpha_c \gg 1$. This prediction is compared in figure 3.11 with the results of numerical computations of the sheath-vaporization problem for $u_c = 1$, yielding excellent agreement over the range of $\alpha_c$ computed.

The length scale $\delta$ defined in (3.57) is modified when $u_c = 0$, because convection in this case enters farther from the spray, in a region whose characteristic radius can be obtained from the convection diffusion balance $r^2/\ln r \sim \delta$, obtained from (3.23)–(3.25) with $u \sim T - T_c \sim Y \sim 1/\ln r$, a scaling that follows from the asymptotic decay of the quasi-steady profiles (3.54)–(3.56). As a result, at the order computed above, the equation that determines $\delta$ becomes

$$\alpha_c \ln[\delta \ln(\delta)]/\delta = 1, \tag{3.65}$$

which should be used instead of (3.57) when $u_c = 0$. It is easy to see that the rest of the development leading to (3.64) remains identical, so that the leading-order asymptotic prediction for the penetration distance of dense spray jets discharging into a stagnant hot atmosphere is given by (3.64), with $u_c = 0$ and with $\delta$ computed from (3.65), equivalent to $\delta = \alpha_c \ln(\alpha_c \ln \alpha_c)$ at this order. This prediction is compared in figure 3.11($a$) with results of numerical integrations. As can be seen, the resulting accuracy is reasonably good, with departures remaining smaller than 20% for the two values of $T_c$ considered, in agreement with the errors of order $(\ln \delta)^{-1}$ associated with the leading-order asymptotic development. It is worth pointing out that these differences in radial scale between the cases $u_c \sim O(1)$ and $u_c = 0$ were also previously encountered in classical boundary-layer analyses in cylindrical geometries, with the scale for the case $u_c \sim O(1)$ corresponding to that found [10] for the boundary layer developing over a stagnant cylinder and that of the case $u_c = 0$ being related to that used in [11] in his analysis of a cylinder moving in a fluid at rest.

### 3.8.3 Higher-order corrections

The leading-order predictions for $Y_v$, $u_v$ and $r_v$ given in (3.61), (3.62) and (3.63) and the accompanying prediction for $x_v$ given in (3.64) can be improved by introducing expansions for the different variables in increasing powers of $(\ln \delta)^{-1}$. The analysis may employ the results $Y = Y_v$ and $v = 0$ for $r < r_v$ along with the quasi-steady profiles given in (3.54), (3.55) and (3.56) for $0 < r - r_v \sim O(1)$, because the associated errors are of order $\delta^{-1} \ll (\ln \delta)^{-1}$. Matching with the far-field solution beyond the order used in deriving (3.61)–(3.63) must be however considered, along with higher-order corrections to $(\partial u/\partial r)_-$ arising from convective effects for $r < r_v$, with the leading-order result (3.53) being replaced by a more elaborate expression involving powers of $(\ln \delta)^{-1}$. As an example, results are given below for the case $u_c = 1$, for which the required development is simpler, because the solution for the velocity field everywhere reduces to $u = 1$, so that corrections to $r_f$ stem only from higher-order matching of the temperature field with the solution for $r \sim \delta^{1/2}$.

The analysis begins by writing the quasisteady profile (3.54) for $r \sim \delta^{1/2}$ in the form

$$\ln \Lambda + \ln\left(1 + \frac{T - T_c}{\beta \Lambda}\right) = -\frac{1}{2} r_v \dot{r}_v \left[1 + \frac{2}{\ln \delta} \ln\left(\frac{r}{\delta^{1/2} r_v}\right)\right]. \tag{3.66}$$

The vaporization front $r_v$ is determined as an expansion of the form $r_v^2 = A_0 + (\ln \delta)^{-1} A_1 + (\ln \delta)^{-2} A_2 + \ldots$ by matching the temperature profile given above with that encountered in the far field, yielding at leading order $\dot{A}_0 = -4 \ln \Lambda$, which can be integrated with initial condition $A_0(0) = 1$ to give

$$A_0 = 1 - 4X \ln \Lambda, \tag{3.67}$$

corresponding to the leading-order result (3.63) with $u_c = 1$. Investigation of the solution in the far field is required to obtain the first-order correction $A_1$. Observation of (3.66) reveals that $T - T_c \sim (\ln \delta)^{-1}$ for $r \sim \delta^{1/2}$, which justifies the selection of the rescaled temperature

$$\theta = \frac{(\ln \delta)(T - T_c)}{2\beta \Lambda \ln \Lambda} \tag{3.68}$$

for the analysis of the far field in terms of the rescaled radius $R = r/(T_c\delta)^{1/2}$, with the term $T_c^{1/2}$ included in the definition for convenience. The governing equation for the leading-order term in the expansion $\theta = \theta_0 + (\ln\delta)^{-1}\theta_1 + \cdots$ can be seen from (3.24) to be

$$\frac{\partial\theta_0}{\partial X} - \frac{1}{R}\frac{\partial}{\partial R}\left(R\frac{\partial\theta_0}{\partial R}\right) = 0, \tag{3.69}$$

which must be integrated with initial conditions $\theta_0 = 0$ at $X = 0$ and with boundary conditions $\theta_0 = 0$ as $R \to \infty$ and $R\partial\theta_0/\partial R = 1$ as $R \to 0$, the latter following from matching with (3.66). The solution reduces to $\theta_0 = -\frac{1}{2}E_1[R^2/(2X)]$, where $E_1$ is the exponential integral [12], with the simplified form

$$\theta_0 = \ln R + \frac{1}{2}\left[\gamma - \ln(2X)\right] \tag{3.70}$$

applying as $R \to 0$, where $\gamma$ is Euler's constant. Matching (3.70) with (3.66) gives $\dot{A}_1/\dot{A}_0 = \gamma - \ln(2XT_c/A_0)$, which can be integrated with initial condition $A_1(0) = 0$ to provide the first-order correction

$$A_1 = (A_0 - 1)[\gamma - \ln(2T_c) - \ln X] + A_0 \ln A_0. \tag{3.71}$$

Solving now $r_f^2 = A_0 + (\ln\delta)^{-1}A_1 = 0$ for the first two terms in the penetration-distance expansion $X_v = X_{v0} + (\ln\delta)^{-1}X_{v1} + \ldots$ yields $X_{v0} = 1/(4\ln\Lambda)$ and

$$X_{v1} = -X_{v0}[\gamma - \ln(2T_c) - \ln X_{v0}], \tag{3.72}$$

with the former corresponding to the leading-order result (3.64) with $u_c = 1$. The expansion for $X_v$ can be used to write

$$x_v = \frac{\delta}{4\ln\Lambda}\left\{1 - [\gamma - \ln(T_c/2) + \ln(\ln\Lambda)]/\ln(\delta)\right\}, \tag{3.73}$$

as a corrected prediction for $x_v$ when $u_c = 1$. Results obtained with this expression are essentially the same as those shown in figure 3.11 for the leading-order predictions coming from (3.64) until $\alpha_c \simeq 30$ but agree slightly better with the exact solution at smaller values of $\alpha_c$. The accuracy of the corrected prediction is therefore comparable with that found at leading order, with differences between both expressions being small, because the factor $\gamma - \ln(T_c/2) + \ln(\ln\Lambda)$ appearing in the logarithmic correction is not very large for the values of $T_c$ and $\beta$ investigated. Improved accuracy must rely on corrections of order $(\ln\delta)^{-2}$ and smaller, which could be computed by carrying on the present analysis to higher orders, a development not further pursued here and not strongly motivated, in that logarithms of large numbers are not often very large.

### 3.8.4 Influence of the coflow velocity

As can be inferred from the comparisons in figure 3.11, the leading-order analysis describes satisfactorily the reduction in penetration distance associated with increasing values of $T_c$; as expected, increasing

the coflow temperature produces a larger heat flux and therefore reduces the penetration distance, an effect clearly seen in the plots. The dependence of $x_v$ on $u_c$ is somewhat more complicated and deserves further attention.

The leading-order result for $u_c \neq 0$ given in (3.64) predicts a linear increase of $x_v$ with $u_c$. The increasing rate is however not very large for the small value of the latent heat of vaporization $\beta = 0.36$ used here, because the accompanying factor $\Lambda^{-1/\mathrm{Pr}}$ is relatively small. This linear increase, due to spray acceleration, competes with a more subtle effect, coming from modifications to the radial heat flux, not accounted for in the leading-order prediction (3.64). As previously mentioned, in the limit of vanishing coflow velocities, the characteristic radius of the far-field region increases, which in turn reduces the radial heat flux reaching the spray, causing the characteristic spray length $\delta$ to increase from the value determined for $u_c \neq 0$ in (3.57) to the value given by (3.65). Since this additional effect is not accounted for in the leading-order analysis for $u_c \neq 0$, as $u_c$ is decreased the value of $x_v$ obtained from (3.57) and (3.64) approaches a limiting value below the asymptotic prediction for $u_c = 0$, determined with use made of (3.65). This is seen in figure 3.12, which compares results of integrations of the sheath-vaporization problem for $\alpha_c = 100$ and different values of $u_c$ with the asymptotic predictions for $u_c = 0$ and for $u_c \neq 0$.

As can be seen in the figure, the numerical integrations of the sheath-vaporization problem exhibit the increase of $x_v$ for decreasing $u_c$ discussed above, contrary to the prediction obtained by use of (3.57) in (3.64), which agrees with the numerical results only at values of $u_c$ appreciably larger than those of the figure. This effect can be captured in the asymptotic solution for $u_c \sim O(1)$ by incorporating corrections to (3.64), of order $(\ln \delta)^{-1}$. Although the required analysis is not attempted here, it is relatively easy to extract the dependence on $u_c$ of the resulting correction term by studying the asymptotic development given in section 3.8.3 for the special case $u_c = 1$. As can be anticipated, in the modified analysis for $u_c \neq 1$, the far-field temperature solution should incorporate the value of $u_c$ in the definition of the radial coordinate $R = r/(T_c\delta/u_c)^{1/2}$. With this definition, the far-field equation for the temperature would reduce to (3.69) and matching the resulting solution with the inner quasisteady temperature field would produce a term $-\ln(2T_c/u_c)$ as a replacement for $-\ln(2T_c)$ in (3.71) and also in (3.72). The associated correction $\ln(u_c)/\ln(\delta)$ can be incorporated when writing (3.64) to give $x_v = [\delta/(4\ln\Lambda)][1 + (u_c - 1)\Lambda^{-1/\mathrm{Pr}} - \ln(u_c)/\ln(\delta)]$, with $\delta$ and $\Lambda$ evaluated from (3.57) and (3.59) respectively. The comparisons shown in figure 3.12 indicate that this corrected expression improves significantly the accuracy of the asymptotic limit $\alpha_c \gg 1$ over the range of $u_c$ shown in the figure, with the logarithmic correction providing the increase in $x_v$ found numerically as $u_c \to 0$. Additional analysis of the distinguished limit $u_c \sim 1/\ln\delta$ could provide the transition between the asymptotic analyses for $u_c \sim O(1)$ and the limiting result for $u_c = 0$ in dense sprays.

## 3.9 The limit $\alpha_c \ll 1$

For sufficiently dilute sprays with $\alpha_c \ll 1$, the amount of heat required to vaporize the spray and the resulting mass addition to the gas stream are both small, so that the solution for the gas temperature and fuel mass fraction is only weakly affected by the vaporization process. The heat flux coming from the coflow easily vaporizes the spray, yielding in the sheath-vaporization regime a vaporization front

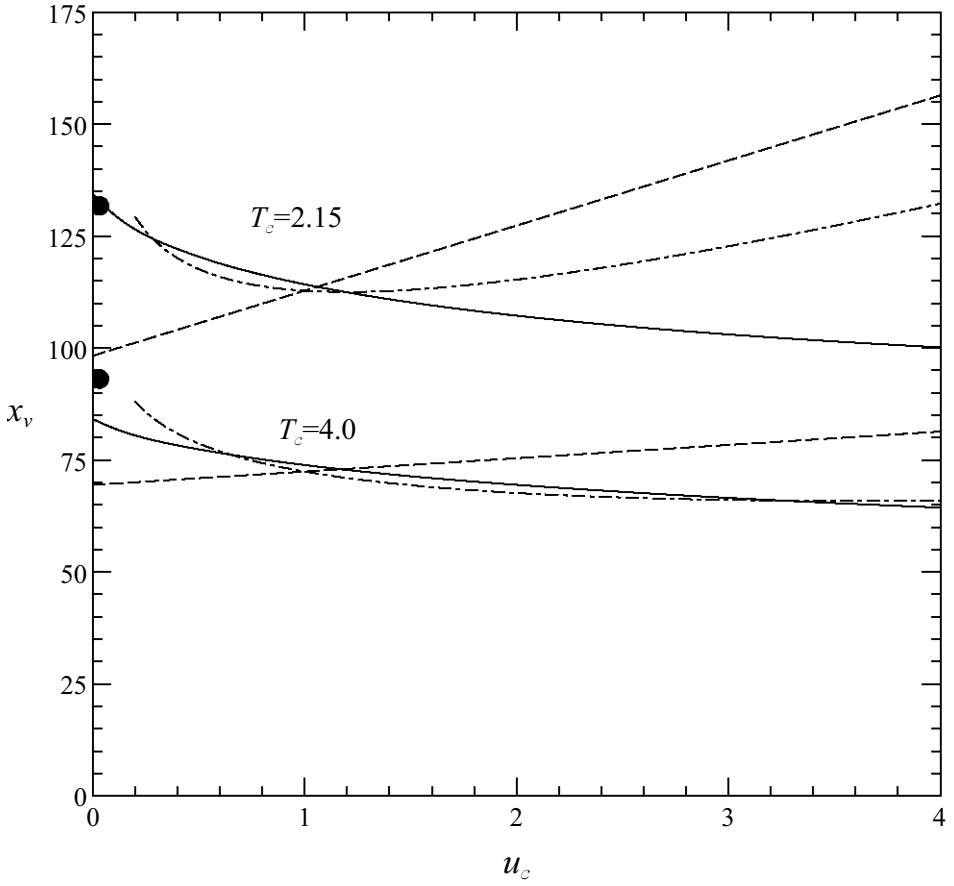


**Figure 3.12:** The spray penetration distance $x_v$ obtained in the limit $\varepsilon \to 0$ with $\beta = 0.36$, $\mathrm{Pr} = 0.7$, and $\alpha_c = 100$ for $T_c = (2.15, 4.00)$ and increasing values of $u_c$. The dashed and dot-dashed curves represent the leading-order prediction $x_v = [\delta/(4\ln\Lambda)][1 + (u_c - 1)\Lambda^{-1/\mathrm{Pr}}]$ and the corrected value $x_v = [\delta/(4\ln\Lambda)][1 + (u_c - 1)\Lambda^{-1/\mathrm{Pr}} - \ln(u_c)/\ln(\delta)]$ with $\delta$ and $\Lambda$ evaluated from (3.57) and (3.59), while the solid dot denotes the prediction $x_v = [\delta/(4\ln\Lambda)][1 - \Lambda^{-1/\mathrm{Pr}}]$ for $u_c = 0$, with $\delta$ evaluated from (3.65).

that propagates rapidly into the spray jet to complete vaporization at a short distance $x_v \ll 1$. Initially, the vaporization front lies on the innermost side of the annular mixing layer that forms downstream from the injector rim, at a location $-\eta_v \gg 1$. On the outer side corresponding to $\eta > \eta_v$, the solution is determined in the first approximation by integration of (3.45), (3.46) and (3.48) with boundary conditions $F_\eta - u_c/T_c = T - T_c = Y = 0$ as $\eta \to \infty$ and $F - \eta = T - 1 = Y - Y_j = 0$ as $\eta \to -\infty$, giving a temperature profile that decays towards the spray side according to

$$T - 1 = -C\exp(-\eta^2/4)/\eta, \tag{3.74}$$

where the constant $C$ is obtained as part of the integration, giving for $T_c = (1.5, 2.15, 3.0)$ the values $C = (0.1404, 0.2764, 0.4082)$ for $u_c = 0$ and $C = (0.1948, 0.3624, 0.5275)$ for $u_c = 1$, respectively. This vaporization-free solution fails as the vaporization front is approached for $\eta - \eta_v \sim -\eta_v^{-1} \ll 1$

where $T-1 \ll 1$ and $F-\eta_v \ll 1$. Introducing the stretched coordinate $\zeta = -\eta_v(\eta-\eta_v)/2$ reduces the description of the temperature to the integration of $T_{\zeta\zeta} - T_\zeta = 0$ with boundary conditions $T-1 = T_\zeta - \beta\alpha_c = 0$ at $\zeta = 0$ and $T-1 \to -C[\exp(-\eta_v^2/4)/\eta_v]e^\zeta$ at $\zeta \to \infty$. Integrating once with the boundary conditions at $\zeta = 0$ yields $T_\zeta - T = \beta\alpha_c - 1$, and a second integration provides $T-1 = -\beta\alpha_c - C[\exp(-\eta_v^2/4)/\eta_v]e^\zeta$. The condition $T = 1$ at $\zeta = 0$ then gives

$$\beta\alpha_c = -C\exp(-\eta_v^2/4)/\eta_v, \tag{3.75}$$

to determine $\eta_v$ as a function of $\beta$ and $\alpha_c$. The accuracy of this asymptotic prediction is very satisfactory, as can be seen in figure 3.9.

As the vaporization front moves into the jet outside the annular mixing layer, effects of curvature enter to modify the heat flux that reaches the vaporization front from outside. In the intermediate region that lies between the mixing layer and the vaporization front, corresponding to radial distances such that $\sqrt{x} \ll 1-r < 1-r_v$, the temperature and velocity differ by exponentially small amounts from the initial jet values $T = 1$ and $u = 1$, whereas the radial velocity is given simply by $v = \partial T/\partial r$, as can be seen by integrating (3.24) with $u = 1$ and with $\alpha_c = 0$ used in (3.34) when evaluating the boundary values $v_+$ and $(\partial T/\partial r)_+$. Introducing this result into (3.22) provides the linear heat equation

$$\frac{\partial T}{\partial x} - \frac{1}{r}\frac{\partial}{\partial r}\left(r\frac{\partial T}{\partial r}\right) = 0 \tag{3.76}$$

which is to be integrated with the boundary condition $T = 1$ at $r = r_v$ and subject as $r \to 1$ to the matching condition with the mixing-layer solution given in (3.74). In the first approximation, the solution is given by

$$T-1 = C\sqrt{x}\left\{\frac{\exp[-(r-1)^2/(4x)]}{r^{1/2}(1-r)} - \frac{\exp[-(r_v-1)^2/(4x)]}{r_v^{1/2}(1-r_v)}\right\}, \tag{3.77}$$

with sample values of $C$ given below (3.74). Using now the additional boundary condition $\partial T/\partial r = -\beta\alpha_c(\mathrm{d}r_v/\mathrm{d}x)$ at $r = r_v$, obtained from (3.34) with $u_v = 1$, provides

$$\frac{C\exp[-(r_v-1)^2/(4x)]}{2r_v^{1/2}\sqrt{x}} = -\beta\alpha_c\frac{\mathrm{d}r_v}{\mathrm{d}x}, \tag{3.78}$$

as an evolution equation for $r_v(x)$, which can be approximately solved for small values of $\alpha_c$ to give

$$r_v = 1 - 2\left(x\ln\left\{\frac{\alpha_c^{-1}}{[\ln(\alpha_c^{-1})]^{1/2}}\right\}\right)^{1/2}. \tag{3.79}$$

According to (3.79), the penetration distance for dilute sprays

$$x_v = \left(4\ln\left\{\frac{\alpha_c^{-1}}{[\ln(\alpha_c^{-1})]^{1/2}}\right\}\right)^{-1}, \tag{3.80}$$

obtained from (3.79) with $r_v = 0$, depends only on the parameter $\alpha_c$, all other parameters, including the velocity and temperature in the coflow, entering only in determining the higher-order corrections. Also of interest is that the modifications associated with curvature do not affect the solution at the order displayed in (3.80) in that the same prediction for the penetration distance is obtained by setting $r_v$ equal to zero in $\eta_v = (r_v - 1)/\sqrt{x}$, derived above as the location of the vaporization front within the annular mixing layer that departs from the injector rim, with $\eta_v$ determined by solving (3.75) for $\alpha_c \ll 1$. The prediction (3.80) is tested in figure 3.10, giving good agreement for the different conditions considered.

## 3.10 Conclusions

For a laminar, equilibrium, monodisperse fuel spray emerging steadily at a constant velocity from a round tube into a hot, chemically inert coflowing stream having a different constant velocity but the same molecular weight as the gas in the spray tube, the axisymmetric two-fluid conservation equations that account for finite-rate, diffusion-controlled evaporation and Stokes drag of spherical droplets in an ideal gas were integrated numerically to demonstrate explicitly the development of a regime of sheath vaporization as the ratio of the characteristic time of jet evolution associated with spray vaporization to the characteristic time for transverse diffusion across the jet approaches zero. This sheath-vaporization regime develops irrespective of whether the ratio of the mass of liquid to the mass of gas in the spray stream is large or small. If that ratio is large, then sample computations for octane sprays in air with a Lewis number of unity show explicitly that the fuel jet initially expands appreciably, its outer boundary being determined by the trajectory of the outermost droplet, until that droplet is completely vaporized, after which the outer boundary contracts, increasingly rapidly as the tip of the spray is approached. If, on the other hand, that mass ratio is small, then there is very little initial expansion of the jet, the shape of which now resembles a pointed icicle, much shorter than the jet for high liquid mass ratio because of the smaller amount of liquid to be vaporized.

In the limit of sheath vaporization, the initial expansion of the jet no longer occurs, there being a narrow vaporization layer, across which jump conditions are derived, connecting solutions of outer droplet-free differential equations to solutions of inner partial differential equations that describe the velocity and gas-phase fuel-concentration fields of the spray, the other variables there retaining their tube-exit values in the first approximation. The resulting free-boundary problem was also integrated numerically, making use of a mixing-layer solution near the injector rim, obtained numerically as well, to provide the necessary initial conditions for this parabolic problem. The numerical results give, for example, the jet penetration length as a function of the liquid-to-gas mass ratio of the spray for various ratios of coflow-to-spray temperatures and velocities, explicitly exhibiting the decrease in jet width and the increase in jet penetration length with increasing liquid-to-gas mass ratio.

Analytical formulae derived for the jet penetration distance in the dense-spray (large liquid-to-gas mass ratio) and dilute-spray (small liquid-to-gas mass ratio) limits agree reasonably well with the numerical results in those limits. In the dilute-spray limit, the penetration length is proportional to the product of the jet exit velocity and the transverse diffusion time, the proportionality constant depending only on the ratio of the liquid mass to the gas mass in the spray and increasing only weakly

(inverse logarithmically) as this ratio increases. It is noteworthy that, in this limit, the penetration distance is entirely independent of the properties of the coflow stream at leading order, being controlled completely by the properties and dimensions of the lightly liquid-loaded spray.

If the coflow velocity is small enough, then the same proportionality of penetration length to the product of the jet exit velocity and transverse diffusion time occurs in the dense-spray limit as well (and therefore for all ratios of liquid-to-gas mass), but the proportionality constant increases much more strongly with increasing liquid-to-gas mass ratios (namely, in proportion to the product of this ratio with its logarithm) and, in addition, depends (relatively weakly) on the coflow temperature and the Prandtl number, decreasing as either of these increases. On the other hand, if the coflow velocity is sufficiently large, then in the dense-spray limit the penetration distance is independent of the initial jet velocity but instead is proportional to the product of the coflow velocity and the transverse diffusion time, the proportionality constant again increasing more strongly with the liquid-to-gas mass ratio, and while it still decreases slowly with increasing coflow temperature, now its dependence on the Prandtl number is reversed. These last dependences, however, apply only for rather large coflow velocities, and at smaller coflow velocities the penetration length actually decreases with increasing coflow velocity, counterintuitively, as a consequence of a decrease in the coflow velocity producing an increase in the radial distance over which external heat conduction occurs, through reduction of entrainment, thereby decreasing the rate of heat transfer to the spray from the surrounding hot gas.

The results, in general, improve our knowledge of fuel-spray jet structure and penetration. Although formally restricted to steady laminar flow, qualitative interpretations for turbulent flows may be achieved by replacing the laminar viscosity by a turbulent viscosity, so long as the development of the spray is not significantly influenced by wall boundary layers and recirculation, for example. The regime of sheath vaporization, in particular, is often likely to be encountered in practice, and the present results may aid in insights into phenomena to be expected in that regime.

# References

[1] G. Chen, A. Gomez, Dilute laminar spray diffusion flames near the transition regime from group combustion to individual droplet burning, Combust. Flame 110 (1997) 392–404.

[2] A. N. Karpetis, A. Gomez, An experimental study of well-defined turbulent non-premixed flames, Combust. Flame 121 (2000) 1–23.

[3] S. Russo, A. Gomez, Physical chracterization of laminar spray flames in the pressure range 0.1-0.9 MPa, Combust. Flame 145 (2006) 339–356.

[4] S. M. Correa, M. Sichel, The boundary layer structure of a vaporizing fuel cloud, Combust. Sci. Tech. 28 (1982) 121–130.

[5] H. H. Chiu, R. Ahluwalia, B. Koh, E. J. Croke, Spray group combustion, AIAA 16th Aerospece sciences meeting.

[6] H. Y. Kim, H. H. Chiu, Group combustion of liquid fuel sprays, AIAA paper 83-0150.

[7] H. H. Chiu, T. Liu, Group combustion of liquid droplets, Combust. Sci. Tech. 17 (1977) 127–142.

[8] M. Labowsky, D. E. Rosner, Group combustion of droplets in fuel clouds, i. quasi-steady predictions, in: J. T. Zung (Ed.), Evaporation-Combustion of Fuels, Americal Chemical Society, 1978, pp. 63–79.

[9] S. M. Correa, M. Sichel, The group combustion of a spherical cloud of monodisperse fuel droplets, Proc. Combust. Inst. 19 (1982) 981–991.

[10] M. B. Glauert, M. J. Lighthill, The axisymmetric boundary layer on a long thin cylinder, Prog. Roy. Soc. Lon. A 230 (1955) 188–203.

[11] L. J. Crane, Boundary layer flow on a circular cylinder moving in fluid at rest, J. Appl. Math. Phys. (ZAMP) 23 (1972) 201–212.

[12] M. Abramowitz, I. A. Stegun, Handbook of Mathematical Functions, Dover Publications Inc., New York, 1965.

CHAPTER
**FOUR**

# Nonpremixed combustion of a hollow cone spray

## 4.1 Introduction

The preceding Burke-Schumann formulation can be used in direct numerical simulations of spray diffusion flames. It can also serve as a starting point in modeling strategies addressed to two-phase turbulent flows. As a simplified illustrative example, the coupling-function formulation is used here to analyze the combustion of a conical spray issuing from a swirl atomizer, as sketched in figure 4.1. The thin liquid sheet issuing from the injector rim opens up as a result of the initial swirling motion to form downstream a trumpet-like sheet. As the azimuthal velocity component decays, a conical sheet of semiangle $\varphi$ is formed [1], as illustrated in figure 4.2. The thickness of the resulting liquid sheet, moving with constant streamwise velocity, decreases due to flow divergence until it eventually breaks up as a result of fluid-mechanical instabilities, forming a hollow-cone spray that vaporizes, mixes and reacts with the outer gas streams, as shown schematically in figure 4.1, where the plot depicts the flow structure appearing in the limit of infinitely fast chemistry.

In the highly simplified analysis that follows, the initial conical liquid-fuel sheet issuing from the injector dissintegrates into droplets at a given breakup distance $l'_{\text{BU}}$, producing a monodisperse spray that is assumed to be steady, axisymmetric and slender. We shall also assume that the velocity of the air coflow, possibly including significant swirling motion in many applications, is small, behaving as a stagnant air atmosphere. Inside the hollow cone, there exists a recirculating stream of hot products, also with small velocity, that contains a nonnegligible amount of fuel vapor, as occurs typically in rich-quench-lean combustion applications [2]. Significant gas motion occurs only in a thin boundary-layer region surrounding the fuel sheet and the spray.

The hot product stream is assumed to be at temperature $T_P$, of the order of, although smaller than, the characteristic flame temperature $T_f = T_A + q/[c_p(1+S)]$ defined above in (2.21), whereas the air feed stream is assumed to be at temperature $T_A$, often somewhat larger than the normal ambient temperature (e.g, because of upstream adiabatic compression in gas-turbine applications). These elevated gas-flow temperatures $T_P$ and $T_A$ are responsible for the initial heating and vaporization of the liquid fuel and also for the autoignition of the resulting fuel-air mixture, leading to the formation of a diffusion flame, where the vaporizing fuel reacts with the surrounding oxygen. Since no significant vaporization can be expected to occur prior to atomization, the diffusion flame originates near the position of droplet formation by liquid-sheet breakup, $l' = l'_{\text{BU}}$. The resulting nonpremixed flame is thin and can be computed accurately in the limit of infinitely fast reaction, except near $l' = l'_{\text{BU}}$, in

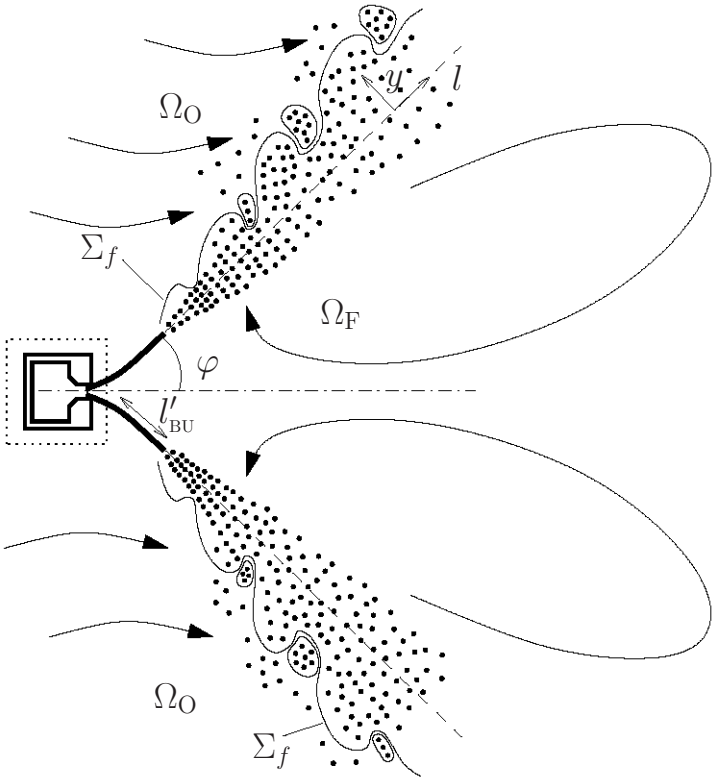


**Figure 4.1:** Schematic illustration of a diffusion flame in a swirl-atomizer spray combustor.

the flame-base region where autoignition and premixed combustion are present. The treatment of finite-rate effects in this near-field solution is not considered in the following analysis, which focuses instead on the application of the coupling-function formulation for the description of the downstream region of diffusion-flame development. Moreover, to exhibit essentials of the methods without excessive clutter and with a minimum number of parameters that need to be addressed, additional simplifying assumptions, such as Lewis numbers of unity, will be adopted. Although it has been emphasized in the formulation that Lewis-number effects are important in practice, their inclusion merely complicates the calculations by increasing the number of equations but does not affect the methods.

## 4.2 Characteristic scales and dimensionless variables

A hollow-cone monodisperse spray, with droplets of initial radius $a_o$, is assumed to be formed at $l' = l'_{\mathrm{BU}}$ as a result of the breakup of the conical liquid sheet of density $\rho_l$. It is considered that, because of upstream liquid-sheet heating, the initial droplet temperature equals the boiling value $T_B$, thereby enabling droplet vaporization to begin inmediately following atomization. The distribution of initial droplet velocities, with values typically comparable to that of the liquid sheet, depends on the details of the atomization process, which may involve different physical mechanisms depending on the injection

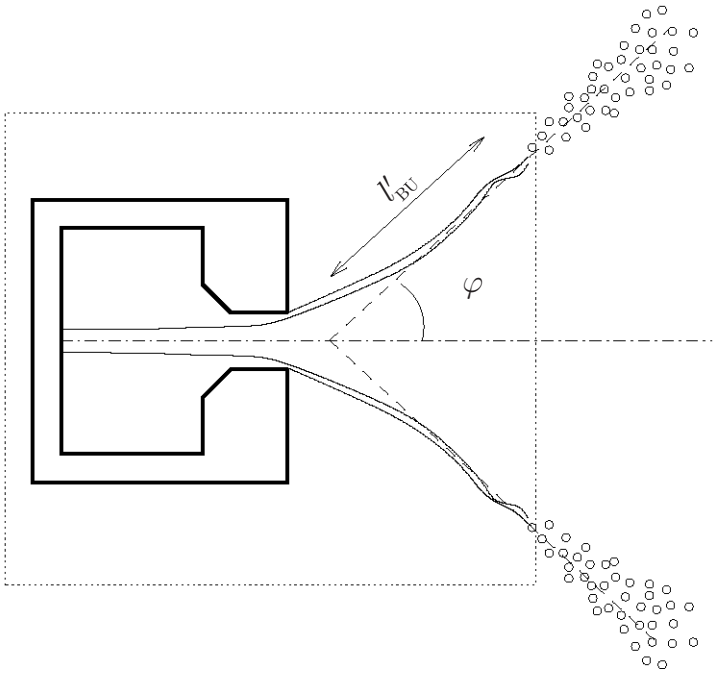


**Figure 4.2:** Illustration of the model of the swirl atomizer [1].

conditions, as discussed in [3]. In the simplified analysis given here, all droplets are assumed to have the same streamwise velocity at the atomization point, with a value $u_o$ equal to that of the conical sheet upstream from the breakup point. Besides $u_o$ and $a_o$, the other parameter characterizing the spray is the value of the liquid volume flux $Q$ defining the total number of droplets injected per unit time $\dot{N} = Q/[(4/3)\pi a_o^3]$.

The conical spray will be treated as slender, in the sense that the transverse coordinate $y'$ will be assumed to be small compared to the distance $l'$ to the vertex of the cone, so that the flow will be described with the steady boundary-layer approximation. The injector size is assumed to be much smaller than the breakup length of the liquid sheet, $l'_{\rm BU}$, which is turn is assumed to be comparable to the length of spray vaporization. Relevant length and time scales for the problem are associated with the droplet response, with comparable time scales emerging for vaporization and acceleration. In the formulation below, the Stokes time, or characteristic droplet acceleration time,

$$t_d = \frac{2}{9}\frac{a_o^2 \rho_l}{\mu_f}, \tag{4.1}$$

obtained from a straightforward order-of-magnitude balance in (2.13) with the drag force given in (2.15), is selected to define the characteristic values of the length and thickness of the conical spray $u_o t_d$ and $(\nu_f t_d/\rho_f)^{1/2}$, to be used in defining dimensionless coordinates $l = l'/(u_o t_d)$ and $y = y'/(\nu_f t_d)^{1/2}$, giving an order-unity value for the dimensionless breakup length $l_{\rm BU} = l'_{\rm BU}/(u_o t_d)$. The subscript $f$ will be used here to denote gas properties evaluated at the characteristic flame temperature $T_f$, with

$\nu_f = \mu_f/\rho_f$ representing for instance the gas kinematic viscosity at that temperature. Using the condition of conservation of the flux of droplets in the conical spray, together with the characteristic spray thickness $(\nu_f t_d)^{1/2}$, yields

$$n_c = \frac{\dot{N}}{2\pi \sin\varphi t_d u_o^2 (\nu_f t_d)^{1/2}} \tag{4.2}$$

as the characteristic value of the number of droplets per unit volume. This value will be used below in defining a dimensionless droplet number density $n$, whereas the droplet radius will be scaled with $a_o$. The streamwise and transverse velocity components will be scaled with $u_o$ and $(\nu_f/t_d)^{1/2}$, yielding $(u, v)$ and $(u_d, v_d)$ for the dimensionless gas-phase and liquid-phase velocity components, respectively.

The characteristic flame temperature $T_f$ and the associated density $\rho_f$ will be used as scales for the dimensionless temperature $\theta$ and density $\rho$, giving, for instance, $\theta_A = T_A/T_f < 1$ and $\theta_P = T_P/T_f < 1$ for the boundary gas temperatures on the air and products sides of the spray. Correspondingly, the characteristic dilution parameter $\alpha_c$ is defined with $\rho_c = \rho_f$ in (1.1). Variations of the mean molecular weight will be neglected, thereby reducing the equation of state (2.9) to

$$\rho\theta = 1. \tag{4.3}$$

A power law will be assumed for the temperature dependence of the different transport properties, according to

$$\frac{\mu}{\mu_f} = \frac{\kappa}{\kappa_f} = \theta^\sigma. \tag{4.4}$$

The analysis will use $\sigma = 0.7$ and a constant specific heat $c_p$, giving a constant Prandtl number $\mathrm{Pr} = c_p\mu/\kappa$, with the value $\mathrm{Pr} = 0.7$ employed in the numerical integrations. Also, unity values of the reactant Lewis numbers are assumed, implying that a reduced description with $Z = \tilde{Z}$ and $H = \tilde{H}$ applies, with the excess-enthalpy variable being scaled with $c_p T_f$ for consistency of the dimensionless formulation to give

$$H = \theta - \theta_A + (\hat{Y}_\mathrm{O} - 1)\bar{q}/S, \tag{4.5}$$

where $\bar{q} = q/(c_p T_f)$. The same scale $c_p T_f$ will be used for the factor $q/S + L_v + c_p(T_A - T_B)$ appearing in (2.27) to give

$$\gamma = \bar{q}/S + l_v + \theta_A - \theta_B \tag{4.6}$$

where $l_v = L_v/(c_p T_f)$.

## 4.3 Conservation equations

For moderately large values of the spray Reynolds number $u_o^2 t_d/\nu_f$, the resulting slender flow remains steady and can be consequently described in the boundary-layer approximation. In terms of the

dimensionless variables defined above, the gas-phase continuity and momentum equations become

$$\frac{1}{l}\frac{\partial}{\partial l}(\rho l u) + \frac{\partial}{\partial y}(\rho v) = \alpha_c n \dot{m} \tag{4.7}$$

$$\frac{1}{l}\frac{\partial}{\partial l}(\rho l u^2) + \frac{\partial}{\partial y}(\rho v u) = \frac{\partial}{\partial y}\left(\theta^\sigma \frac{\partial u}{\partial y}\right) + \alpha_c n \dot{m} u_d + \alpha_c \theta^\sigma a n (u_d - u), \tag{4.8}$$

while the evolution equations for the mixture fraction $Z$ and excess enthalpy $H$ reduce to

$$\frac{1}{l}\frac{\partial}{\partial l}(\rho l u Z) + \frac{\partial}{\partial y}(\rho v Z) = \frac{1}{\mathrm{Pr}}\frac{\partial}{\partial y}\left(\theta^\sigma \frac{\partial Z}{\partial y}\right) + \alpha_c n \dot{m} \tag{4.9}$$

and

$$\frac{1}{l}\frac{\partial}{\partial l}(\rho l u H) + \frac{\partial}{\partial y}(\rho v H) = \frac{1}{\mathrm{Pr}}\frac{\partial}{\partial y}\left(\theta^\sigma \frac{\partial H}{\partial y}\right) - \alpha_c \gamma n \dot{m}, \tag{4.10}$$

to be integrated together with the liquid-phase conservation equations (2.10) and (2.12)–(2.13), which take the dimensionless form

$$\frac{1}{l}\frac{\partial}{\partial l}(n l u_d) + \frac{\partial}{\partial y}(n v_d) = 0, \tag{4.11}$$

$$u_d \frac{\partial a^3}{\partial l} + v_d \frac{\partial a^3}{\partial y} = -\dot{m}, \tag{4.12}$$

$$u_d \frac{\partial u_d}{\partial l} + v_d \frac{\partial u_d}{\partial y} = \frac{\theta^\sigma}{a^2}(u - u_d), \tag{4.13}$$

$$u_d \frac{\partial v_d}{\partial l} + v_d \frac{\partial v_d}{\partial y} = \frac{\theta^\sigma}{a^2}(v - v_d). \tag{4.14}$$

Droplet heating need not be described, since the droplets are assumed to be released at the boiling temperature, so that the condition $T_d = T_B$ replaces in the computation the integration of (2.11), with $\dot{q}_d = 0$ employed in writing (4.10).

In dimensionless form, the vaporization rate (2.17) yields

$$\dot{m} = \frac{2a\theta^\sigma}{3\mathrm{Pr}} \ln\left(1 + \frac{\theta - \theta_B}{l_v}\right), \tag{4.15}$$

corresponding to droplets vaporizing on the fuel side of the flame. The relationships (2.26) are to be used to compute the reactant mass fractions. Similarly, the temperature is determined from (2.28), written in the dimensionless form

$$\begin{cases} \theta - \theta_A = H + \bar{q}/S & \text{if} \quad Z \geq Z_s \\ \theta - \theta_A = H + (Z/Z_S)\bar{q}/S & \text{if} \quad Z \leq Z_s \end{cases} . \tag{4.16}$$

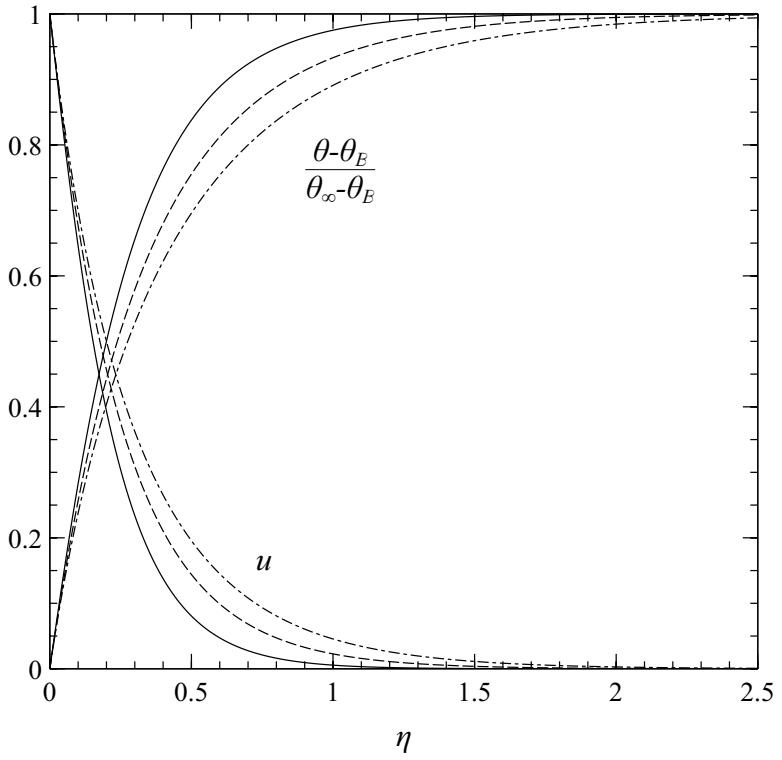


**Figure 4.3:** Self-similar boundary-layer profiles of streamwise velocity and temperature obtained with $\mathrm{Pr} = 0.7$ and $\sigma = 0.7$ by integration of (4.17) and (4.18) for $\theta_\infty/\theta_B = (1.5)$ (solid curves), $\theta_\infty/\theta_B = (2.5)$ (dashed curves), and $\theta_\infty/\theta_B = (3.5)$ (dot-dashed curves).

## 4.4 Boundary and initial conditions

The boundary conditions for the gas velocity, $u = 0$ as $y \to \pm\infty$ and $v = 0$ at $y = 0$, follow from assuming that the gas motion outside is induced only by the spray entrainment and that $y = 0$ is a stream surface, the latter being an arbitrary selection consistent with the boundary-layer approximation. No fuel is present in the air stream, so that $Z = 0$ as $y \to +\infty$. Inside the conical spray, the recirculating mixture of hot products contains vapor fuel with mass fraction $Y_{\mathrm{F}_P}$, giving $Z = Z_P = (SY_{\mathrm{F}_P} + 1)/(1 + S) > Z_s$ for the boundary value of the mixture fraction as $y \to -\infty$. Correspondingly, the boundary conditions for dimensionless excess enthalpy (4.5) are given by $H = 0$ as $y \to \infty$ and $H = H_P = \theta_P - \theta_A - \bar{q}S$ as $y \to -\infty$.

Upstream from the breakup point $l = l_{\mathrm{BU}}$ the liquid sheet sets the surrounding gas in motion, leading to the formation of two boundary layers that develop independently on each side of the sheet. The solutions for these boundary layers determine the initial profiles of velocity and temperature found at $l = l_{\mathrm{BU}}$, to be used in the integration of the spray problem for $l > l_{\mathrm{BU}}$. These boundary layers do not affect the liquid-sheet velocity in the first approximation, so that the boundary condition $u = 1$ at $y = 0$ applies for the gas velocity. Vaporization upstream from the breakup point will be neglected, along with variation of the liquid-sheet temperature, yielding the simplified boundary

condition $\theta = \theta_B$ at $y = 0$, a good approximation when the liquid-injection temperature is close to the boiling temperature, as is typically the case in applications. With these simplifications the resulting boundary-layer solution for the gas flow is selfsimilar. In terms of the stream function $l^{3/2}F(\eta)$, defined such that $\rho u = F_\eta$ and $\rho v = l^{-1/2}(\frac{1}{2}\eta F_\eta - \frac{3}{2}F)$, with the subscript $\eta$ denoting differentiation with respect to the self-similar coordinate $\eta = |y|/\sqrt{l}$, the problem reduces to that of integrating the momentum and energy conservation equations

$$\left[\theta^\sigma \left(F_\eta/\rho\right)_\eta\right]_\eta + (3/2)F\left(F_\eta/\rho\right)_\eta = 0 \tag{4.17}$$

$$(\theta^\sigma \theta_\eta)_\eta + (3/2)\mathrm{Pr}F\theta_\eta = 0 \tag{4.18}$$

with boundary conditions $F = F_\eta - 1 = \theta/\theta_B - 1 = 0$ at $\eta = 0$ and $F_\eta = \theta/\theta_B - \theta_\infty/\theta_B = 0$ as $\eta \to \infty$, where $\theta_\infty$ denotes the dimensionless free-stream temperature. The resulting solution, shown in figure 4.3 for different values of the parameter $\theta_\infty/\theta_B$, can be used to evaluate the initial profiles of velocity and temperature at $l = l_{\mathrm{BU}}$, with $\theta_\infty = \theta_A$ and $y = l_{\mathrm{BU}}^{1/2}\eta$ for $y > 0$ and $\theta_\infty = \theta_P$ and $y = -l_{\mathrm{BU}}^{1/2}\eta$ for $y < 0$. The corresponding initial profile for the mixture fraction is given by $Z = 0$ for $y > 0$ and $Z = Z_P$ for $y < 0$, while the initial profile for $H$ can be computed from (4.5) in terms of the temperature profile, with $\hat{Y}_{\mathrm{O}} = 1$ for $y > 0$ and $\hat{Y}_{\mathrm{O}} = 0$ for $y < 0$.

In the initial region $l - l_{\mathrm{BU}} \ll 1$, the force acting on and the vaporization rate of the droplets have a negligible effect on the droplet evolution, so that each droplet maintains the initial values of its radius $a = 1$ and velocity $u_d = 1$ as follows from (4.12) and (4.13). With $u_d = 1$ and negligible drag force, the conservation of droplet transverse momentum (4.14) indicates that $v_d$ is conserved along the trayectories $\mathrm{d}y/\mathrm{d}l = v_d$, which are therefore straight lines with $v_d = y/(l - l_{\mathrm{BU}})$, thereby providing the initial condition for $v_d$ as well as the characteristic spray thickness $y \sim l - l_{\mathrm{BU}}$. On the other hand, the droplet number density in this region is a large quantity of order $(l - l_{\mathrm{BU}})^{-1}$, as follows from the integral conservation equation

$$l\int_{-\infty}^{+\infty}(nu_d)\mathrm{d}y = 1, \tag{4.19}$$

obtained by integration of (4.11) across the spray. The corresponding droplet distribution, given by

$$n = \frac{\mathcal{N}(\xi)}{l_{\mathrm{BU}}(l - l_{\mathrm{BU}})}, \tag{4.20}$$

includes an arbitrary shape function $\mathcal{N}$ of the rescaled coordinate $\xi = y/(l - l_{\mathrm{BU}})$ that depends in general on the atomization process, the only constraint being $\int_{-\infty}^{+\infty}\mathcal{N}\mathrm{d}\xi = 1$ as dictated in this region by the droplet conservation law (4.19). The function

$$\mathcal{N} = \frac{\exp[-(\xi/\delta)^2]}{\delta\sqrt{\pi}} \tag{4.21}$$

was tested in the numerical integrations, with a scaling factor $\delta$ used to characterize the initial spray thickness. For the concentrated sprays considered here, this parameter was seen to exert a negligible

influence on the vaporization and combustion processes, in that numerical integrations employing different values in the range $0.1 < \delta < 5$ gave virtually the same solution away from the breakup point.

## 4.5 Numerical results

Integration of (4.7)–(4.10) and (4.11)–(4.14) with the initial and boundary conditions defined in the previous section provides the evolution of the spray for $l > l_{\text{BU}}$. The numerical scheme employed in the computation is similar to that previously utilized in [4] for the integration of vaporizing spray jets. The fuel properties considered are those of octane, i.e., $S = 15.3$, $T_B = 398.7$ K, and $q = 44.7 \times 10^{-6}$ J/Kg. With the air-side temperature assumed to be $T_A = 800$ K, the corresponding flame temperature defined in (2.21) is $T_f = 2766$ K, yielding dimensionless values $\bar{q} = 11.55$, $l_v = 0.077$, $\gamma = 0.98$ for the different energetic parameters, evaluated with a value $c_p = 1400$ J/(Kg K) assumed for the specific heat. Correspondingly, with the temperature of the burnt products taken to be $T_P = 1200$ K, the boundary value $H_P = -0.612$ is obtained for the dimensionless excess enthalpy on the products side, where the mixture fraction takes on a value $Z_P = (1 + SY_{\text{F}_P})/(1 + S)$ that, for the nonzero values of $Y_{\text{F}_P}$ considered here, is always larger than the stoichiometric mixture fraction $Z_s = 1/(1 + S) = 0.061$ found at the flame.

Although different values of $Y_{\text{F}_P}$ in the range $0.075 \leq Y_{\text{F}_P} \leq 0.3$ were used in the computations, this parameter was found to have a negligible influence on the solution, because the presence of a nonzero fuel concentration in the gas mixture is important for the initial flame establishment but becomes irrelevant as soon as the spray begins to vaporize for $l > l_{\text{BU}}$, thereby not affecting the downstream flame development. As a result, for values of $\alpha_c$ of order unity the spray contours and flame shapes obtained with different $Y_{\text{F}_P}$ were seen to be virtually indistinguishable. Because of this independence, a fixed value $Y_{\text{F}_P} = 0.2$ was selected for all of the integrations shown below in figures (4.4)–(4.6), which were performed with $\text{Pr} = 0.7$, $\sigma = 0.7$, and $\delta = 1$ for different values of the dilution parameter $\alpha_c$ and breakup length $l_{\text{BU}}$.

Figure 4.4 shows transverse profiles of temperature, gas and droplet velocity, droplet radius, and reactant mass fractions obtained for $Y_{\text{F}_P} = 0.2$, $\alpha_c = 1$, and $l_{\text{BU}} = 0.25$, at different downstream locations. A thick dashed line is used to represent the flame surface $\Sigma_f$ and the outer boundary of the spray $\Sigma_s$, the latter coinciding initially with the outermost droplet trajectory. The radii of the boundary droplets, seen to decrease because of vaporization for $l > l_{\text{BU}}$, vanish at a finite distance from the injector, given by $l \simeq 0.9$ for the flame-side droplet and $l \simeq 1.07$ for the products-side droplet, with the former being smaller because of the larger conductive heating rate provided by the flame. The downstream boundary of the spray is defined as the location where $a = 0$ for the different vaporizing droplets located initially within the spray jet.

Because of droplet vaporization, the temperature gradient exhibits a sharp variation across the spray and, correspondingly, $Y_{\text{F}}$ peaks in its interior. The fuel diffuses from the spray to react at the flame with the oxygen transported by the air stream. As can be seen, for the large value of $S$ corresponding to octane, the flame migrates far from the spray, to a location such that the diffusive flux of oxygen into the flame is that needed to meet the reaction stoichiometry, with the strong transverse velocities induced initially by the vaporizing droplets being responsible for the large flame displacement observed

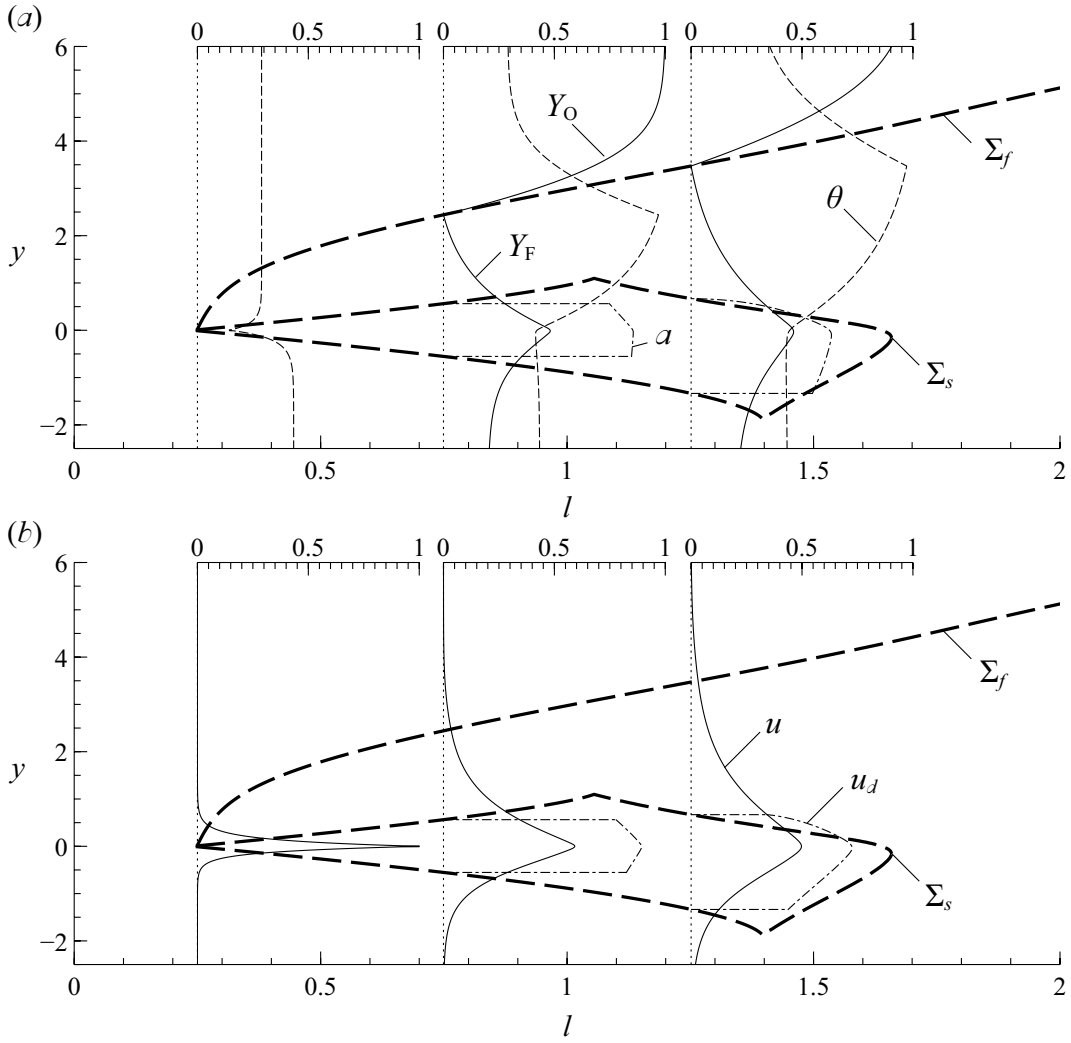


**Figure 4.4:** ($a$) shows transverse profiles of temperature (thin dashed curves), reactant mass fractions (solid curves), and droplet radius (dot-dahed curves), while ($b$) shows the corresponding profiles of streamwise velocity components for the gas (solid curves) and droplets (dot-dashed curves), as obtained for $\mathrm{Pr} = 0.7$, $\sigma = 0.7$, $\delta = 1$, $\alpha_c = 1$, $Y_{\mathrm{F}_P} = 0.2$ and $l_{\mathrm{BU}} = 0.25$ at $l = (0.75, 1.25)$; the thick dashed lines represent in both plots the flame surface $\Sigma_f$ and the contour of the spray $\Sigma_s$.

near $l = l_{\mathrm{BU}}$.

Also shown in figure 4.4 are profiles of gas and droplet streamwise velocities $u$ and $u_d$. Two-way exchange of streamwise momentum occurs within the spray due to the Stokes force present in (4.8) and (4.13). Appreciable gas motion is observed in a boundary layer of increasing thickness surrounding the spray, which is accelerated by viscous stresses. Initially, the peak values of the gas and droplet velocities, both unity at $l = l_{\mathrm{BU}}$, decrease downstream according to $1 - u \sim l^{1/2}$ and $1 - u_d \sim l^{3/2}$, as can be infered from order-of-magnitude estimates in (4.8) and (4.13); the gas decelerating therefore at a much more pronounced rate within the spray, resulting in the values $u < u_d$ displayed in figure 4.4. The

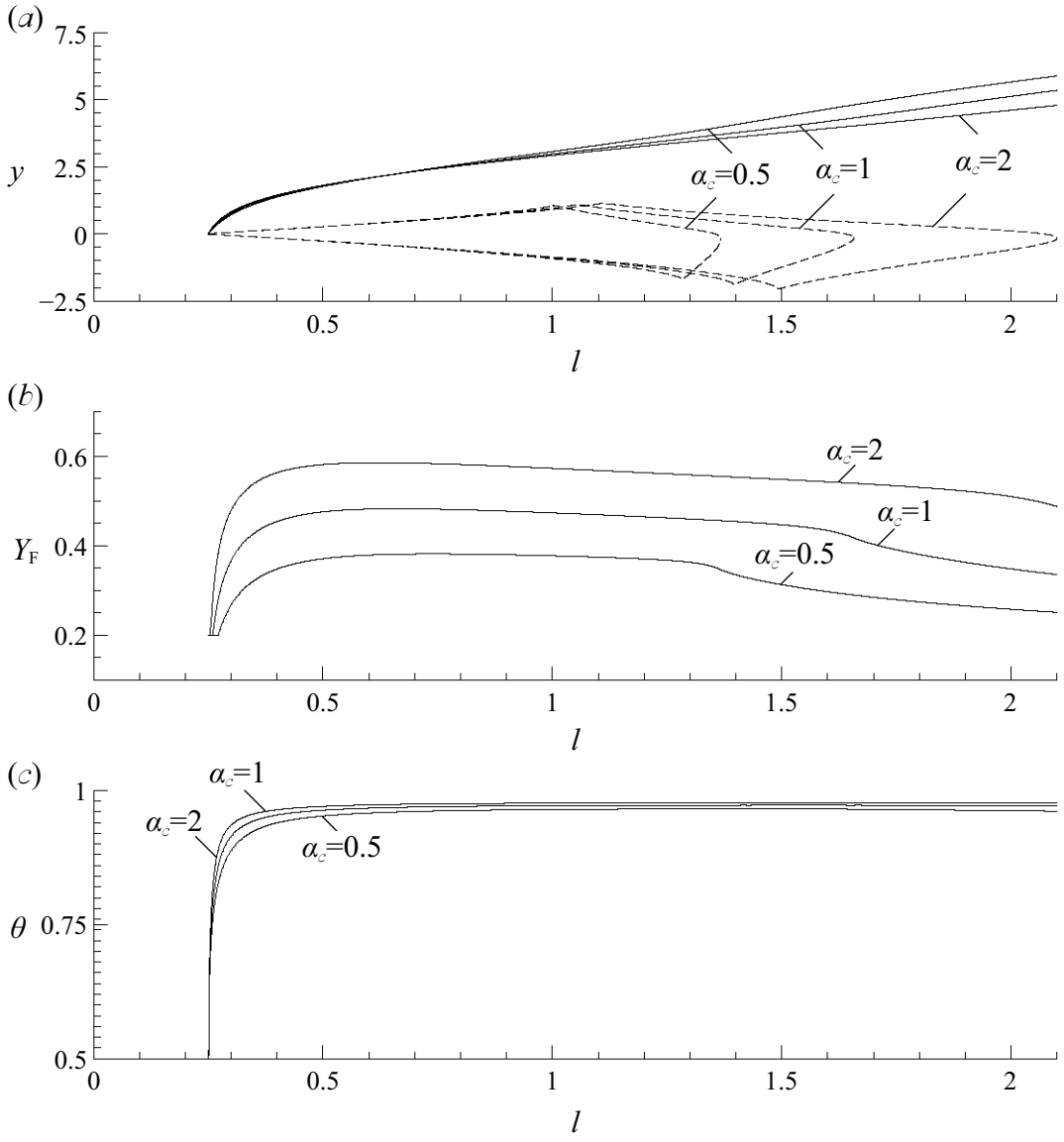


**Figure 4.5:** Reactive spray solutions for $\mathrm{Pr} = 0.7$, $\sigma = 0.7$, $\delta = 1$, $Y_{\mathrm{F}_P} = 0.2$, $l_{\mathrm{BU}} = 0.25$, and $\alpha_c = (0.5, 1, 2)$ including flame surface and spray contour ($a$), peak fuel mass fraction ($b$), and flame temperature ($c$).

decrease in droplet radius due to vaporization reduces inertial effects, causing the associated droplet velocity to naturally converge to that of the surrounding gas. This result can be anticipated from (4.13), where it is seen that the droplets become flow tracers with $u = u_d$ as $a \to 0$, as seen, for instance, for the boundary droplet of vanishing radius located on the flame side of the spray for $l = 1.25$.

The peak temperature at the flame is not constant, as can be seen in the lower plot of figure 4.5, which investigates the effect of dilution on the spray structure. The temperature increases quickly in the initial region where the flame lies close to the spray and the burning rate relies partly on the fuel

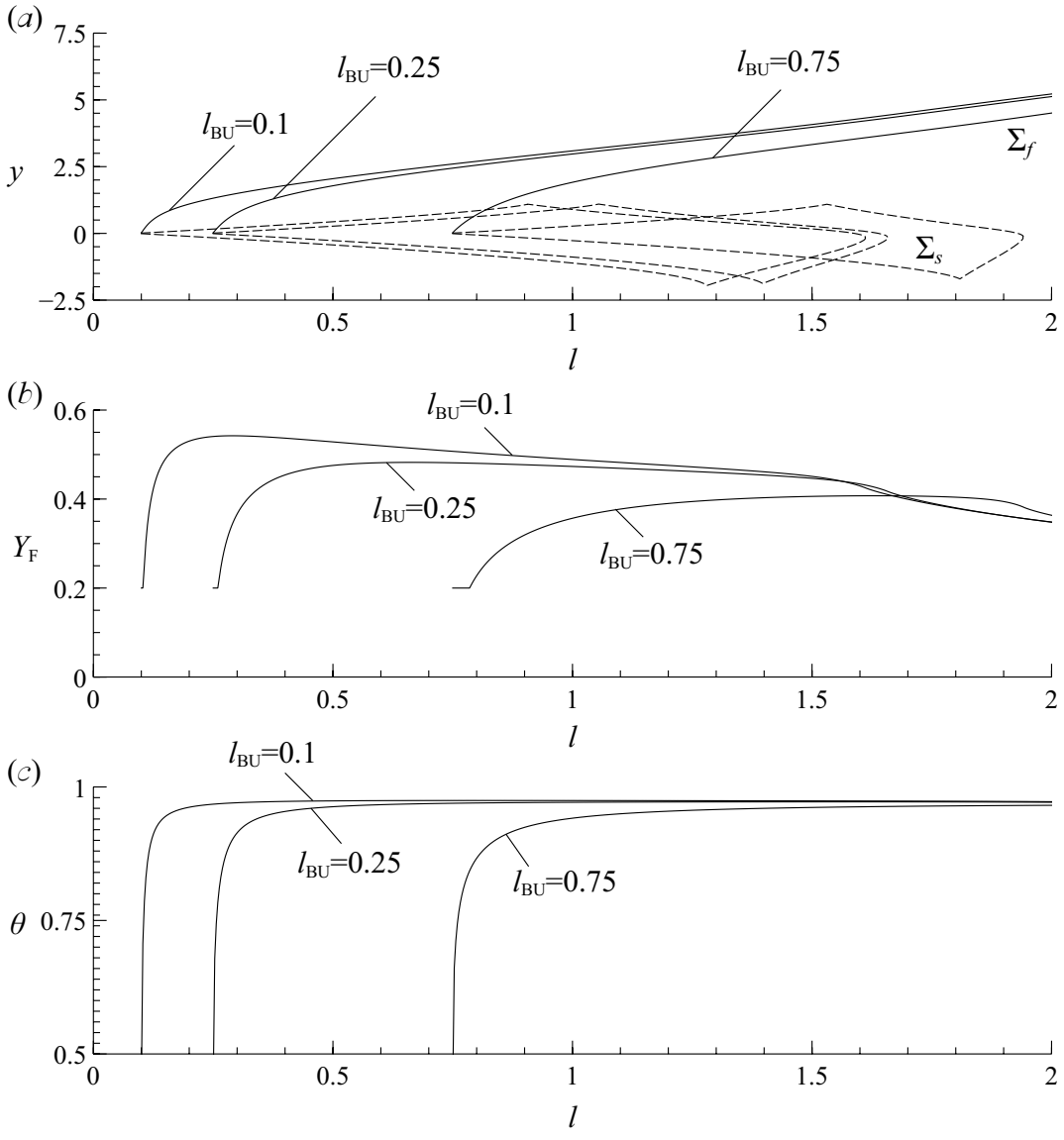


**Figure 4.6:** Reactive spray solutions for $\mathrm{Pr} = 0.7$, $\sigma = 0.7$, $\delta = 1$, $Y_{\mathrm{F}_P} = 0.2$, $\alpha_c = 1$, and $l_{\mathrm{BU}} = (0.1, 0.25, 0.75)$ including flame surface and spray contour ($a$), peak fuel mass fraction ($b$), and flame temperature ($c$).

provided by the products stream. Once a fully vaporizing spray is established and the flame moves away towards the air side, the dimensionless temperature is seen to reach an almost constant value, not far from unity, as expected from the flame-temperature scale defined in (2.21). The resulting temperature evolution is practically identical for the values of $\alpha_c$ of order unity considered in the figure.

The spray contours shown in the upper plot of figure 4.5 exhibit an increment in spray penetration distance as the relative liquid-to-gas mass ratio $\alpha_c$ increases, a behavior also encountered in vaporizing spray jets [4]. By way of contrast, the flame location is almost independent of this parameter, with the flame surface moving only slightly towards the spray for increasing values of $\alpha_c$.

Higher fuel concentrations appear in the spray region for larger values of $\alpha_c$. As can be seen in the plots of peak $Y_{\text{F}}$ shown in figure 4.5, a sharp rise in $Y_{\text{F}}$ accompanies the onset of vaporization. The fuel mass fraction soon reaches a maximum value, larger for larger values of $\alpha_c$, which is followed by a slow decay as the amount of fuel generated by the vaporizing spray steadily decreases. Note that, once the spray dissapears, the resulting lack of fuel supply inmediately leads to a more pronounced decay of $Y_{\text{F}}$. However, this varying fuel concentration does not modify appreciably the corresponding flame temperature, which is seen to remain unperturbed downstream at distances larger than the spray penetration distance.

Variations of breakup length are considered in figure 4.6. The axial derivative operators in (4.7)–(4.11) introduce in principle a nonnegligible geometrical dependence on $l_{\text{BU}}$, beyond that of a simple translation, but the resulting effects on the shape of $\Sigma_f$ and $\Sigma_s$ are only moderate, as can be seen in the upper plot. An additional effect emerge in connection with the gas boundary layers that develop on both sides of the liquid sheet for $0 < l < l_{\text{BU}}$, whose thicknesses at $l = l_{\text{BU}}$ scale with $l_{\text{BU}}^{1/2}$ (see the discussion following (4.18)), thereby affecting spray vaporization in the near field through the value of the initial conductive heating rate, proportional to the reciprocal of the boundary-layer thickness. A reduced spray vaporization rate is present for larger values of $l_{\text{BU}}$, limiting the accumulation rate of gaseous fuel within the spray, as is clearly visible in the plots of peak $Y_{\text{F}}$ in figure 4.6. The effect is also noticeable, although to a somewhat lesser extent, on the development of the flame, with the flame temperature increasing towards its peak value at a smaller rate for larger $l_{\text{BU}}$ in the lower plot of figure 4.6. Note, however, that the final peak temperature achieved seems to be quite independent of the breakup length for the three values of $l_{\text{BU}}$ investigated here.

## 4.6 Conclusions

As an illustration of the application of the formulation presented in chapter 2, a simplified analysis of the combustion of a hollow-cone, swirl-atomized spray was completed. That analysis revealed a number of properties of that spray-combustion process, such as nonuniform fuel-vapor distributions with diffusion flames on the oxidizer side of the spray, spray boundary contours and variations of spray penetration distances with the extent of spray dilution and the breakup length of the liquid fuel sheet. The analysis demonstrates how spray-combustion quantities of interest can be derived from the general formulation. While the maximum extent of analytical simplification was employed in this analysis, the general formulation is readily applicable to fully numerical investigations, which may address more general configurations and may be applied, with turbulence modelling for diffusivities, in turbulent spray combustion.

## References

[1] G. Taylor, The mechanics of swirl atomizers, Proc. 7th Intl. Congress for Appl. Mech. 2 (1948) 280–285.

[2] K. Luo, H. Pitsch, M. G. Pai, O. Desjardin, Direct numerical simulations and analysis of three-

dimensional n-heptane spray flames in a model swirl combustor, Proc. Comb. Inst. 89 (2011) 1447–1460.

[3] A. Lefebvre, Atomization and sprays, Hemisphere Publishing, 1989.

[4] J. Arrieta-Sanagustín, A. Sánchez, A. Liñán, F. Wiliams, The sheath vaporization of a monodisperse fuel-spray jet, J. Fluid Mech. 675 (2011) 435–464.

CHAPTER
**FIVE**

# Concluding remarks and future prospects

This final chapter summarizes the main conclusions of this dissertation and suggests lines of future research in the general field of spray combustion.

## 5.1 Conclusions and summary of the results

### 5.1.1 Coupling-function formulation for spray diffusion flames with infinitely fast chemistry

A two-continua homogenized formulation has been derived for the description of spray flows including droplet vaporization and diffusion-controled group combustion. The formulation can be applied to the description of sprays containing many droplets when the interdroplet spacing is much larger than the droplet radii, the latter condition corresponding in particular to sprays with characteristic values of the liquid-to-gas mass ratio per unit volume $\alpha_c$ of order unity or smaller, the case often found in combustion applications. The formulation includes a Eulerian description for the gas phase, including source terms in the conservation equations collectively describing the exchange of mass, momentum and energy of the vaporizing droplets with their local surrounding environment. The fuel generated by droplet vaporization burns with the oxygen of the air in a gaseous flame, with the chemical reaction described as a single irreversible reaction. The Burke-Schumann limit of infinitely fast chemistry is analyzed, in which the flame appears as a surface separating a region without fuel from a region without oxygen. Following the procedure introduced by Shvab and Zeldovich, the singular reaction term is eliminated by linear combinations of the conservation equations for energy and chemical species. Correspondingly, the mass fractions and the temperature are replaced in the integration by appropriate coupling functions, which appear modified in the diffusion terms to account for nonunity-Lewis-number effects and include sources proportional to the vaporization and heating rates of the droplets and the number of droplets. The formulation accounts for droplets crossing the flame to vaporize on the air side, as may occur when the droplets have sufficient inertia, leading to distributed fuel oxidation that may be described as a perturbation to the Burke-Schumann solution.

The description of the liquid phase includes a Eulerian conservation equation for the droplet number density and equations for the heating, vaporization and acceleration of the droplets. Although the expressions for the force, vaporization rate and heating rate of each individual droplet are written explicitely only for the case of small values of the droplet Reynolds number, more complicated expressions including dependences on droplet Reynolds number could easily be incorporated. A monodisperse

spray is assumed, so that a single droplet-number density can be used to describe the spray population. Nonetheless, it is indicated how the analysis could be extended to account for droplet families of different radii by using either a Eulerian description with several different droplet-number variables or Lagrangian tracking of individual particles.

### 5.1.2 Sheath vaporization of a monodisperse fuel-spray jet

The homogenized formulation is employed to investigate vaporization of a monodisperse fuel-spray jet discharging into a hot atmosphere for moderately large values of the jet Reynolds number. To focus directly on the vaporization process, the discharging spray has been assumed to be in saturated equilibrium with the surrounding gas. Besides the dilution parameter $\alpha_c$, the vaporizing jet is found to be controlled by a second parameter, the inverse of the group combustion number, $\varepsilon$, which determines the thickness of the vaporization region. The numerical integrations reveal that as $\varepsilon$ decreases the vaporization region becomes thinner, leading to a regime of sheath vaporization that is investigated by considering the asymptotic limit $\varepsilon \to 0$. The problem is seen to reduce to the integration of a parabolic free-boundary problem that determines the position of the vaporization front, which separates an inner stream where the spray remains unperturbed from an outer droplet-free region. The inner structure of the vaporization layer, of characteristic thickness $\varepsilon^{1/2}$, is also addressed. The results of the sheath vaporization limit are in good agreement with those obtained by integrating numerically the original governing equations for moderately small values of $\varepsilon$. The study of the sheath vaporization limit includes consideration of the limits $\alpha_c \gg 1$ and $\alpha_c \ll 1$, which provide in particular explicit analytic expressions for the spray penetration distance.

### 5.1.3 Burke-Schumann analysis of nonpremixed combustion of a hollow cone spray

The general coupling-function formulation was applied to study the group combustion of a hollow cone spray issuing from a pressure-swirl atomizer, in a simplified steady laminar configuration that neglects the swirling motion of the surrounding gaseous streams often found in applications. For the moderately large value of the stoichiometric ratio $S$ employed in the integrations, the flame lies on the air side far from the spray, so that vaporization and combustion are seen to occur in different places. Besides the dilution parameter $\alpha_c$, the solution is seen to depend on the ratio $l_{\mathrm{BU}}$ of the distance from the injector at which the liquid film breaks up to the characteristic spray valorization length, although the observed dependences on this last parameter are weak, whereas the parameter $\alpha_c$ is much more influential and affects both the spray penetration distance and the relative distance of the diffusion flame to the spray boundary.

## 5.2 Future prospects

Although monodisperse sprays are considered in all of the examples investigated, it has been indicated how the coupling-function formulation can be extended to account for droplet classes of different

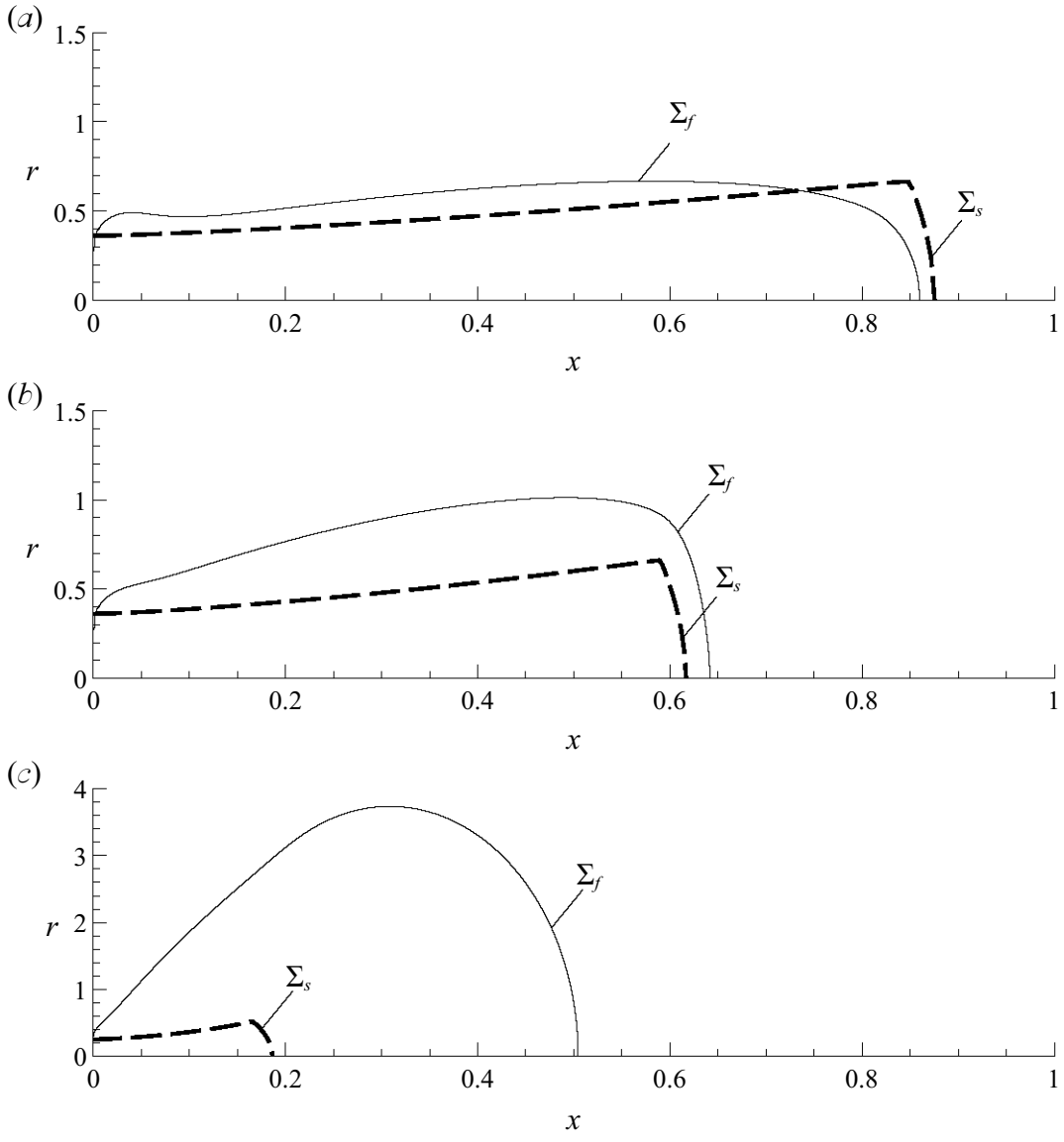


**Figure 5.1:** Diffusion flame in a round jet spray with $T_c$=2.0, $u_c$=0.5 and $\alpha_c$ =0.5 for values of the Stokes number (*a*) St =2.0, (*b*) St =1.0 and (*c*) St =0.25.

radii. Atomization often leads to the formation of small satellite droplets. Although the total volume fraction of these satellite droplets is typically small, they vaporize rapidly because of their small size and are therefore responsible for providing the initial gaseous fuel, fundamental for spray-combustion stabilization near the injector. Studies addressing this effect could make use of an extended form of the formulation including two different droplet classes, described by different variables.

Combustion of liquid-fuel sprays has been addressed in this dissertation in the Burke-Schumann limit of infinitely fast chemical reaction. Indications have been given as to how to treat effects of finite chemistry to describe the oxidation of the fuel coming form the vaporizing droplets crossing into the

air-side of the flame. Additional finite-rate effects are worth further investigation, including conditions for flame extinction and flame anchoring as well as autoignition of the spray.

In a series of recent reactive spray computations[1–3] employing a single irreversible step for the description of the fuel oxidation, it has been observed that regions of premixed and diffusion-controlled combustion may coexist in the vicinity of the atomizer. Clarification of the parameters that determine the type of predominant burning mode and of the conditions that enable the simultaneous appearance of premixed and nonpremixed combustion are worth pursuing in future work. Studies of influences of droplet size and droplet concentration on spray-flame anchoring characteristics could employ simple geometrical configurations, similar to that previously utilized for the investigation of gaseous lifted flames [4].

The study of spray vaporization of round fuel jets presented in chapter 3 could be extended to describe the chemical reaction between the fuel and the oxidizer. For the large value of $S$ corresponding to typical liquid fuels, the flame length and the accompanying characteristic residence time in the flame region scale with $S$, whereas the flame radius scales with $\sqrt{S}$. When these scalings are accounted for in formulating the problem, the solution is seen to depend mainly on two parameters, namely, the dilution parameter $\alpha_c$ and the Stokes number, St, the latter defined as the ratio of the droplet acceleration time to the characteristic diffusion time across the flame. Results of numerical integrations of the resulting boundary-layer problem are shown in figure 5.1 for different values of the Stokes number. As can be seen, droplets with a sufficiently large value of St may cross the flame to vaporize on the air side. For the large Reynolds numbers typically found in applications the flow is turbulent, and droplet transport across the flame would be further facilitated by turbulent dispersion, another phenomenon worth of further investigation in the context of the coupling-function formulation.

As previously mentioned, in reactive fuel-spray jets the flame typically lies far from the spray, at radial distances that are a factor $\sqrt{S}$ larger that the injector radius, so that the discharging spray appears as initially localized when measured with the characteristic scales of the flame. Canonical solutions associated with point sprays, described as concentrated sources of momentum and droplets, can therefore provide considerable understanding of jet-spray flows for $S \gg 1$ while reducing to the minimum the associated parametric dependence. Inclusion of models for turbulence transport could extend the applicability of the solutions to more realistic configurations, enabling simple laws to be derived for spray penetration distances or flame heights, for instance.

# References

[1] J. Reveillon, L. Vervisch, Analysis of weakly turbulent dilute-spray flames and spray combustion regimes, J. Fluid Mech. 537 (2005) 317–347.

[2] L. P. Domingo, Vervisch, J. Reveillon, DNS analysis of partially premixed combustion in spray and gaseous turbulent flame-bases stabilized in hot air, Combust. and Flame 140 (2005) 172–195.

[3] K. Luo, H. Pitsch, M. G. Pai, O. Desjardin, Direct numerical simulations and analysis of three-dimensional n-heptane spray flames in a model swirl combustor, Proc. Comb. Inst. 89 (2011) 1447–1460.

[4] E. Fernández-Tarrazo, M. Vera, A. Liñán, Liftoff and blowoff of a diffusion flame between parallel streams of fuel and air, Combust. and Flame 144 (2006) 261–276.

APPENDIX

# A

# Numerical method

The numerical scheme used to integrate (3.8)–(3.18) and (4.7)–(4.10) is second-order accurate, with an implicit marching procedure considered for the gas-phase equations, account being taken of the sources and sinks that appear in the conservation equations (3.8)–(3.11) and (4.7)–(4.10). Since changes in molecular weight are neglected, the solution for the temperature field becomes independent of the composition. The conservation equations are discretized in a non-uniform mesh designed to cluster points where the spteepest gradients are expected in the flow, i.e. , around $r = 1$ for the jet spray and around $y = 0$ for hollow-cone spray. In order to achieve an appropiate node distribution, the integration procedure uses the transformation proposed by Roberts [1] which maps the uniformly spaced computational domain $\bar{y} \in [0, 1]$ to the non-uniform physical domain according to

$$\bar{y} = B + \frac{1}{\tau} \sinh^{-1} \left[ \left( \frac{y}{y_c} - 1 \right) \sinh(\tau B) \right], \tag{A.1}$$

with

$$B = \frac{1}{2\tau} \log \left[ \frac{1 + (e^{\tau} - 1)(y_c/y_{max})}{1 + (e^{-\tau - 1})(y_c/y_{max})} \right], \tag{A.2}$$

where $\tau$ is the stretching parameter of the mesh, $y$ denotes the radial variable and $y_{max}$ represents the length of the physical domain. In the computational domain the second-order-accurate backward finite-difference formula

$$\left. \frac{\partial \phi}{\partial x} \right|_{i+1}^{j} = \frac{3\phi_{i+1}^{j} - 2\phi_{i}^{j} + \phi_{i-1}^{j}}{2\Delta x}, \tag{A.3}$$

and the second-order accurate centered finite-difference formulae

$$\left. \frac{\partial \phi}{\partial \bar{y}} \right|_{i+1}^{j} = \frac{\phi_{i+1}^{j+1} - \phi_{i+1}^{j-1}}{2\Delta \bar{y}}, \quad \left. \frac{\partial \phi}{\partial \bar{y}^2} \right|_{i+1}^{j} = \frac{\phi_{i+1}^{j+1} - 2\phi_{i+1}^{2} + \phi_{i+1}^{j-1}}{\Delta \bar{y}^2}, \tag{A.4}$$

are employed to discretize streamwise and tranverse derivatives, yielding

$$\rho_{i+1}^{j} u_{i+1}^{j} \left.\frac{\partial \phi}{\partial x}\right|_{i+1}^{j} + \rho_{i+1}^{j} v_{i+1}^{j} \left.\frac{\mathrm{d}\bar{y}}{\mathrm{d}y}\right|^{j} \left.\frac{\partial \phi}{\partial \bar{y}}\right|_{i+1}^{j} - \frac{1}{\Gamma} \left.\frac{\mathrm{d}\bar{y}}{\mathrm{d}y}\right|^{j} \frac{1}{y^{j+1/2}} \left( \left.\frac{\mathrm{d}\bar{y}}{\mathrm{d}y}\right|^{j+1/2} \left.\frac{\partial \phi}{\partial \bar{y}}\right|_{i+1}^{j+1/2} - \left.\frac{\mathrm{d}\bar{y}}{\mathrm{d}y}\right|^{j-1/2} \left.\frac{\partial \phi}{\partial \bar{y}}\right|_{i+1}^{j-1/2} \right) - S_{\phi}|_{i+1}^{j} (1 - \phi_{i+1}^{j}) = 0, \quad \text{(A.5)}$$

for the gas-phase conservation equations with $\Gamma = (Pr, 1, L)$ and $\phi = (u, \theta, Y_{\alpha})$ for (3.9)–(3.11), respectively. $S_{\phi}$ denotes the source terms appearing in (3.9)–(3.11) An iterative method similar to that proposed in [2] is used to determine the values of the gas-phase variables at a given axial location. Convergence is achived when the error falls below a prescribed tolerance. The continuity equation is discretized at the node $(i + 1, j + 1/2)$, yielding

$$\left.\frac{\partial}{\partial x}(\rho u)\right|_{i+1}^{j+1/2} + \frac{1}{r^{j+1/2}} \left.\frac{\partial}{\partial r}(\rho r v)\right|_{i+1}^{j+1/2} - S_{m}|_{i+1}^{j+1/2} = 0, \quad \text{(A.6)}$$

determining the dowstream evolution of $v$. Similarly (4.8)–(4.10) are discretized at the node $(i + 1, j)$ whereas (4.7) is discretized at the node $(i + 1, j + /2)$ yielding similar expressions to (A.5) and (A.6).

The liquid phase is treated as a continuum, hence it can be discretized, defining a finite number of droplets, the outermost droplet of which defines the liquid-phase boundary, beyond which $n = 0$. The liquid-phase equations are written with use made of the Lagrangian description; thus, the systems (3.13)–(3.15) and (4.12)–(4.14) of partial differential equations are reduced to a system of ordinary differential equations, with $u_d \partial/\partial x + v_d \partial/\partial r = u_d \mathrm{d}/\mathrm{d}x$, and

$$\frac{\mathrm{d}y_d}{\mathrm{d}x} = \frac{v_d}{u_d}, \quad \text{(A.7)}$$

as an additional differential equation to determine the radial position of each droplet as a function of its corresponding radial velocity.

The gas-phase properties at each droplet position, needed to evaluate the source terms in (3.13)–(3.15) and (4.12)–(4.14), are obtained by linear interpolation. Similarly, the source terms are distributed to the neighbouring gas-phase mesh points by linear approximation. Therefore, the method used for the numerical integrations is very similar to that proposed in [3] and [4]. However, in order to avoid numerical errors resulting from the stiffness of the source terms in (3.13)–(3.15) when $\varepsilon \ll 1$, the implicit trapezoidal rule is preferred and was employed for the integration of the differential equations of the liquid phase, whereas a two-step Runge-Kutta scheme was utilized to integrate (4.12)–(4.14) as proposed in [3].

The integration of the droplet-density equations (3.12) and (4.11) was carried out by the finite-volume method with a cell-vertex scheme having dual control volumes [5], with the control volume defined in figure A.1. Once the droplet axial velocity, radial velocity and corresponding radial position are calculated, the fluxes at each cell face are determined, providing the downstream evolution of the

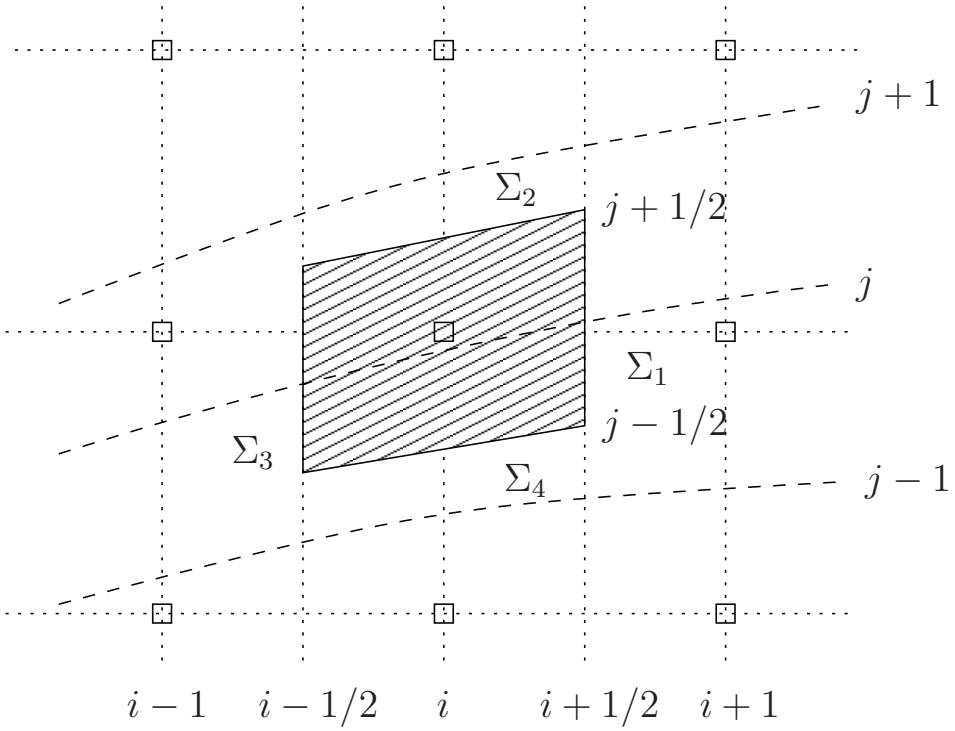


**Figure A.1:** Control volume defined to determine the droplet density distribution. Trajectories of the droplets are represented by dashed lines – – – – whereas the Eulerian mesh nodes are represented by the squared symbols.

droplet density number.

The integration of the free-boundary parabolic problem (3.22)–(3.25) in the sheath vaporization limit was carried out with the front-fixing method described in [6]. To perform the integration the normalized variable $R = r/r_v$ was defined. The inner non-vaporizing stream is integrated in $R \in [0, 1]$, whereas the outer non-vaporizing stream is integrated in $R \in [1, R_\infty]$ with the jump conditions at $R = 1$ (3.34)–(3.35) and $r_v$ determined as part of the solution.

# References

[1] G. O. Roberts, Computational meshes for boundary layer problems, in: Lecture Notes in Physics 8, Vol. 61, Proc. Second Int. Conf. Num. Methods Fluid Dyn., Springer, Berlin, 1971, pp. 171–177.

[2] D. A. Anderson, J. C. Tannehill, R. H. Pletcher, Computational Fluid Mechanics and Heat Transfer, Hemisphere, New York, 1984.

[3] S. K. Aggarwal, G. J. Fix, W. A. Sirignano, Two-phase laminar axissymmetric jet flow: explicit, implicit and split-opperator approximations, Numer. Methods Partial Differential Eq. 1 (1985) 742–756.

[4] J. K. Dukowicz, A particle-fluid numerical model for liquid sprays, J. Comp. Phys. 35 (1980) 229–253.

[5] J. Blazek, Computational Fluid Dynamics: Principles and Applications, Elsevier, 2001.

[6] J. Crank, Free and moving boundary problems, First ed., Oxford Uniersity Press, New York, 1984.

# Alphabetical list of references


Abramowitz, M. & Stegun, I. A. 1965 *Handbook of Mathematical Functions*. Dover Publications Inc., New York.

Aggarwal, S. K., Fix, G. J. & Sirignano, W. A. 1985 Two-phase laminar axissymmetric jet flow: explicit, implicit and split-opperator approximations. *Numer. Methods Partial Differential Eq.* **1**, 742–756.

Anderson, D. A., Tannehill, J. C. & Pletcher, R. H. 1984 *Computational Fluid Mechanics and Heat Transfer*. Hemisphere, New York.

Annamalai, K. & Ryan, W. 1992 Interactive processes in gasification and combustion. Part I: Liquid drop arrays and clouds. *Prog. Energy Combust. Sci.* **18**, 221–295.

Arrieta-Sanagustín, J., Sánchez, A.L., Liñán, A. & Wiliams, F.A 2011 The sheath vaporization of a monodisperse fuel-spray jet. *J. Fluid Mech.* **675**, 435–464.

Bermúdez, A., Ferrín, J.L., Liñán, A. & Saavedra, L. 2011 Numerical simulation of group combustion of pulverized coal. *Comb. Flame* **158**, 1852–1865.

Bermúdez, A., Ferrín, J. L. & Liñán, A. 2007 The modelling of the generation of volatiles, $H_2$ and CO, and their simultaneous diffusion controlled oxidation, in pulverized coal furnaces. *Combus. Theor. Modell.* **11**, 949–976.

Bilger, R.W 2011 A mixture fraction framework for the theory and modeling of droplets and sprays. *Comb. Flame* **158**, 191–202.

Blazek, J. 2001 *Computational Fluid Dynamics: Principles and Applications*. Elsevier.

Bollig, M., Liñán, A., Sánchez, A. L., & Wiliams, F.A 1998 A simplified approach to the numerical description of methane-air flames. *Proc. Combust. Isnt.* **27**, 595–603.

Burke, S.P. & Schumann, T.E.W. 1928 Diffusion flames. *Indust. Eng. Chem.* **20**, 998–1009.

Chen, G. & Gomez, A. 1997 Dilute laminar spray diffusion flames near the transition regime from group combustion to individual droplet burning. *Combust. Flame* **110**, 392–404.

Chiu, H. H., Ahluwalia, R.K., Koh, B. & Croke, E. J. 1978 Spray group combustion. *AIAA 16th Aerospece sciences meeting* .

Chiu, H. H., Kim, H.Y. & Croke, E. J. 1982 Internal group combustion of liquid droplets. *Proc. Combust. Inst.* **19**, 971–980.

Chiu, H. H. & Liu, T.M. 1977 Group combustion of liquid droplets. *Combust. Sci. Tech.* **17**, 127–142.

Correa, S. M. & Sichel, M. 1982*a* The boundary layer structure of a vaporizing fuel cloud. *Combust. Sci. Tech.* **28**, 121–130.

Correa, S. M. & Sichel, M. 1982*b* The group combustion of a spherical cloud of monodisperse fuel droplets. *Proc. Combust. Inst.* **19**, 981–991.

Crane, L. J. 1972 Boundary layer flow on a circular cylinder moving in fluid at rest. *J. Appl. Math. Phys. (ZAMP)* **23**, 201–212.

Crank, J 1984 *Free and moving boundary problems*. First ed., Oxford Uniersity Press, New York.

Crowe, C., Sommerfeld, M. & Tsuji, Y. 1998 *Multiphase flows with droplets and particles*. CRC Press.

De, S. & Lakshmisha, K. N. amd Bilger, R.W 2011 Modeling nonreacting and reacting turbulent spray jets using fully stochastic separated flow approach. *Comb. Flame* **158**, 1992–2008.

Dukowicz, J. K. 1980 A particle-fluid numerical model for liquid sprays. *J. Comp. Phys.* **35**, 229–253.

Faeth, G.M 1977 Current status of droplet and liquid combustion. *Prog. Energy Combust. Sci.* **3**, 191–224.

Faeth, G. M. 1983 Evaporation and combustion of sprays. *Prog. Energy Combust. Sci.* **9**, 1–76.

Fernández-Tarrazo, E., Vera, M. & Liñán, A. 2006 Liftoff and blowoff of a diffusion flame between parallel streams of fuel and air. *Combust. and Flame* **144**, 261–276.

Glauert, M. B. & Lighthill, M. J. 1955 The axisymmetric boundary layer on a long thin cylinder. *Prog. Roy. Soc. Lon. A* **230**, 188–203.

Godsave, G. A. 1953 Studies of the combustion of drops in a fuel spray – the burning of single drops of fuel. *Proc. Combust. Inst* **4**, 818–830.

Janicka, J. & Kollmann, W. 1978 Two variables formalism for the treatment of chemical reactions in turbulent $H_2$-air diffusion flames. *Proc. Combust. Inst.* **17**, 421–430.

Karpetis, A. N. & Gomez, A. 2000 An experimental study of well-defined turbulent non-premixed flames. *Combust. Flame* **121**, 1–23.

Kim, H. Y. & Chiu, H. H. 1983 Group combustion of liquid fuel sprays. *AIAA paper 83-0150* .

Labowsky, M. 1980 Calculation of the burning rates of interacting fuel droplets. *Combust. Sci. Tech.* **22**, 217–226.

Labowsky, M. & Rosner, D. E. 1978 Group combustion of droplets in fuel clouds, i. quasi-steady predictions. In *Evaporation-Combustion of Fuels* (ed. J. T. Zung), pp. 63–79. Americal Chemical Society.

Lasheras, J. C. & Hopfinger, E. J. 2000 Liquid jet instability and atomization in a coaxial gas stream. *Annu. Rev. Fluid Mech.* **32**, 275–308.

Lee, D., Kim, H. Y., Yoon, S. S. & Cho, C. P. 2010 Group combustion of staggeringly arranged heptane droplets at various Reynolds numbers, oxygen mole-fractions and separation distances. *Fuel* **89**, 1447–1460.

Lefebvre, A.H. 1989 *Atomization and sprays*. Hemisphere Publishing.

Lépinette, A., . Liñán, A., Lázaro, B. & Sánchez, A. L. 2005 Reduced kinetics and coupling functions for calculating CO and NO emissions in gas-turbine combustion. *Combust. Sci. Tech.* **177**, 907–931.

Li, S.C. 1997 Spray stagnation flames. *Prog. Energ. and Combust. Sci.* **23**, 303–347.

Liñán, A. 1985 Theory of droplet vaporization and combustion. In *Modélisation des phénoménes de combustion* (ed. R. Borghi, P. Clavin, A. Liñán, P. Pelcé & G. I. eds Sivashinsky), pp. 73–103. Editions Eyrolles.

Liñán, A. 1991 The structure of diffusion flames. In *Fluid dynamical aspects of combustion theory* (ed. M. Onofri & A. Tesei), pp. 11–19. Longman Scientific Technical Essex.

Liñán, A., Orlandi, P., Verizzco, R. & Higuera, F. J. 1994 Effects of non-unity Lewis numbers in diffusion flames. In *Proc. Summer Program*, pp. 5–18. Center for Turbulence Research, NASA-Ames, Stanford University, Standford University.

Liñán, A. & Williams, F.A. 1993 *Fundamental aspects of combustion*. Oxford University Press, New York.

Luo, K., Pitsch, H., Pai, M. G. & Desjardin, O. 2011 Direct numerical simulations and analysis of three-dimensional n-heptane spray flames in a model swirl combustor. *Proc. Comb. Inst.* **89**, 1447–1460.

Massot, M., Kumar, M., Smooke, M.D. & Gomez, A. 1998 Spray counterflow diffusion flames of heptane: experiments and computations with detailed kinetics and transport. *Proc. Combust. Inst.* **27**, 1975–1983.

Moin, P. & Apte, S.V. 2006 Large-eddy simulation of realistic gas turbine combustors. *AIAA Journal* **44**, 698–708.

P. Domingo, Vervisch, L. & Reveillon, J. 2005 DNS analysis of partially premixed combustion in spray and gaseous turbulent flame-bases stabilized in hot air. *Combust. and Flame* **140**, 172–195.

Peters, N. & Rogg, B. 1993 *Reduced kinetic mechanisms for applications in combustion systems, Lecture notes in Physics 15*. Springer-Verlag.

Reveillon, J. & Vervisch, L. 2005 Analysis of weakly turbulent dilute-spray flames and spray combustion regimes. *J. Fluid Mech.* **537**, 317–347.

Roberts, G. O. 1971 Computational meshes for boundary layer problems. In *Lecture Notes in Physics 8*, , vol. 61, pp. 171–177. Proc. Second Int. Conf. Num. Methods Fluid Dyn., Springer, Berlin.

Russo, S. & Gomez, A. 2006 Physical chracterization of laminar spray flames in the pressure range 0.1-0.9 MPa. *Combust. Flame* **145**, 339–356.

Sadhal, S.S & Ayyaswamy, P.S. 1983 Flow past a liquid drop with large non-uniform velocity. *J. Fluid Mech.* **133**, 65–81.

Sánchez, A. L., Lépinette, A., Bollig, M., . Liñán, A. & Lázaro, B. 2000 The reduced kinetic description of lean premixed combustion. *Combust. Flame* **123**, 436–464.

Sánchez, A. L., Liñán, A. & Wiliams, F.A 1997 A generalized Burke-Schumann formulation for hydrogen-oxygen diffusion flames mantaining partial equilibrium of the shuffle reactions. *Combust. Sci. Tech.* **123**, 317–345.

Shvab, V. A. 1948 Relation between the temperature and velocity fields of the flame of a gas burner, *Issledovanie protessov gorenia naturalnogo topliva. Gos. Energ. izd.* .

Sichel, M. & Palaniswamy, S. 1984 Sheath combustion of sprays. *Proc. Combust. Inst.* **20**, 1789–1798.

Sirignano, W.A 1983 Fuel droplet vaporization and spray combustion theory. *Prog. Energy Combust. Sci.* **9**, 291–322.

Sirignano, W.A. 1999 *Fluid dynamics and transport of droplets and sprays*. Cambridge University Press, Cambridge, UK.

Suzuki, T. & Chiu, H. H. 1971 Multi-droplet combustion of liquid propellants. *Proceedings of 9th International on Space Technology Science* pp. 145–153.

Taylor, G.I 1948 The mechanics of swirl atomizers. *Proc. 7th Intl. Congress for Appl. Mech.* **2**, 280–285.

Williams, F.A. 1985 *Combustion Theory*. Second ed., Benjaming Cummings, Menlo Park, CA.

Williams, F.A 1992 The role of theory in combustion science. *Proc. Combust. Inst.* **24**, 1–17.

Zeldovich, Y. B. 1949 Teorii gorenia neperemeshannykh, *English translation*: On the theory of combustion of initially unmixes gases, NACA, Tech. Memo. 1296, 1951. *Zhurnal Tekhnicheskoi Fiziki* **19**, 1199–1210.